University of Zurich[UZH]

How do wood anatomy and physiological processes influence maximum tree height?

GEO 511 Master's Thesis

Author
Mattias Barigazzi
15-730-989

Supervised by
Prof. Dr. Paolo Cherubini (paolo.cherubini@wsl.ch)
Prof. Dr. John David Marshall (john.marshall@slu.se)

Faculty representative
Prof. Dr. Markus Egli

29.09.2022
Department of Geography, University of Zurich

University of Zurich[UZH]

How Do Wood Anatomy and Physiological Processes Influence Maximum Tree Height?

GEO511 Master's Thesis

Author

Mattias Barigazzi

15-730-989

Supervised by

Prof. Dr. Paolo Cherubini

Prof. Dr. John David Marshall

Faculty representative

Prof. Dr. Markus Egli

Table of Contents

List of figures

List of tables

Acknowledgements

Firstly, I would like to thank Prof. Dr. Paolo Cherubini for suggesting this project and at the same time I would like to thank him for his constant support throughout the last year. Similarly, I would like to thank my co-supervisor Prof. Dr. John David Marshall, for the availability of meeting with me and discussing every next step in this thesis, as well as providing useful suggestions for the interpretations of my results.

A special thanks goes to Dr. Meisha Holloway-Phillips for providing the samples for the thesis, as well as sending me many useful information about the Swiss Canopy Crane II research site, and lastly also for helping me kickstart the thesis during the first few months. Another special thanks must go to Prof. Dr. Ansgar Kahmen from the University of Basel. Without his permission, the project could not have started in the first place.

I also would like to thank Loïc Schneider for his constant assistance during my lab work, also providing much needed help during all the analyses. In the same way, I would like to thank Dr. Matthias Saurer for his kind help during the isotope measurements and, at the same time, assisting me during the interpretation of the isotope results. Moreover, recognition must be given to Dr. Avni Malhotra from the University of Zürich for helping me with the statistical analysis. I also would like to give recognition to Dr. Tamir Klein for providing me with additional information, which was very useful in interpreting my results.

A special thanks goes to Martina Nasca for supporting me throughout this journey and providing at the same time a lot of help. Firstly, she thought me the appropriate way of using R for data analysis as well as giving me a hand with statistics with R. Secondly, I would like to thank her for proofreading the final version of this manuscript. I would also like to thank my flat mates Leonardo Rodoni and Cristina Haldemann for the constant support and for putting up with me this last year.

Next up. I would like to say thank you to Anne Verstege for putting up with me as well. In that sense, I wish to apologize for leaving my samples scattered around the tree-ring lab for so much time without putting them away. Also, thanks to Daniel Nievergelt for being available to accompany me to Basel for returning them.

Finally, a special thanks goes to the other master students, civil service workers, and interns at WSL. They provided a very friendly and light-hearted atmosphere throughout my stay.

Abstract

Studying maximum height in plants poses an interesting insight in the possible consequences of changing climatic condition in the next decades. Since trees are long-lived organisms that could reach ages well over 1000 years, researching what are the factors limiting their vertical growth is rather peculiar. The principal hypothesis which will be tested in this thesis states that hydraulic limitations are the main cause of limiting growth in vascular trees. As such, it can be said that theoretically, it exists a maximum height at which the plant is not able to transport water against the increasing forces of adhesion, cohesion, and gravity. The main goal of this thesis is to see if it is possible to determine said maximum height in European beech (*Fagus sylvatica* L.) and Norway spruce (*Picea abies* (L.) H. Karst.). In order to do that, a combination between wood anatomical measurements and isotope analysis will be applied to a few trees from both species. More specifically, the lumen area will be measured via image analysis of previously cut microsections. Following that, the hydraulic diameter and the hydraulic conductivity will be calculated using the Hagen-Poiseuille equation. For the isotope analysis, the ratio $^{13}C/^{12}C$ for whole wood samples will be computed. In the end, it was found that the lumen area, as well as the hydraulic conductivity for the beech samples decreased with increasing tree height. At the same time, the spruce samples did not show the same trend. Instead, they were found to not have any significant height trend. Moreover, for the carbon isotope measurements, both species did not show any particular height related trend. However, it was found that the spruce samples showed constantly higher values of $d^{13}C$ (i.e., less negative) than the beech ones. Finally, it was not possible to determine concretely if hydraulic constraints did indeed limit maximum tree height in both species, while, at the same time, isotopic data did not contribute to that sense.

1 Introduction

1.1 Background and motivation

The latest IPCC report (April 2022) shows that greenhood gas emissions (mainly CO_2) are continuing to rise to unprecedented levels. Also, current plans to mitigate these emissions are not being followed enough thoroughly by government officials to limit the global increase in temperature to 1.5 °C above preindustrial levels. That is the universally agreed threshold that climatologist believe is the point where the world will face even more catastrophic impacts from climate change (IPCC, 2022). Since CO_2 is the only substrate used for plants' photosynthesis, fluctuation in the atmospheric concentration of carbon dioxide can influence greatly plant functions. Small increases for restricted period of times usually lead to increased photosynthetic activity, while on the other hand persistent increase in atmospheric CO_2 concentrations can well enough act as a stress for the plant, leading to short-to-long term reduced or stopped growth (Marshall and Monserud, 1994). In this sense, studying how plants physiological processes respond to increasing temperatures, carbon dioxide concentrations, and frequency of extreme meteorological events (such as droughts and floods) can be a very important insight into what the future has in store for us (Pesendorfer et al., 2021). Furthermore, looking in depth at plant growth and senescence (i.e., cellular ageing) can give an even more peculiar insight in the plant – climate change dualism mentioned previously.

There are two principal ways of seeing cellular ageing. One way sees senescence as universal, in which cellular wear and tear is inevitable, and to contrast that cells must replace themselves or the organism will eventually die. On the other hand, the second way assumes that cells are potentially immortal and immune to senescence. In this sense, there is a difference between multicellular animals and plants, whereas the first eventually stop growing, age, and die. The latter, however, could potentially grow indefinitely as, in the literature, for example, the growing tips of certain plant species were found to not senesce at all (Sheldrake, 2022). Indeed, trees are examples of long-lived organisms, which are able to set the record for the longest living multicellular organisms: for example, the Great Basin bristlecone pine, which some of their individuals can exceed 4000 years of age, with the record holder of at least 4862 years. With many other tree species reaching 1000 years, such long lives should be reflective of the fact that trees are very adaptive and successful organisms. They are also able to remain reproductive into old age, making it possible for many tree species to outlive many other organisms (Lanner, 2002). This fact is one of the reasons why studying growth trends in trees could be very much indicative of ageing phenomena in all kinds of organisms (i.e., not only trees), also in a philosophical sense. While for animals the term senescence is used usually to refer as the deteriorating effect of ageing on, in plant the term indicated a highly regulated physiological process that eventually leads to death at an organ or tissue level, without necessarily meaning that the entire organism will perish. Therefore, plants can outlive animal by many hundreds of years and could serve as a very good indication on how plants can also adapt to future climatic and environmental conditions, due to the effect of climate change (Pesendorfer et al., 2021; Watson and Riha, 2011).

In this sense, dendrochronology can be the way to assess both questions, since via tree-ring based analyses, it is possible to connect both the influence that changing climatic conditions have on plants, as well as the more philosophical one regarding cell ageing and senescence. In order to do the latter, it is convenient to assume that senescence is directly connected to growth in plants, therefore the immediate way to answer that question is to study maximum tree height.

Generally, trees eventually stop growing past a certain height threshold which is specific to each tree species and influenced by the environmental conditions that the organism finds itself in (Koch et al., 2004; Ryan and Yoder, 1997; Yoder et al., 1994). Some models predict maximum height for all trees at around 120 meters in absence of mechanical damage. However, it was recorded that taller trees existed in nature. Moreover, we now know, that maximal tree height is very species dependent, meaning that each different tree species has an intrinsic range of maximum height that is able to sustain (Koch et al., 2004; Mencuccini et al., 2005). This happens, usually because after a certain height it is not sustainable according to the tree's perspective to keep

investing resources in growing upwards (Mencuccini et al., 2005). According to the literature, there is the possibility that maximal tree height and eventually tree mortality is regulated by hydraulic properties rather than as a consequence of ageing itself (Ryan and Yoder, 1997; West et al., 1999). More specifically it was found that water potential decreases going up towards the top of the tree, making difficult for the organism to transport water at those heights (Koch et al., 2004; Ryan and Yoder, 1997). A concrete way to possibly verify this hypothesis is to study the trees' anatomical features, focusing on the width of the tracheids and vessels present on each tree ring. This is the case, because if at greater heights it would be more difficult to transport water against the gravitational pull, then the width of the tracheids or vessels would consequently be smaller (Ryan and Yoder, 1997). Another useful approach is to investigate carbon isotopes in each annual ring. Indeed, if the tree really is impaired in the transport of water r at higher regions, this would be shown in the $^{13}C/^{12}C$ ratio of the wood (Cherubini et al, 2021; Yoder et al, 1994). More specifically, if less water is available for photosynthesis because of difficulty in transport due to anatomical constraints, then the $d^{13}C$ ratio should consequently become less negative (Cherubini et al., 2021; West et al., 1999).

Based on the theoretical background, this thesis will indeed follow the same procedure presented above. Firstly, from six trees belonging to 2 different species (namely *Fagus sylvatica* L. and *Picea abies* (L.) H. Karst.), tree-ring measurements will be done at different height intervals along the height of the tree. Secondly, wood anatomical measurement will be also conducted at the same height intervals used for ring-width measurements for three years: 2017, 2018, and 2019. Finally isotopic measurements (namely $^{13}C/^{12}C$ and N-percentage) will be done on the entire woody composition of both plant species at the same height intervals, also in this case for the years 2017, 2018, and 2019. The aim of this procedure is to analyze the two aspects presented above. In the first place, the tree-ring data will allow to make comparisons and correlation between tree growth and past climactic events. On the other hand, wood anatomical data and carbon isotope data will be used to assess tree growth and maximal tree height; moreover, a combination of the two could theoretically help understand maximal tree height, since both wood anatomy and isotope data reflect the same process of water transport in plants.

1.2 Research objectives and hypotheses

The research objectives of this project are as the following. Principally, this thesis focuses on determining whether tree height is regulated by both anatomical and hydraulic features; alternatively, to assess if one has stronger influence than the other, or conversely, no influence at all. Moreover, another objective is also to identify consistencies within anatomical features that would suggest that plant growth is indeed limited by tree height, due to hydraulic constraints. Thirdly, this project also wants to assess whether isotope ratios, namely $^{13}C/^{12}C$, have a correlation in plant height trends caused by hydraulic constraints. For these reasons, the main research question of this thesis is the following: "*How do wood anatomy and physiological processes influence maximum tree height in Norway spruce and European beech in a Swiss mixed forest*?".

Together with this main overarching research question, there are also a few smaller research hypotheses. Those consist of a more in-depth analysis of each individual part of this project. The hypotheses are four and are as follow:

- **i.** *The lumen size of the cells of both plant species will decrease going up towards the top of the tree; at the same time isotopic carbon measurements will reflect this trend as well.*
- **ii.** *Interspecific differences will be found between European beech and Norway spruce samples for both wood anatomy and carbon isotope analyses.*
- **iii.** *Hydraulic constraints will be found to limit tree height after a certain threshold".*
- **iv.** *13C/12C will be less negative in wood of higher parts of the tree, due to higher consumption of 13C for photosynthesis*

2 Study area

The Swiss Canopy Crane II in Hölstein, BL (47°26'19.7'' N, 7°46'34.5'' E) is a research site of the University of Basel focused on studying and processing results of 250 trees of 12 different species (Figure 1).

Figure 1 Map of Switzerland. The red marker indicates the location of the Swiss Canopy Crane II research site in Hölstein (BL) (Source: map.geo.admin, 2022a)

2.1 Site description

The Swiss Canopy Crane II research site has the goal to answer the ever so important question of which role could temperate forests provide to the extreme climatic conditions that we will be faced in the near future. Focusing mainly on rising temperatures, changing precipitation patterns, and increasing extreme drought events (SCC, 2022). In the middle of the research site lies a 50 m tall crane equipped with a 50 m long jib, capable of reaching an area of around 7850 m^2 (Figure 2). The trees inside this area are analyzed at different heights. The research area is also equipped with a 3100 m^2 interchangeable roof under the canopy of the trees. The panels making up the roof are able to be moved and shifted as needed. The main focus of this area is to simulate tree growth under different environmental conditions, namely dryer and hotter climates similar to the ones approaching us in the future (Kahmen et al.,2017; University of Basel, 2022).

The research site is located at an elevation of 550 m above sea level and is positioned on top of a gentle hillslope. The size of the plot is around 1.6 ha, while the soil is made of rendzina, which is a calcareous soil with clay content up to 40%. Moreover, the vegetation is constituted by a mixed, uneven-aged temperate forest, with trees reaching maximal heights of up to 35 m. Also, the research site hosts up to 250 trees from 12 different species (Kahmen et al., 2017; SCC, 2022).

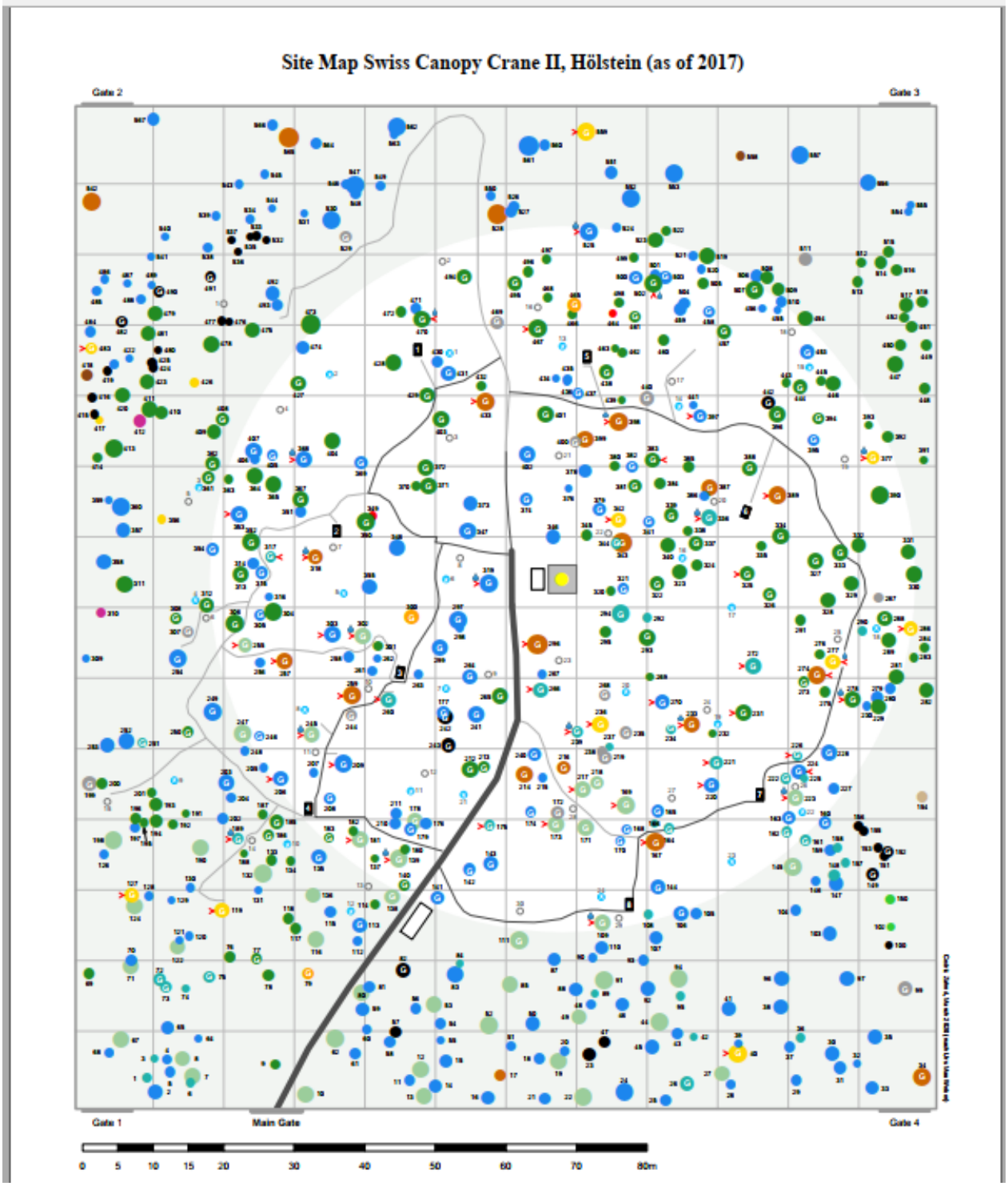

Figure 2 Map of the Swiss Canopy Crane II research site in 2017. The central area (white circle) indicates the reach of the crane. The different colored circles correspond to different tree species present at SCC II (Image kindly given by Dr. Meisha Holloway-Phillips, University of Basel).

2.2 Climate

The mean annual temperature at the Hölstein research site is 9.0 °C and the mean annual precipitation is 1009 mm, which is considerably lower than the Swiss mean (Kahmen et al., 2017). The temperature maximum is found in the months of July and August with average temperature at around 23 °C, and peaks up to 32 °C. The temperature minimum, on the other hand, is found between January and February, with an average temperature of around -2 °C, while the lowest individual temperature values can reach -10 °C. The peaks in mean daily precipitation are found in December, with values reaching around 80 mm/day (Meteoblue.com, 2022).

2.3 Geology

The region around Hölstein and the whole canton of Basel Country (Figure 3) lies over the geological Hauptorgenstein-formation. This is a lithostratigraphic formation from the south-German Jura, belonging to the brown Jura formation, mainly composed of calcareous ooliths or ooids (Bloos et al., 2005).

The geological formation around the area is called folded Jura (in German: *Faltenjura*), which compared to the flatter table Jura (in German: *Tafeljura*) is made of many hillslopes of differing sizes. The Jura hills are built up vertically with decreasing size horizontally along an imaginary northwest-southeast line. This depression accommodates the compression from the alpine mountain range, which moves roughly northwards (Becker, 2000).

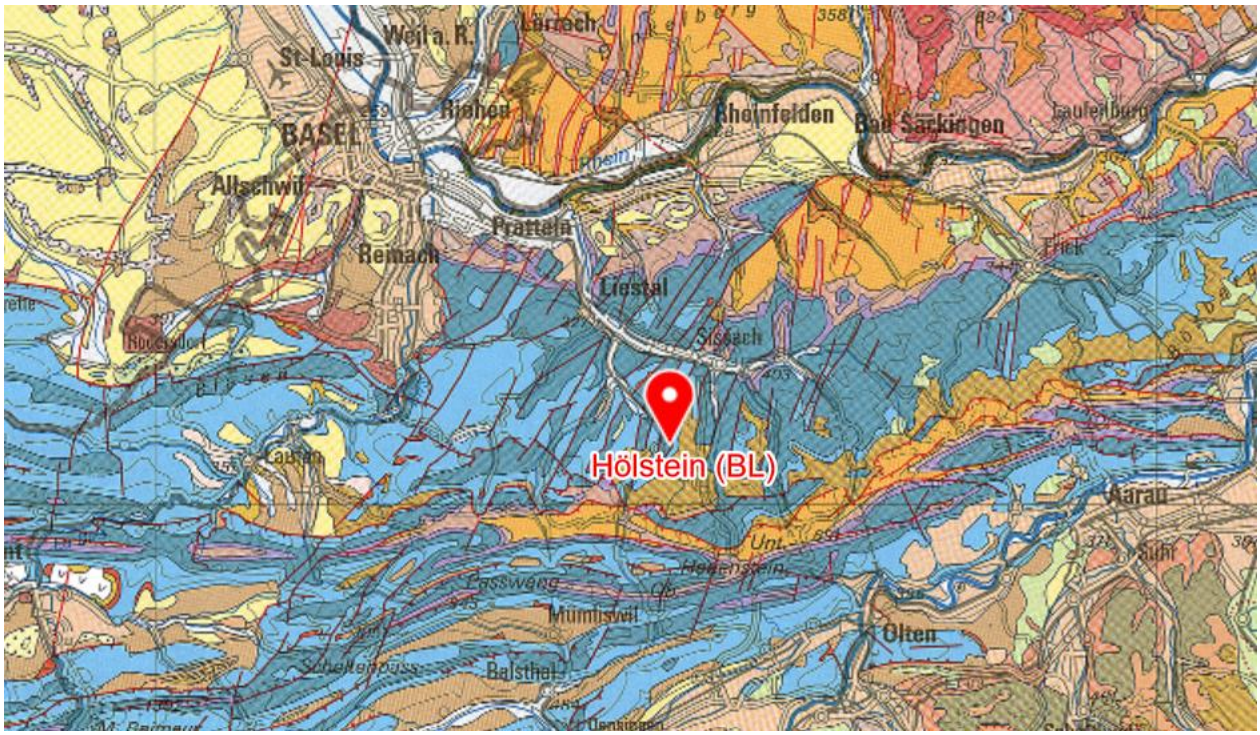

Figure 3 Geological map of the area surrounding Hölstein (BL). The ground sediments are composed of Jura "Malm" rocks belonging to the Hauptrogenstein formation and the folded Jura mountain range (map.geo.admin, 2022b).

2.4 Tree species

From the 12 different species present at SCC II, two of them will be analyzed in this thesis: European beech (*Fagus sylvatica* L.; Figure 4a) and Norway spruce (*Picea abies* (L.) H. Karst.; Figure 4b).

Figure 4 *Fagus sylvatica* L. (a) and *Picea abies* (L.) H. Karst. (b). Image taken in Dübendorf, ZH. (Mattias Barigazzi).

2.4.1 Ecology and distribution

The European beech (also known as common beech) is a deciduous tree belonging to the Fagaceae family (Royal Botanic Gardens, 2017). It is a relatively large tree capable of reaching heights of 50 m and 3 m width diameter at the base of the trunk and has a lifespan of around 150 – 200 years, even if some individuals can live to more than 300 years. Even if it is considered a deciduous species, the European beech in some cases do not drop thier leaves in autumn, instead they remain on the tree until spring, where they become brownish red before withering in a process called marcescence (Wühlisch, 2008). The European beech's habitat ranges all across Europe from southern Sweden to northern Sicily, and from northern Spain to eastern Europe and the entire Greek peninsula, with a considerable hotspot of individuals in Southern England. Some individuals are also found in the Middle East and in northern Turkey (Caudullo et al., 2017). However, it is projected that due to consequences related to climate change many areas that are nowadays suitable for beech will probably disappear or be rendered unable to fulfill the conditions for European beech to grow on. Various physiological studies have defined the European beech as being a very drought sensitive species with evident signs of increased mortality during prolongates drought events (Miranda et al., 2022; Zimmermann et al., 2021).

In Switzerland, European beech is found practically everywhere through every canton with a few small exceptions for the canton of Ticino, Wallis, Bern, and Grisons, where the tallest mountains of the Central Alps are found. In the Swiss Plateu, on the other hand, the European beech is commonly found and with similar intensity (Figure 5). A small increase in number of individuals is found in the western-most regions of Switzerland, namely in the cantons of Vaud, Geneva, and Neuchatel (Infoflora.ch, 2022a)

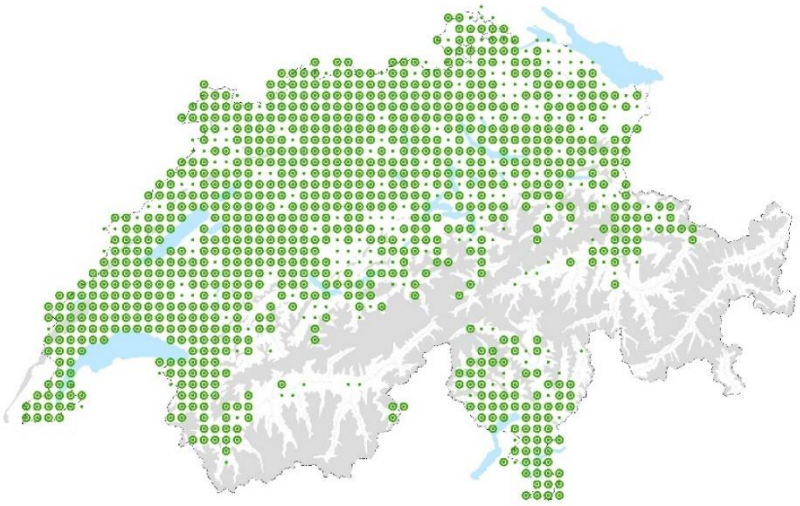

Figure 5 Distribution of *Fagus sylvatica* L. in Switzerland in 2019. Apart from the alpine region, the European beech is equally found in almost all cantons at a similar magnitude. Most individuals are found in the Swiss Plateau with an increasing magnitude in the more western regions (Infoflora.ch, 2022a).

Norway spruce (commonly known also as European spruce) is a species native to central and eastern Europe and it belongs to the Pinaceae family (Sullivan, 1994). It is a large evergreen coniferous tree that can reach heights of around 35 – 55 meters with a trunk diameter of 1 – 1.5 meters. It is usually fast growing in its initial life stages, until it reaches about 20 m height, where it starts growing slower. The leaves are needle-like, and they range from 12 – 14 mm in length (Taylor, 1993). The Norway spruce grows throughout North-Eastern Europe. There are two main regions where the spruce is found in Europe. The first extends from Southern Norway through Scandinavia and then it extends further South through the Baltic region with also a small extension in the westernmost parts of Russia. The second region is located in Central Europe around the central Alps. It extends from the southern-most part of Germany, through Switzerland until the northern-most regions of Greece, passing through the Carpathians (Farjon, 2017).

In Switzerland, the distribution of Norway spruce is somewhat constant throughout the whole nation's territory (Figure 6). There are a few regions where the tree is not found, which coincide with the tallest mountaintops of the Central Alps. These consist in the eastern-most part of Wallis, Grisons, Uri and the southern-most part of for the canton of Bern. In the Swiss Plateu, the Norway spruce is commonly found across the whole area. However, there is a considerable increase in magnitude in the South-western region of Switzerland, namely in the cantons of Geneva, Neuchatel, Fribourg, Vaud, and the western part of the canton of Wallis. A small increase in magnitude is also found in the western-most regions of Switzerland, namely in the cantons of Vaud, Geneva, and Neuchatel (Infoflora.ch, 2022b).

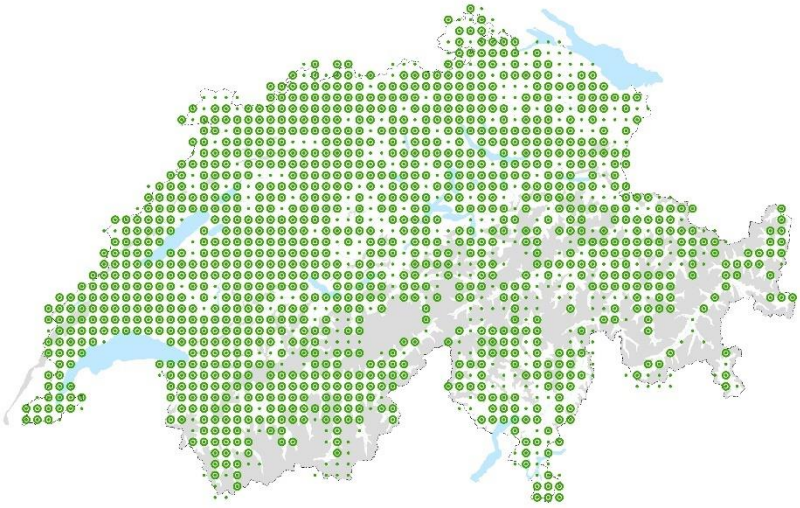

Figure 6 Distribution of *Picea abies* (L.) H. Karst. in Switzerland in 2019. Apart from some very high mountaintops of the alpine region, the Norway spruce is equally found in almost all cantons at a similar magnitude. A small increase in frequency of individuals in the South-western part of Switzerland can be noticed (Infoflora.ch, 2022b).

2.4.2 Internal structure and composition

The wood anatomical structure of European beech (Figure 7a) and Norway spruce (Figure 7b) differs considerably. The principal differences that the two species present are probably due to the fact that they are two completely different kinds of plants; the first being a broadleaf and the second being a conifer (Sperry et al., 2006). In European beech the lumen of the vessels responsible to transport water and nutrients upwards are much different in size and their shape is predominantly elliptical, or sometimes circular (depending on the eccentricity of the cell). Moreover, their distribution does not follow any recognizable pattern or structure. On the other hand, in Norway spruce, the shape of the lumen is mainly rectangular, and their size is fairly constant across every annual ring. Also, the cells are aligned vertically and horizontally, following a very well-defined structure (Fan et al., 2009; Sperry et al., 2006). Moreover, within the European beech's internal structure there are rays, which are extended in all directions form the pith of the tree out towards the bark. Their function is to help with stability within the tree and to "separate" the interior of the tree in sorts of compartments (Lev-Yadun and Aloni, 1995). These structures are not present in the wood of the Norway spruce. Also, the Norway spruce, as for all other conifers, present so called tracheids scattered within the cell matrix. These structures differ quite evidently with all other "regular" cells both in size and shape. The latter are usually larger and most importantly are circular shaped instead of the rectangular shape that most of all other cell have. The function of the trachieds is to help with vertical transport due to their larger conduits and they also act as supporting structures thanks to their extension from the base to the top of the tree (Fan et al., 2009; Ryan and Yoder, 1997).

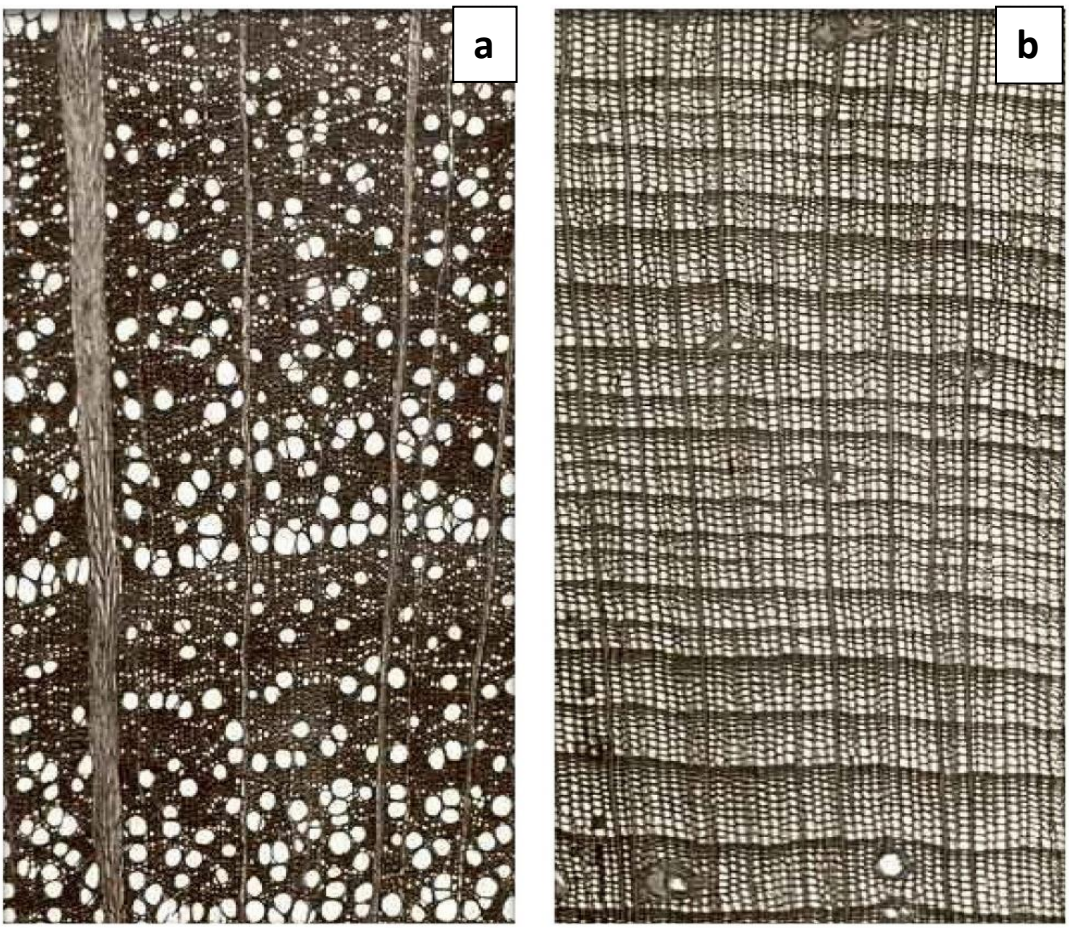

Figure 7 Wood anatomical structures of *Fagus sylvatica* L. (a) and *Picea abies* (L.) H. Karst. (b) (WSL, 2022)

3 Background

3.1 Dendrochronology

Dendrochronology is the study of the connections between trees and dating. More specifically, it focuses on the study of tree growth related with environmental conditions and characteristics, enabling the possibility to establish connection between the two of them. The terms originate from the ancient Greek dendron (δένδρον – tree), chronos (χρόνος – time), as well as logos (λόγος – science), literally meaning the science of using tree ages (Cherubini et al., 2004; Schweingruber, 1996). Before the advent of radiocarbon dating in the late 1940s, dendrochronology was the only reliable method to determine the age of a tree. This method consists of marking the outermost tree ring of a living tree as the current year and then counting inwards to determine its age (Libby, 1946; Schweingruber, 1996).

Even if the first mentions of dendrochronology date back to Leonardo da Vinci (1452 – 1519) thanks to his preliminary studies about tree ring and wood anatomy, the pioneer of dendrochronology is the American astronomer Andrew Ellicot Douglass (1867 – 1962), who set the foundation for the study of tree-ring patterns in trees. Furthermore, the subfield of dendroecology only was developed later in the 1970s starting effectively the study of ecological processes related with trees and the environment (Cherubini et al., 2004; Speer, 2010). Douglass noticed a pattern in the tree rings of various trees growing in similar environmental conditions. Thanks to this finding, he was able to build a chronology that enabled him to also date dead tree stumps. Therefore, practically birthing the so-called cross-dating method of determining tree ages as we know it today. Nowadays, tree-ring analysis is used in many ecological studies as a firm point in determining tree-environment relationships (Cherubini et al., 2004; Douglass, 1941).

3.1.1 Tree-ring analysis

Tree-ring width, coupled with the age of the tree, is the principal measurement parameter of dendrochronology: also, annual tree-rings are an artifact of the tree's biological growth. Moreover, it is widely accepted that tree rings are among the most common and reliable source of data for past environmental characteristics and phenomena. Indeed, tree-ring records have a high degree of confidence in the dating; mainly in its temporal resolution and most of all in the easiness to build extensive time series, also known as chronologies (Cherubini et al., 2004; Von Arx and Carrer, 2013; Zimmermann et al., 2021). In this sense, different structures can be found within a tree ring series (Figure 8). For example, reaction wood can be present if the tree was growing at a slanted angle along a mountain slope or a hillside. In this case, the denser wood is built by the plant to correct for the stress due to different gravitational pull on the body. For angiosperm plants the reaction wood is formed on the side of the plant that is under tension and it is called tension wood, while in gymnosperms it is formed on the side of the plant that is under compression and it is therefore called compression wood (Shigo, 1986). Another example are scars left by damaged wood; either by physical damage (e.g., rockfall) or by burn scars due to wildfires. Another possible cause of either damaged rings or very small and narrow rings are diseases or pest outbreaks which reduce greatly tree growth. Generally, when dealing with pest outbreaks (e.g., *Coloradia pandora* or *Zeiraphera dinian*) the main effects of the attacks in the trees is the great defoliation, which in turn leads to diminished tree growth, noticeable by an abrupt reduction in tree-ring width. These artifacts help greatly the cross-dating procedure since they represent a concrete link between an actual known climatic event and the tree itself. And vice versa, scarred tissue can help reconstruct unknown climate events just by analyzing tree ring data (Baltensweiler et al., 2007; Pohl et al., 2006; Rother et al., 2018).

Currently, the information obtained from tree-ring analyses is used in a wide variety of fields, from law (e.g., dating objects for criminal cases), to astrophysics. Primarily, however, they are used in archeology, climatology, and increasingly in the geoscientific field such as geomorphological studies. Another important application of tree-ring analysis is the use of dendrological data in the testing and calibration of numerical models (Cherubini et al., 2004).

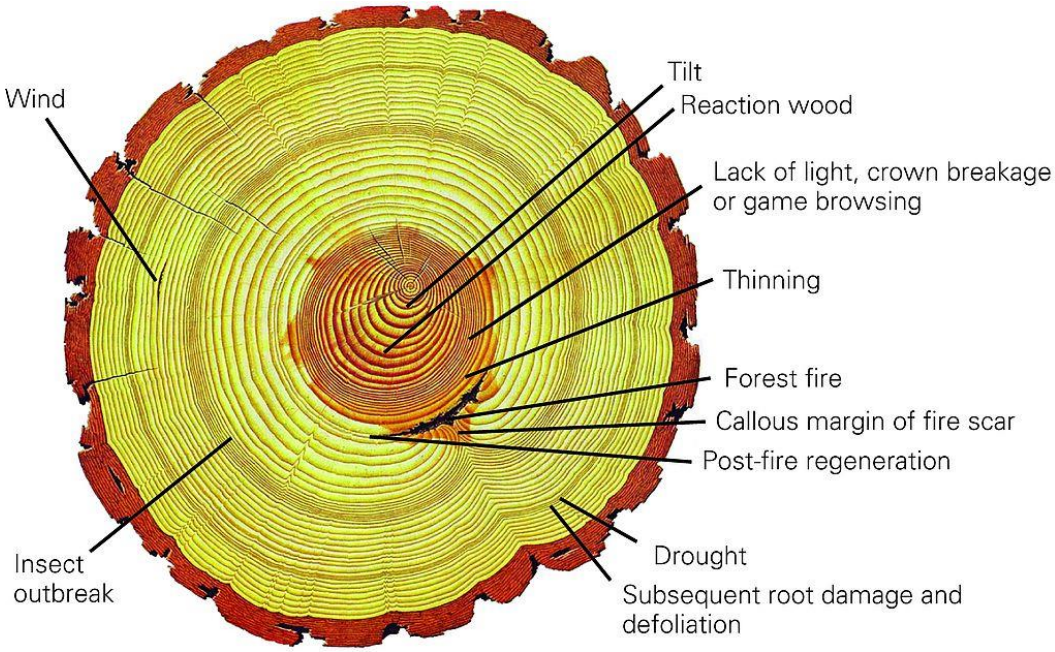

Figure 8 Cross-section indicating the many applications that tree-ring analysis can have to assess climatic and environmental conditions (WSL, 2017).

To extract the climatic information form tree rings, it is necessary to analyze them in a meaningful way. Usually, this is achieved by counting the number of rings, as well as measuring their width (Figure 9). The ring width for an annual ring is determined as the extension from the boundary of its late wood to the beginning of the late wood of the following ring (Burns, 1976). While measuring the ring widths, it is common to then build curves consisting of ring width plotted against each year. Later, it is needed to cross-date each generated curve with reference data (if available) or within the dataset, in order to create a complete chronology. Its features consist on the possibility to identify patterns or abnormalities within the chronology, which are then usually reconducted to climatic events (Martinez, 1996).

Tree-rings act as proxies for climate information and can provide extended climate records distributed in many regions around the world. This allows the possibility to study and evaluate in depth the historical natural climatic variations, as well as determining the frequency and magnitude of climatic events. A clear advantage of using a dendrochronological based series is the ability to obtain annual or intra-annual information about the environment. Moreover, thanks to the clear distinction between earlywood and latewood, it is possible to assign specific climatic events to precise years. Another advantage is that given a representative sample size for a location, one can then extrapolate the climatic information for a broader region, given that the same environmental conditions apply also there (Carlón Allende et al., 2021).

Figure 9 Sample P3_24m analyzed through a binocular with viewfinder. The darker boarders represent latewood, while the lighter regions are the earlywood. To measure ring width of an annual ring one must trace the region between two latewood boarders using the viewfinder (CC Mattias Barigazzi).

3.1.2 Cross-dating

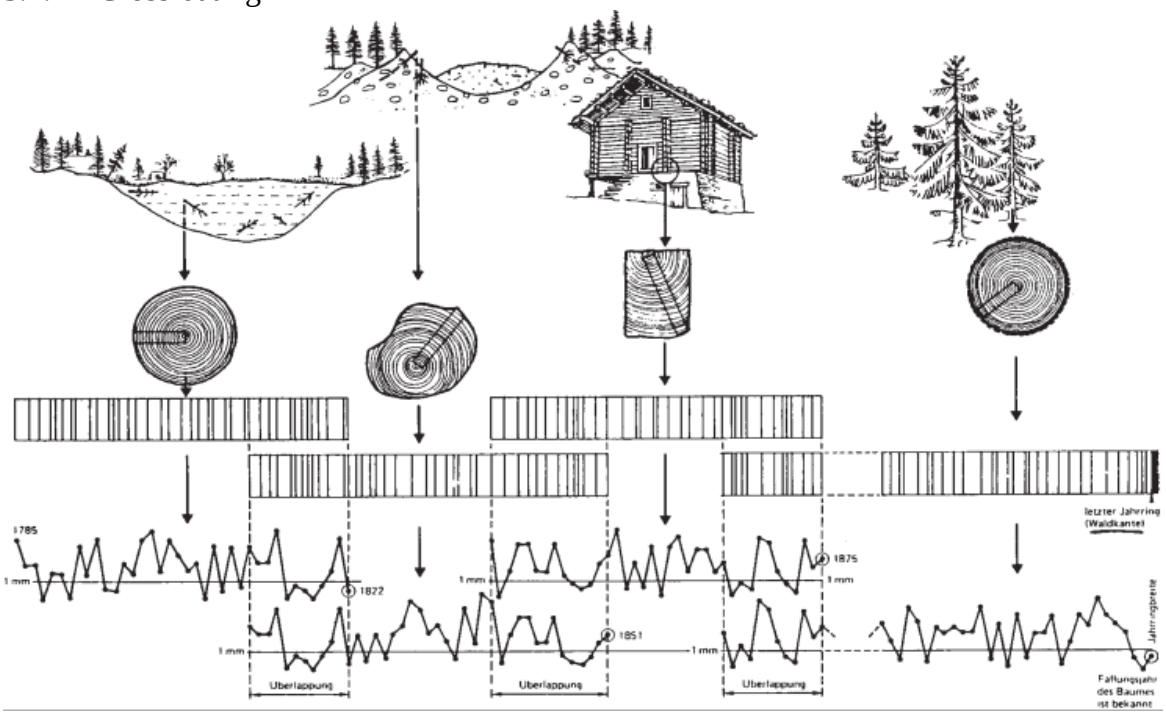

Figure 10 Example of the cross-dating process. Here it is shown how one can reconstruct the chronology of a non-specified region by cross-dating the tree-ring curves from many wood samples across that region (Cherubini et al., 2004).

The cross-dating principle (Figure 10) must be referred as the foundation of all scientific methods regarding dendrochronology. The theoretic principles of cross-dating are based on the knowledge that trees living and

thriving in the same environmental conditions show similar patterns in their tree-ring sequences. The Introduction of cross-dating in dendrochronological studies allowed scientists to use two or several trees to date and assign specific years to individual tree rings. Subsequently, it was possible to confront the growth pattern in trees from nearby regions, which are characterized by similar climatic or environmental conditions and then place each tree in its correct location along a temporal sequence known as a master chronology. The latter consist of a long series of synchronized ring-width pattern that can cover an enormous timespan from nowadays even up to prehistoric times. (Cherubini et al., 2004; Fritts, 1976; Schweingruber, 1988).

3.1.3 Gleichläufigskeitskoeffizient (GLK)

The Gleichläufigskeitskoeffizient (GLK) is a non-parametric measure of growth similarity when comparing tree-rings. The GLK is usually expressed in percentage and indicated as the proportion of simultaneous annual growth changes between two ring-width series. The measure was proposed by Bruno Huber (1899 – 1969) as it also was the Gegenläufigskeitskoeffizient (GGLK), which is the opposite of the GLK and indicates the percentage of dissimilarities between two tree-ring series. However, in later years, the GLK became the method of reference when comparing tree-ring series (Visser, 2021).

To assess the value of GLK, each segment composed of 4 tree rings from the two ring-width curves (two tree ring for each curve), as shown in Figure 11, are compared with each other to see if both curves are either synchronous or asynchronous. If the two curves in a segment increase or decrease together, that part is defined as synchronous growth change. On the other hand, if in a segment the one of the curve increases (respectively decreases), while the other one goes the opposite way, then that part is defined as an asynchronous growth change. Lastly, the third case scenario is that one of the two curves have the same ring width value for two consecutive years, while the other one either increases or decreases. In that case, the segment is defined as semi-synchronous growth change (Huber, 1943; Visser, 2021).

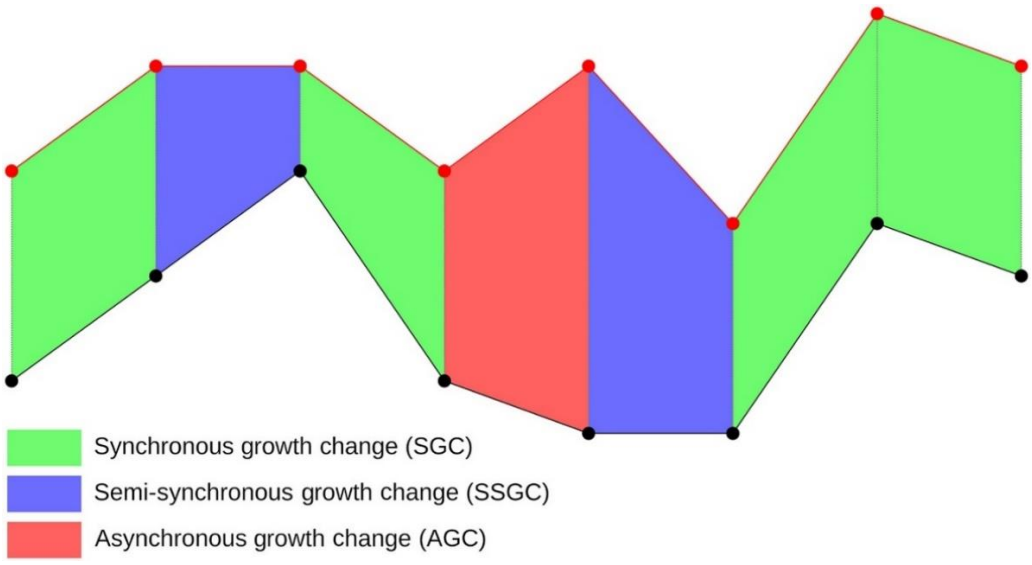

Figure 11 Method used to calculate the Gleichläufigskeitskoeffizient (GLK) using two tree-ring curves. Two series are shown over a period of eight years. In these, seven show growth changes; five of them are synchronous (green), two, are semi-synchronous (blue), and one is asynchronous (red) (Visser, 2021).

3.1.4 Tree growth

Tree growth occurs in two ways. Primary growth is the increase in height and length of the main tree stem and the protruding branches. On the other hand, secondary growth is the increase in diameter of both the main stem as well as the branches.

Primary growth is directly connected with the production of leaves at the top of the stem or at the point of branches. For most plant species, primary growth is directly linked with environmental and climatic conditions

that the plants are affected with. Usually good and constant light and nutrient availability has a positive impact on generating new leaves, leading to increased primary growth. On the other hand, secondary growth is the direct result of cambial activity in plants. Between the xylem and the phloem of the tree lies a softer wood structure called the cambium (Figure 12), which is responsible for generating new wood and new inner bark, leading to increase in the width of the tree (Gaertner, 1964; Kozlowski and Pallardy, 1997). Xylem is mainly composed of dead cells with thickened cell walls rich in cellulose and lignin, which are responsible for providing mechanical support to the tree, as well as conducting water and minerals. In broadleaf trees these cells are differentiated by the tree in fibers that provide support to the structure and vessel cells which specialize in the transport. For conifers, tracheid cells play the double role of support and transport at the same time. On the other hand, phloem is made of alive cells which specify in transport of products of the photosynthesis together with signaling molecules including growth regulating hormones. (Lanner, 2002; Wang et al., 2021).

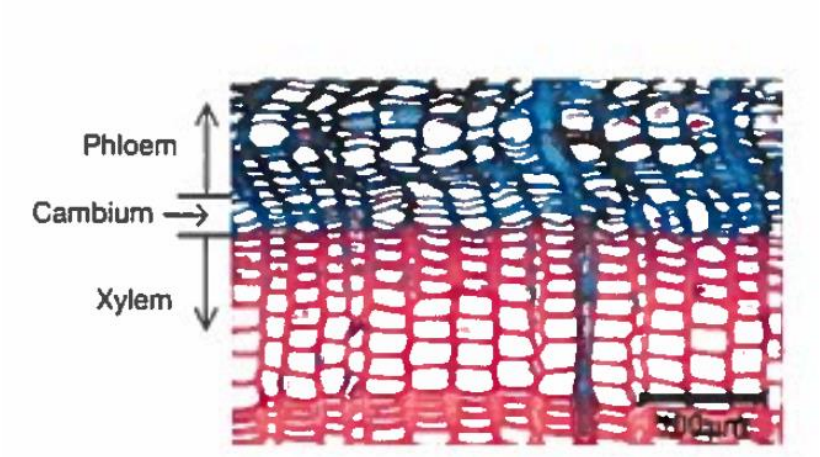

Figure 12 Microscopic thin section showing the outer most ring (red) of a European larch (*Larix decidua* Mill.) including the bark (blue). The cambium responsible for cellular division and secondary tree growth is indicated between the wood (xylem) and the bark (phloem) (Gärtner and Heinrich, 2013).

In trees growing in temperate climates, the cambium usually does not produce new cells during the winter, resulting in an abrupt change in color in the wood at the year's end. This pattern leads to the formation of annual rings of alternating earlywood produced in the summer and latewood generated in the fall (Figure 13). As well as for the primary growth, also cambial activity is very much dependent form climatic and environmental conditions. Usually, temperate to warm temperatures with moderate to abundant precipitation favor secondary growth, leading to wider tree rings, while, on the other hand, rigid temperatures as well as prolonged periods of drought lead to diminished cambial activity, which results in smaller and thinner tree rings (Bose et al., 2020; Higuchi, 1997). The transition from earlywood and latewood is also evident in the cell size of the plants. Analyzing each annual ring it can be noticed an evident transition where the cells go from being wide and very thin to be more narrow and thicker. This change is due to the amount of lignin produced by the cambium at different stages during the growing season. Earlywood is characterized by less lignin resulting in thinner cell walls, while on the other hand latewood typically presents thicker cells walls due to higher lignin content (Wimmer, 2002).

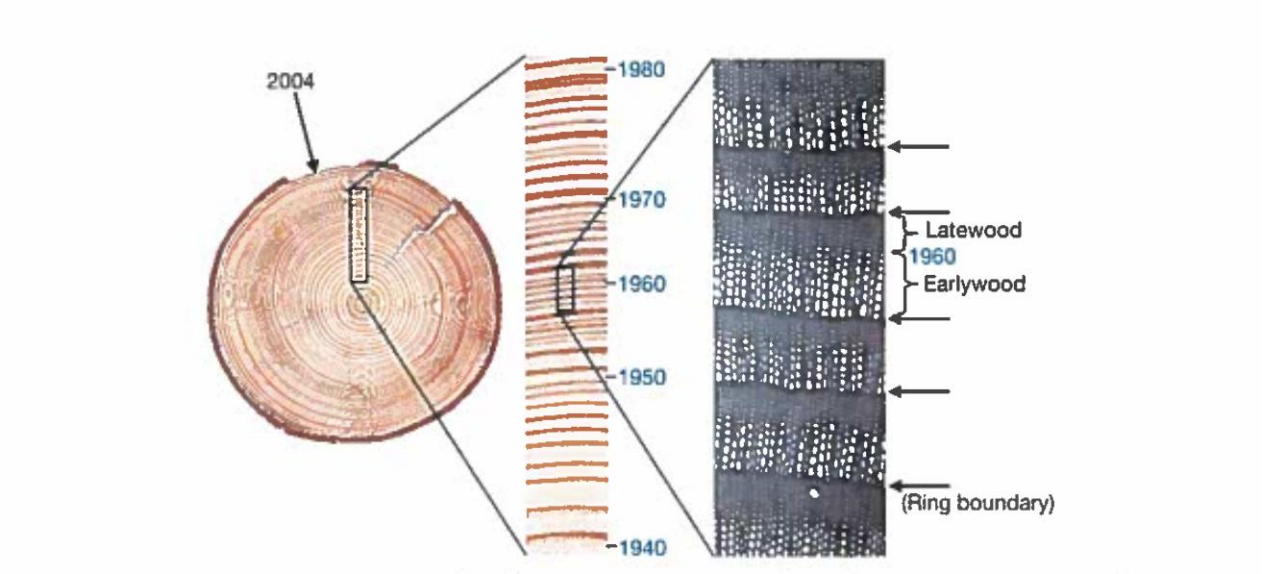

Figure 13 Tree-ring pattern of earlywood and latewood in a cross section. The alternation of darker shaded latewood and lighter early wood is used to count annual ring in wood samples. A ring is determined to be what lies between two latewood boundaries. (Gärtner and Heinrich, 2013).

Tree growth is influenced by a combination of climatic and environmental conditions at the growing site and water and nutrient availability. As for climatic conditions, drought events are one of the factors that influence tree growth the most. At low-to-moderate drought intensity and duration, tree growth is initially stimulated, at least for tree species that thrive at warmer temperatures. On the other hand, at severe drought conditions, tree growth is usually hindered mainly due to the elevated temperatures and the lack of water (Gärtner, 1964; Saurer et al., 2020). Indirectly, also pest outbreaks and diseases are commonly connected with the availability of nutrients and water and their presence can hinder tree growth substantially (Fritts, 1976). Moreover, tree growth is also influenced by geophysical and geomorphological characteristics of the growing site. For example, factors such as topography, substrate composition and texture, elevation, and sunlight exposure due to shading from either other plant competitors or obstacles (e.g., mountains, buildings, etc.) can negatively affect trees at any steps of their growth (Carrer et al., 2007).

3.2 Wood anatomy

Wood anatomy is the study of the structure and composition of the hard fibrous substance that makes up the parts of trees beneath the bark. Wood is composed mostly of hollow cells arranged in parallel fashion to each other along the whole extension of the tree (Gärtner et al., 2014; Miller 2018; Von Arx et al., 2016). Figure 14 shows a schematic representation of the principal components of a wood cell. The thicker outer layer is called the cell wall and it is primarily made of cellulose. The region responsible for the transport of water and nutrients is the cell lumen, which is the hollow potion contained within the cell walls ("LA" in Figure 14). This region is crucial in assessing the hydraulic capability of the cell, meaning that the total hydraulic conductivity of a tree is directly proportional to its cells' lumen area (Carteni et al., 2018; Koch et al, 2004). These vessels, relevant for the transport of water, nutrient, and hormones are usually localized within an annual ring. This means that, it is possible to identify those anatomical characteristics in every year ring along a core or cross-section sample, which in turn allows to identify interannual trends and patterns (Ryan and Yoder, 1997; Von Arx et al., 2016).

The characteristics of these fibrous cells and their arrangement affect strength properties, appearance and resistance from water, chemicals, decay, and many other properties. Thus, wood anatomy is an important field of study for natural scientists, botanists, forest engineers, and manufacturers of lumber or other wood products (Miller 2018). Again, the main characteristics of wood anatomical features such as cell size, cell perimeter, and cell wall thickness gather very relevant information about physiological characteristics of the tree itself, as well as environmental patterns that the tree is affected with (Bass and Wheeler, 2011; Gärtner et al., 2014; Von Arx and Carrer, 2013). A single tree experiences a multitude of different climatic conditions during its

lifetime, which is then imprinted on the wood: both at an annual ring level and at the cellular level. Because vessel properties are closely related to water and nutrient transport, wood anatomical data, might provide an even better insight in climatic characteristic rather than ring width data (Zimmermann et al., 2021).

The main perk of wood anatomy is the possibility to analyze in detail the cellular characteristics and build long chronologies of the whole extension of a tree; either via reducing a cross-section to smaller pieces and later rebuilding the original structure (usually via digital imagery), or by means of increment cores (Gärtner et al., 2014). It is important to note here that the thickness of the microsection is crucial to the truthfulness of the retrieved data. Indeed, the optimum lies around 10 – 20 µm (depending on the plant species and the hardness of the wood); too thicker sections lead to over- and underestimation of anatomical features, de facto causing imprecise measurements, which lead to heavy uncertainties in the final results. Moreover, the orientation of the cut is very important to obtain valuable data. If the microsections are not cut perpendicularly to the xylem cells, that would also lead to over- or underestimation of the anatomical features. (Von Arx et al., 2016).

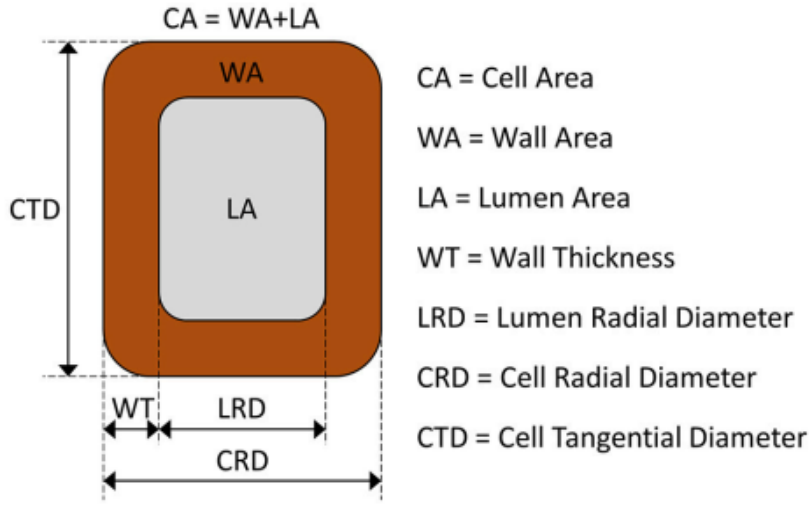

Figure 14 Schematic representation of a tree cell. The cell area, wall area, lumen area, cell wall thickness, lumen diameter, cell diameter and cell tangential diameter are represented (Carteni et al., 2018).

3.3 Stable carbon isotopes

Stable isotope ratios (principally $d^{13}C$, $d^{18}O$, $d^{15}N$, D/H) in terrestrial plants are known for many decades to vary among different species and also among trees growing in different environments. For this reason, they are employed across a diverse range of environmental applications in plant science (Cernusak et al., 2013; Cherubini et al., 2004; Woodley et al., 2012). For example, they can be used to reconstruct paleoclimate using fossilized plant remains, or also they can used to analyze hydraulic properties in plants, mainly related to height trends across the plant structure (Cernusak et al., 2013; Ryan and Yoder, 1997). Carbon isotopes are used in plant physiology to determine photosynthetic activity, since they are directly correlated with water availability in the leaves. They can be used as integrative indicators of tree vitality over time, since the $^{12}C/^{13}C$ isotopic ratio is indicative of hydraulic relationships inside the tree. This can be applied at different tree regions to build photosynthetic and hydraulic height trends along individual plants (Cherubini et al., 2021; Ryan and Yoder, 1997). $d^{13}C$ is defined as balance between the leaf's demand for carbon dioxide with the diffuse supply of CO_2 through the leaves. More precisely, $d^{13}C$ is associated with the ratio of the partial pressure of CO_2 within the leaves to the partial pressure of CO_2 outside the leaves, the so-called P_{int}/P_{amb} ratio (Hultine and Marshall, 2000).

There are many categories of study where $d^{13}C$ measurements have been utilized. Usually, they are employed to determine temporal changes in various environmental parameters. The main way of doing this is to analyze carbon isotopic composition in dated tree-ring series, in order to find trends with a precise temporal resolution (Gessler et al., 2014; Leavitt, 1993). Photosynthesis is obviously carbon dependent since it utilized carbon dioxide and combining it with water to produce glucose and oxygen. For this reason, it can be said that

photosynthesis rate changes for different CO_2 concentrations; this is based on the assumption that until CO_2 is available, photosynthesis will happen, and when the carbon dioxide stock starts to deplete, the rate of photosynthesis will slow down (Bryant and Frigaard, 2006). When water availability in the leaves is ensured, plants discriminate against the heavier carbon isotope ^{13}C for photosynthetic activity, favoring the atomically lighter isotope ^{12}C. On the other hand, when in a situation of diminished water availability (i.e., water stress), the stomata of the leaves will be either closed or semi-closed to keep as much moisture as possible inside. For this reason, gas exchanges cannot occur properly, therefore the plant is not able to discriminate against ^{13}C anymore and it will be used in the same manner ^{12}C is utilized. This physiological adaptation is shown in the resulting sugars from that photosynthesis reaction and can be measured through the woods' $^{12}C/^{13}C$ ratio, which will show less-negative values in water stress conditions compared to normal water availability conditions. Generally, water stress is more prominent at higher tree regions, therefore it is expected that at those regions the $^{12}C/^{13}C$ ratio should be less negative than at lower portions of the same tree (Cherubini et al., 2021; Koch et al., 2004; Marshall and Monserud, 1996; Ryan and Yoder, 1997). However, water availability is not the only factor influencing stomatal conductance; water demand is also one. This means that other variable such as air humidity, vapor pressure deficit, and potential evapotranspiration also affect ^{13}C discrimination. Furthermore, other stress factors, rather than only water availability, can influence stomatal conductance leading to increased photosynthetic rates, which in turn will decrease ^{13}C discrimination dependent on the CO_2 availability inside the leaves. The increased photosynthesis leads then to an overall decrease in the difference between the carbon in the air inside the leaves and the one outside (C_i/C_a), causing plants again to discriminate less against ^{13}C. These stress factors are mainly abrupt changes in temperature, light, CO_2 concentration in the air and nutrient availability in the soil (Cherubini et al., 2021; Leavitt, 1993)

3.4 Maximum tree height and tree hydraulics

3.4.1 Defining maximum tree height

Height growth of trees is one of their most characteristic features. It is generally accepted that tree height is dependent not only on age, but also on tree species, tree diameter, and the quality of the growing site (Petras et al., 2014). Trees grow tall where resources are abundant, water is constantly available, stresses are minor, and competition for light with other trees is minimal. There is no absolute maximum height that a plant can reach; it mainly depends on the previously mentioned conditions, as well as its own species. Some models predict height up to 120 m in the absence of mechanical damage as threshold for maximum height, but there are historical records of taller trees (Koch et al., 2004). In the past, it was noticed that the maximum height a tree can reach is directly correlated with the speed at which it grew vertically when young (Ryan and Yoder, 1997).

There are different hypotheses for which factor influences maximal tree growth the most. One of these is the senescence hypothesis which bases its explanation for the reduced growth in older trees in genetics. The latter, states that some genetic processes, which are found to regulate the tree's growth period, are active during the passing from juvenility to sexual maturity but are absent during the later stages of its life; mainly, they disappear in late adulthood (Mencuccini et al., 2005). A second set of hypotheses for maximum growth is based on physiological or environmental burdens on the plant. These theories are largely based on the premise that energy is allocated differently in relation with mass. This means, that in larger and taller trees there is less energy available for growth due to all other physiological process that occur at the same time. This result in reduced or even absent growth in those kinds of trees (Mencuccini et al., 2005; Ryan and Yoder, 1997). Another set of hypotheses concern nutrient availability. As Ryan and Yoder (1997) describe, in large trees, nutrients become sequestered in living biomass, and as the forest age, more nutrients end up in woody debris and decaying wood. The subsequent decline in nutrient availability may ultimately reduce tree growth either by allocation of photosynthetic product to roots instead of higher parts of the tree, or by the fact that foliage of older trees, might have reduced photosynthetic capacity. This hypothesis is named the nutrient limitation hypothesis. Even if the latter may sometimes be valid for slower growth in older tree, it is unlikely to be generally applicable to all kinds of tree species. Nutrient availability in the soil cannot be used as a discriminative variable to determine correctly growth rate in plants, since it is possible that the presence of

nutrients in soils of older forests can be as much as or greater than in that of younger forests (Entry and Emmingham, 2011; Ryan and Yoder 1997).

Currently the main hypothesis of height limitation in plants concerns increasing water transport constraints in taller tree resulting in reduced photosynthetic activity. According to the adhesion-cohesion theory, water transport in plants occur along a gradient of negative pressure inside the xylem, with transpiration, water adhesion to cell walls, and surface tension as the driving forces. Hydraulic resistance increases as trees grow taller because water must travel a longer path inside the tree. Moreover, to move the same amount of water through a path with higher resistance require higher tension. This usually continues to be the case until a certain height threshold is reached, where the plants start having difficulties transporting water against the increasing tension. However, at higher tensions it is more likely for air bubbles to form in the xylem water column, in a process called cavitation. Cavitation and subsequent xylem embolism are the consequence of diminished water, which in turn decreases drastically hydraulic conductivity, which can lead to the death of either regions of or the whole tree itself (Hunt and Manzoni, 2015; Koch et al., 2004; Ryan and Yoder, 1997; Sperry et al., 1994; Tyree and Sperry, 1988). Moreover, it was found out that fast growing species have consequently larger and more efficient xylem conduits, which are however more vulnerable to cavitation compared to smaller, less efficient conduits belonging to slower growing trees (Tyree, 2003). To prevent cavitation as well as temporary loss of hydraulic conductivity, leaf stomata in taller trees close earlier during the day or during a drought event. The result is the lowering of stomatal conductance and photosynthesis, leading to reduced carbon availability for wood growth. This main hypothesis for maximum tree height is called the hydraulic limitation hypothesis. The hydraulic limitation hypothesis can explain why height growth rates and maximum height can vary with nutrient availability. On a resource-poor environments, trees will most likely have low rates of photosynthesis and stomatal conductance, therefore having also slower wood growth. This means that in nutrient-poor growing sites, hydraulic resistance for a tree at a given height will be greater than for another tree growing in a resource-rich environment at the same height. Further, decreasing water availability usually causes the formation of smaller xylem conduits, which in turn can lead also to beneficial effects such as an increased resistance against drought-induced hydraulic failure. Furthermore, the hydraulic limitation hypothesis can also explain why different tree species might achieve different maximum heights even if they grow in the same environment. Generally, species that can endure very low xylem tensions or have limited hydraulic restrictions in their architecture are more likely to reach greater maximum heights. On the other hand, individuals that have been exposed to mechanical stresses, and therefore produce reaction or compression wood with inherent low permeability, are more likely to reach smaller maximum heights (Petrik et al., 2022; Ryan and Yoder, 1997; Schulze et al., 1994; Zimmermann et al., 2021).

3.4.2 Plant hydraulic properties

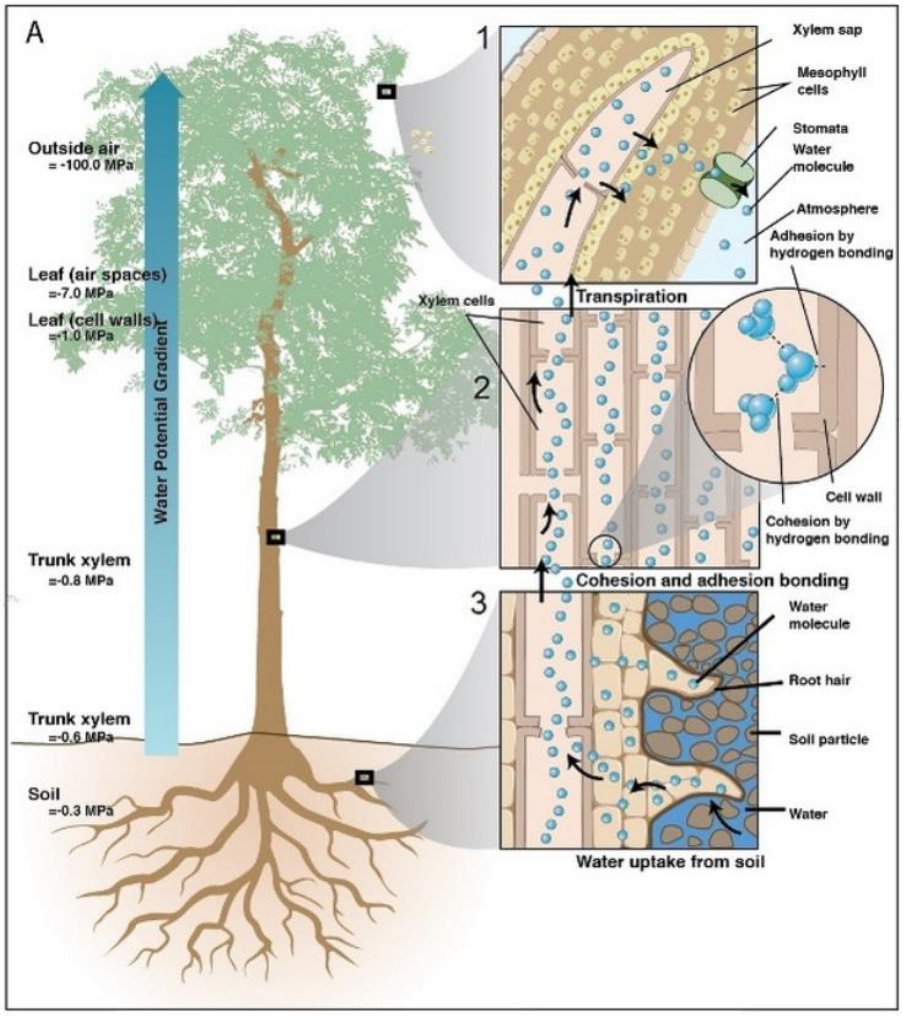

Figure 15 schematic representation of the water transport process form roots to the crown of the tree. Each numbered images show in detail an individual step belonging to the whole transport process. The main forces driving water transport against gravity are the cohesion-adhesion bonding and transpiration. The first happen throughout the entirety of tree from the root to the leaves, while the latter is strictly confined to the leaves (McElrone et al., 2013).

Trees transport water to from the roots to the leaves through a long pathway of xylem conduits, utilizing the cohesion-tension properties of water to raise it against gravity driven by transpiration of water from the stomata of the leaves (Figure 15). As the trees grow taller, the gravitational pull on the water column increases, resulting in increased difficulties of transporting the water to the leaves at higher tree regions (Anfodillo et al., 2005; Prendin et al, 2018; Tyree, 2003). The pattern of water transport is dependent on the architecture and spatial distribution of the trees' xylem (Kotowska et al., 2015). Furthermore, crucial role for tree performance is played by the water transport system. If water availability is not compromised and the environmental conditions of the growing regions are stable, a highly conductive xylem favors high photosynthetic rates. On the other hand, however, during periods of drought, the hydraulic system of the tree needs to be less conductive to better resist against hydraulic failure, in order to maintain acceptable photosynthetic rates. This means that the quality and durability of the xylem conduits are essential for a tree, since they allow the latter to achieve good enough photosynthetic rates without taking into consideration environmental conditions (Tyree, 2003; Zimmermann et al., 2021). There are also other factors that influence greatly the hydraulic properties in plants, which are not strictly related to the wood anatomical structure of the plant itself. For example, soil texture and composition play a decisive role in determining water movement in the unsaturated zone of the topsoil. Also, the ratio between leaf area and absorption area at the crown region of the tree is very important in ensuring proper water transport throughout the entire structure (Trillo and Fernández, 2005).

3.4.3 Hagen-Poiseuille law

In determining theoretical hydraulic conductivity through the xylem of plants, the Hagen-Poiseuille equation for laminar flow through conduits is often used. The Hagen-Poiseuille equation (1) provides the exact solution for laminar flow in ideal capillaries with circular transverse sections, while the application of this equation to conduits with non-circular transverse section needs a correction factor.

$$J_v = -\frac{\pi D^4}{128\mu} * \frac{\Delta p}{\Delta x}; \quad (1)$$

Where J_v indicates the hydraulic conductivity, D indicates the diameter of a circular conduit, μ is the viscosity of water, and $\Delta p/\Delta x$ is the pressure gradient. The minus sign shows the direction of flow, which it moves in the direction of decreasing pressure. As the Hagen-Poiseuille law indicates (1), even a small increase in mean vessel diameter can cause an exponential increase in hydraulic conductivity. (Kotowska et al., 2015; Lewis and Boose, 1995).

Since the hydraulic conductivity is proportional to the fourth power of the conduit's lumen diameter, if said conduit diameter decreases (e.g., at higher regions of the tree), the pressure difference forms the roots to the leaves that is required to maintain an adequate water flow has to increase. This results then in a limitation in conduit dimeter in order to maintain flow. Below said limit, water transport is not possible anymore, which practically stops vertical growth at that threshold. So, this can be used as further evidence that wood anatomical hydraulic properties might limit maximum tree height (Tyree, 2003).

3.4.4 WBE model

West et al., (1999) proposed a model for the hydrodynamics, biomechanics and branching geometry of vascular plants (Figure 16) The so called WBE model (from the last names of their three creators West, Brown and Enquist) achieved many breakthrough findings about plant hydraulics correlated with tree heights. The most important of them is that conductive conduits in vascular plant were shown to taper with height independently from their total length as well as the plant size. This is theoretically applicable to any kinds of plants that possesses a vascular system for the transport of water and nutrients. Mainly the model quantitatively predicts how vessels must taper to compensate for variation in the vessel system, which in turn quantify the theoretical maximal height in plants. This should theoretically resolve the problem of resistance increasing with increasing height, therefore allowing plants to reach maximum heights of more than 100 meters.

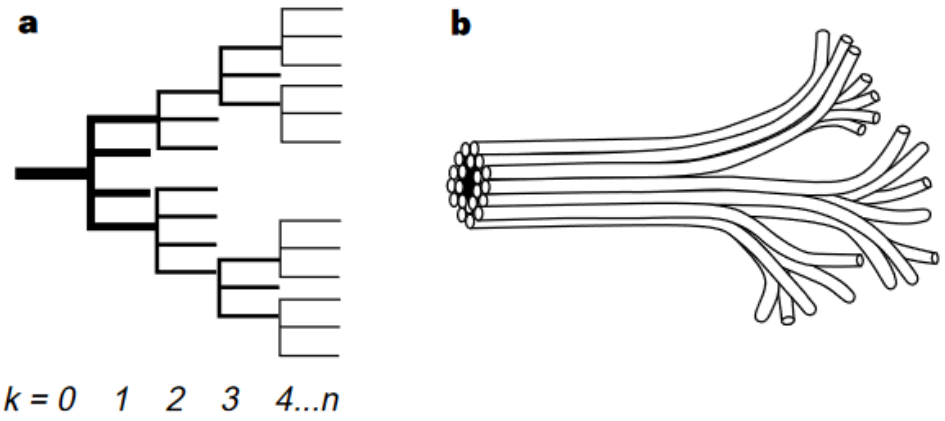

Figure 16 Trees' branching structure proposed by the WBE model. Figure 9a indictes the topology of a plant branching network, where it is shown that the conduit tapers more, the more they branch out. Figure 9b is a schematic representation of the branching network in Figure 9a (West et al., 1999).

However, Anfodillo and Petit, (2009) discuss the validity of the WBE model stating that the ideal plant described by West and colleagues is too simplistic to depict all of nature's scenarios. Mostly, they argue that the geometry and morphology of the water conduits proposed from West and colleagues differ from those of real plants, and also some assumptions made to achieve this universal model can be disproved by evidence

form plant anatomy and physiology. Mainly, it is hard to find plants that universally have the same branch length and geometry as those proposed by the WBE model, as well as the fact that tapering rate sometimes do not correspond to the real case scenarios in all of the plants (Anfodillo et al., 2005; Anfodillo and Petit, 2009).

Moreover, it can be said that the WBE model is not completely reliable because it deals only with actively growing plants put in a hypothetical situation where there is no limitation in increasing the dimension of xylem conduits at the stem base. In reality, this situation is achieved only during the juvenile stage where the height increase rate is extremely high compared to later stages during the plant life cycle. Also, after the juvenile stage, most trees' vascular system becomes suboptimal for the efficient transport of water. Therefore, in these cases, the WBE model cannot be applied anymore, since it would mean that the plant hydraulic conductivity decreases non-linearly with height, which is a crucial assumption for its validity (Anfodillo et al., 2005).

4 Materials and methods

4.1 Sampling strategy

The samples for this project (Table 1) consist of six trees; of those six trees, 5 different heights along each tree will be analyzed, for a total of 30 samples (15 for European beech and 15 for Norway spruce). The number of samples was chosen arbitrarily with the aim of finding a compromise between workload and reliability in the results. In the end, it was decided that a total of 30 samples was the correct amount to satisfy both criteria. Each tree was sampled in 2019, after being taken down during a heavy storm, therefore the outermost year correspond to that of 2019. This information is crucial when conducting the analyses, mainly for the tree-ring width measurements.

Each sample was given an identification code according to its tree of belonging and the height that corresponds to that sample. The chosen heights differ from tree to tree since they were chosen according to regions of the stem along the tree instead of using fixed heights. The tree regions of choice for this project are the base samples (*Bas*), the base of the crown (*BoC*), the top of the tree (*Top*) and the two regions between the *Bas* sample and the *BoC* sample and between *BoC* and *Top* respectively (*Int1* and *Int2*). The *BoC* sample is identified as the closest 2-meter-interval to the first branch along the tree trunk. Each tree has different heights associated with the 5 tree regions; the only fixed height are the *Bas* samples that are always labelled with 0 meters. The top sample does not necessarily correspond to the highest point along the tree trunk, but it is the highest available sample for that specific tree within the pool of cross-sections made available by the SCC II.

A consideration has to be made here. Each labelled sample might not perfectly represent its corresponding height, since each cross-section was different in thickness with each other; some are considerably thinner than other samples. This translates to small imprecisions if one wants to consider exact height for each tree regions, since the labels on each sample (e.g., F1_0m, F2_10m, P1_24m, etc.) do not correspond exactly to the real height along the tree trunk. However, the difference is in the order of tens of centimeters, which should not create too large uncertainties in the results. Therefore, the exact height will not be taken into consideration while conducting the analyses, instead only the corresponding tree regions will be used.

Table 1 Sampling strategy for the master thesis. The dataset consists in three spruce trees and three beech trees, each sampled at five different heights. The height intervals from bottom to top are as follows: Base (*Bas*), intermediate region between base and the top of the crown (*Int1*), base of the crown (*BoC*), intermediate region between base of the crown and top of the tree (*Int2*), top of the tree (*Top*).

Height (m)	0	2	4	6	8	10	12	14	16	18	20	22	24	26	28	30	32
Beech tree name																	
F1	**X**						**X**					**X**		**X**		**X**	
F2	**X**					**X**				**X**			**X**			**X**	
F3	**X**				**X**	**X**							**X**	**X**			
Spruce tree name																	
P1	**X**				**X**				**X**				**X**				**X**
P2	**X**					**X**				**X**			**X**			**X**	
P3	**X**				**X**				**X**				**X**				**X**

4.2 Tree-ring width measurements

4.2.1 Sample preparation

After the sample were collected from the Basel study site, they were all labelled according to their height and their respective tree. The entirety, of the stem for each tree was sampled, and thus all 2-meter-height intervals were labelled accordingly. Each sample was then searched for integrity along the cross-section to see whether it could then be used to conduct all needed analyses. After the samples were identified as in well enough conditions, they were then ready for the second step of sample preparation.

The second step of sample preparation consisted in sanding each cross-section (Figure 17) The sanding process has the objective to help in other analyses such as ring-width measurement and wood anatomy. The sanding was done using different sanding paper, each of them with different grain size; used in ascending order (i.e., from coarser to finer grain). To achieve a smooth enough surface, but at the same time to avoid burning the cross-section only 5 sanding paper sized were utilized (Figure 18). The process started with sandpaper with grain size 120 µm, then 180 µm, 240 µm, 360 µm, and finally 400 µm. The treatment with the 360 µm and 400 µm sanding paper was done rather lightly and quickly, since the risk of burning the surface increases considerably at finer grain sizes.

Figure 17 Sanding machine at WSL (Höfer, Graf Machinen & Service GmbH). The machine allows to sand both wood cores and cross sections, thanks to its dual function. The upper part of the machine allows the user to sand smaller sections or cores, while the bottom part is equipped with a press which is used to sand larger cross-sections while resting them onto an installed moving table (Mattias Barigazzi).

Figure 18 Sample F1_22m after being sanded. The sanding process was achieved by repeatedly scratching the surface of the sample, using different sized sanding paper each time. The result is a cross section with very smooth surface, where each annual ring is clearly visible by the naked eye. In some cases, there are a few burn marks on the surface caused by prolonged contact with the sanding paper and the wood; those are not problematic for the type of analysis that will be conducted (Mattias Barigazzi).

During the sanding process, some spruce samples got lightly burned, mostly at the edges. This could mean an inappropriate use of the sanding machine, or also that the cross-sections were too large, which in turn lead to a prolongated exposure of the sanding paper to the surface of the sample. However, this is not a problem, since for the tree-ring width measurements the burnt parts do not cause any concerns; it can even be easier to identify ring boundaries if burnt. For the isotope analysis, however, it is important that all burnt parts are removed from the wood that is going to be analyzed. For the beech cross-sections, they do not burn as easily, but they are also harder to sand properly, needing more time with each different sanding paper to achieve an acceptably smooth surface.

4.2.2 Laboratory analysis and procedure

The measurements were done with the aid of a binocular equipped with a rotating measuring table (LINTAB measuring table by Rinntech, Heidelberg, Germany), which allows the user to move the samples easily across the binocular's vision (Figure 9). The apparatus is then connected with the software TSAP (Time Series Analysis and Presentation, Rinntech, Heidelberg, Germany). This software allows the user to measure the ring width of both cross-sections and core samples. Moreover, it is also possible to build, save and retrieve multiple chronologies based on the measured samples or even based on preexisting data. The software also allows the user to modify directly the tree-ring curves to add or delete tree rings that were wrongly measured with the binocular (Rossi et al., 2013)

Each cross-section was measured two times, following two different radii along the same surface. This was done to minimize uncertainty, since in this way there are less possibility to have measured a region with tree rings that might cause problems when building the ring width curves. (e.g., reaction wood, burn scars, signs of infection, etc). Afterwards, from the measured curves, an average curve for each sample was built. When every average curve was built, each one was then cross dated with each other curve belonging to the same tree to find potential errors of measurement. Since the average curves belonged to the same tree, it was possible to cross-date with them without worrying about using a pre-existing reference chronology. Afterwards, the lines were then adjusted accordingly adding or removing rings that were measured incorrectly, so that, in the end, there were only curves with the same trend that belongs to each individual tree.

Then in a second stage, each resulting curve was tested for reliability, based on the Gleichläufigskeit (GLK) value. An arbitrary threshold of 75% GLK was chosen to identify a reliable enough tree-ring curve; as well as a statistical significance of $P < 0.01$. To do so, curves of the same tree were tested for GLK within each other, as well as different trees from the same species. In a final stage, average curves for each species beech and spruce were build, as well as final curves for each height sections.

4.3 Wood anatomy measurements

4.3.1 Method background

The cutting of microsections is usually achieved through the use of a specific tool called microtome (Figure 19). There are different models of microtomes with different functionalities and characteristics. The most common ones are the rotatory microtome (mainly used in medicine for biopsies), the sledge microtome, and the core microtome (used mainly to cut tree cores; developed at the WSL lab) (Gärtner et al., 2014; McMillan and Harris, 2018). Using the sledge microtome allows the user to quickly cut the necessary amount of wood material for analysis. Commonly, this consists in microsections of about 10 – 20 µm in thickness, which are to be cut perpendicularly to the annual rings, in order to achieve a smooth surface and to keep all cellular structures intact (Von Arx et al., 2016). The advantage of using this kind of microtome is indeed to have minimal time consumption, in contrary to using the rotatory microtome, which needs the samples to be first submerged in paraffin before cutting. The main drawback of the sledge microtome is that it can be sometimes a bit rough when creating the microsections. Indeed, if the samples are brittle, it can be considerably hard to cut with it without breaking apart the slices (Gärtner et al., 2014; McMillan and Harris, 2018; Von Arx et al., 2016).

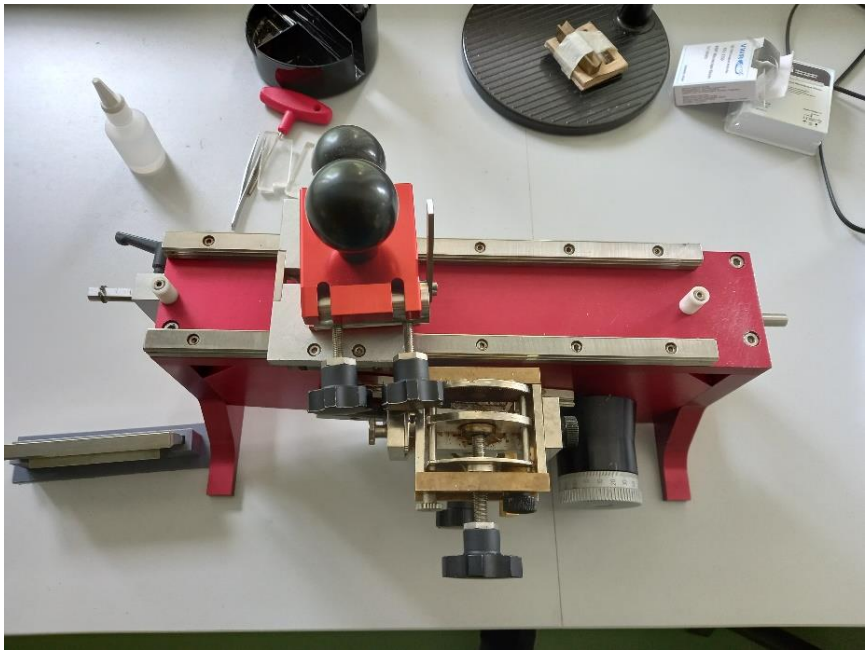

Figure 19 Lab microtome used for cutting microsections for this thesis. The lab microtome is designed to cut microsections of all kinds of woody samples. The knife holder as well as the sample holder are adjustable in all directions. Semi-automated uplift of the sample allows constant thickness of the micro-slices as well as a quicker and more efficient cutting process (Mattias Barigazzi).

The next fundamental procedure to obtain reliable wood anatomy data is to stain the previously created microsections with the appropriate staining agent and to create permanent microscope slides. This allows the different cellular structure to be more distinguishable and be identified more easily. Common staining agents for wood microtomy are astrablue[1], safranin[2], and toluidine blue[3] (Von Arx et al., 2016). Later, those stained microscope slides will be digitized via scanner to then be analyzed with the appropriate software. For this purpose, at WSL there are two available software for analyzing cellular structures in wood microsections: ROXAS and WinCell. These two programs allow the user to measure precisely the main features of wood internal structure, for examples lumen area, lumen wall length, and lumen perimeter (Von Arx and Carrer, 2014).

4.3.2 Sample preparation

After having measured the tree-ring width, the next step is to prepare all of the cross-sections for the wood anatomy measurements. In order to be as time efficient as possible, only the three outermost rings will be analyzed (i.e., 2017, 2018, and 2019) for all the height sample of all six trees. In order to cut the micro-slices, it is necessary that the samples are reduced in size. Every cross-section has to be cut down to a small cube of about 2 – 3 cm size, so that it can fit properly in the microtome holder. To achieve this, each cross section was cut with a linear wood saw (D7300, Kölle Machinenbau GmbH from 1991) in the WSL carpentry into long wood strips of about 3 cm width. Afterwards, each wood strip was cut down into small pieces using a knife and a hammer. It is important to note here that when cutting with the knife it is crucial that each segment is cut diagonally in respect to the year rings. Otherwise, it would be nearly impossible to reconstruct the original wood strip when reconnecting the individual small segments. In a second step all wood pieces were cut down again to be of about 1 – 2 cm width since it facilitates considerably the microtome slicing.

4.3.3 Laboratory analysis and procedure

The first step in achieving wood anatomy results is to obtain the microsections with the microtome (Lab microtome at WSL, Figure 19) In order to do that, the previously reshaped wood pieces have to stay submerged in water at least 6 hours for spruce wood and 12 hours for beech wood. When the samples were soaked enough, they were then cut with the high-profile blade, which, in contrast to the low-profile one, grants a smoother cut and damages less the cells when performing the cut (Figure 20). The cut wood slices were then transferred onto temporary microscope slides with a few drops of glicerin to avoid drying and shriveling the samples. The microsections were obtained only for the outermost wood piece for each height sample, since the goal is to analyze the wood anatomical structure of the years 2017, 2018, and 2019.

[1] Astra Blue: Empirical formula: $C_{47}H_{52}CuN_{14}O_6S_3$, CAS-Number: 82864-57-1, molecular weight: 1068.75 g/mol, MDL-Number: MFCD00070974 (Sigma Aldrich, 2022a)

[2] Safranin O: Empirical formula: $C_{20}H_{19}ClN_4$, CAS-Number: 477-73-6, molecular weight: 350.84 g/mol, MDL-Number: MFCD00011759, H318: Eye damage 1. (Sigma Aldrich, 2022b)

[3] Toluidine blue: Empirical formula: $C_{15}H_{16}ClN_3S$, CAS-Number: 92-31-9, molecular weight: 305.83 g/mol, MDL-Number: MFCD00011934. (Sigma Aldrich, 2022c)

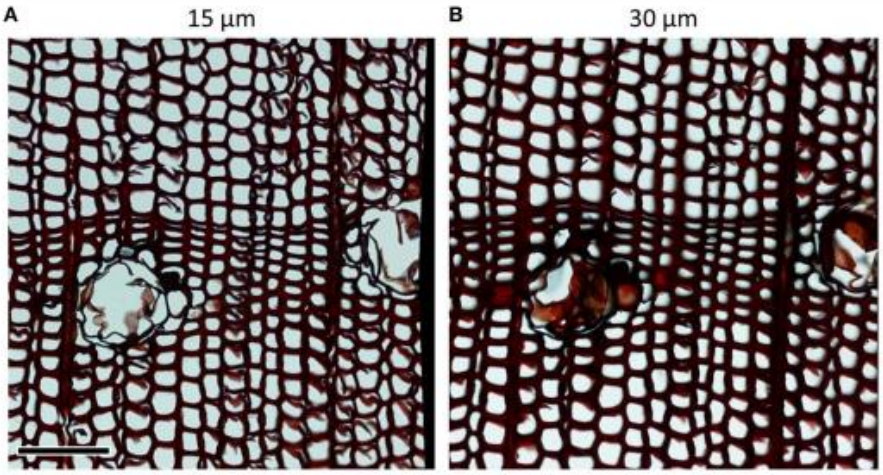

Figure 20 *Pinus heldreichii* (H.Christ) microsections at different thickness. A is at 15 µm thickness, B is at 30 µm thickness. The difference in the 2 microsection is evident. The thinner section (A) displays easier to identify cell lumens and tracheids than the thicker section (B). However, it is noticeable that in the thinner section (A) there are more broken cells on the upper-right part of the slice compared to B. This is caused by the use of dull blades: the effects of reduced sharpness in the blades are increased in thinner sections (Von Arx et al., 2016).

Later, after all samples were ready, they were stained using safranin as the staining agent. The staining process consists in submerging the microsection in few drops of safranin and then wash them multiple times using water and ethanol (EtOH) at different concentrations (C_2H_6O (75%), C_2H_6O (96%), C_2H_6O (100%), as well as xylol[4] (Figure 21). After this procedure is completed, the samples were coated with a small amount of Canada balsam and covered with a small glass panel to form the permanent microscope slides. Afterwards, the slides are places inside a drying oven (Binder oven from 2018) set to 60 °C overnight. When all of the permanent slides were dried, they were cleaned from the excess dried Canada balsam[5] with the help a small razor blade. The next step in the procedure is to digitize the slides (Figure 22); this is achieved by using a scanner and the appropriate computer tools (Zeiss, Axio Scan.Z1).

[4] O-Xylol: CAS-Number: 95-47-6, H-Sätze: H226, H304, H312, H315, H319, H335, H412 (GESTIS, 2019)
[5] Canada balsam, CAS-Number: 8007-47-4, MDL-Number: MFCD00123800, H-Sätze: H226 (Sigma Aldrich, 2022d)

Figure 21 Series of solutions used for the staining process of the thesis. From left to right the solutions are safranin (the staining agent), ethanol (75%), ethanol (96%), ethanol (100%), and xylol. The bigger beaker contains tap water to rinse the solutions off the samples. The left-most bottle of sodium hypochlorite was not used for this kind of staining process (Mattias Barigazzi).

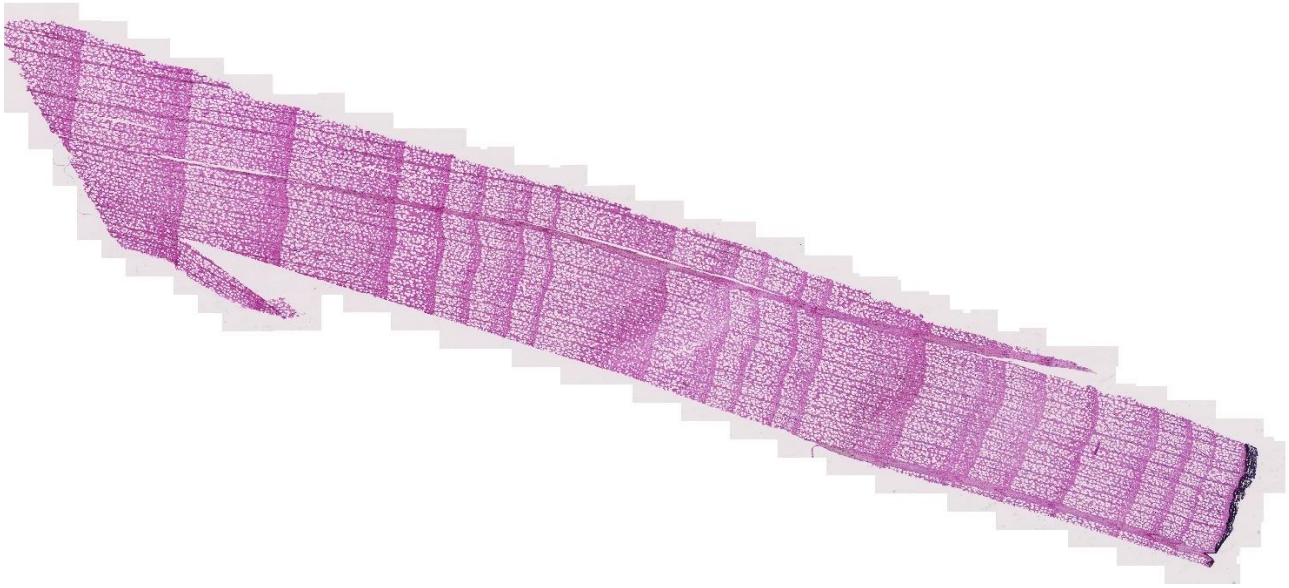

Figure 22 Digitized image of sample F1_0m using the Zeiss Axio Scan.Z1 scanner set at 25% image resolution. The Ring boundaries are clearly noticeable as well as the difference between the regions of latewood and earlywood (Mattias Barigazzi)

Since the microsections in each microscope slide are quite big, the scanning process will last for a considerably long time. To avoid that, it was chosen to reduce the resolution of the obtained images to 25% of the "high-resolution" setting. This allows a quicker scan time, and at the same time keeps the final images at good enough

quality. Lastly, the images are then transferred on a storing device to be analyzed using the WinCell software (Figure 23)

Figure 23 Sample F1_0m (41_0m old name shown in the image) analyzed using the WinCell software. The cells highlighted in yellow are the ones considered good enough to be measured. The gray colored cells are the ones that do not enter in the criteria to be considered good enough cells. There are either too small or broken. The red regions represent the area deemed to be too big to be considered cells. Usually, those areas correspond to either resin canals or big breaks in the sample (Mattias Barigazzi)

4.4 Carbon Isotope measurements

4.4.1 Sample preparation

After each cross-section was cut into wood strips to be used in the wood anatomy analyses, what was discarded was used to conduct isotopes measurements. From the big pieces of wood left behind while trimming the wood strips, all the outer most parts for each cross-section were collected. After that, the aim is to obtain very small cubes of around 0.5 – 1 cm side. This was achieved via a hand saw (when possible) or with a knife and hammer. Later, the cubes were cut at the top and at the bottom with the microtome. This allows to better identify the individual years while separating them, moreover, cutting the top and bottom surface ensures that there is no residual pollution coming from the sanding process done at the beginning. After all small cubes were ready, they were stored in appropriately labelled plastic bags and kept on a shelf in dry conditions.

4.4.2 Laboratory analysis and procedure

The first step in analyzing the carbon isotope content in the wood for each year is to split the different annual ring and store them in different containers. To achieve this the small 1 cm cubes were places under a binocular microscope, and, with the aid of a scalpel, the individual rings were split or shaved off form the cube. After the entire year was removed, the shavings were then placed into Eppendorf tubes and stored in an appropriate tube rack and were labelled accordingly. It is important to consider that not always it was possible to shave off the entire ring with maximal precision; this is caused mainly by the stiffness and plasticity of the wood. Notably, the spruce samples were easy to cut at the ring border with only a few exceptions. In the other hand, beech samples were very hard to cut and therefore, sometimes, the end portion of a few rings was not collected[6].

[6] Theoretically, this fact could lead to some uncertainties and unreliability during data analysis. However, according to the literature, the carbon rich part of each annual ring is found around their middle point, thus on the edges the carbon content should be smaller. Hopefully, for this reason, the results are reliable either way.

Afterwards, when all of the years were separated, they were then milled with a rotation mill (Retsch, ZM200). The powder was then collected back into the same Eppendorf tubes ready for the next step. It is important to note here that between the milling of one sample to the other, the machine has to be thoroughly cleaned to avoid cross-contamination. Later, from each sample, 1 mg ± 0.1 mg were weighted with a high precision balance (Mettler, MT5; 1 ± 0.001 mg) and inserted in tin capsules. Each capsule was then rolled up into a very small ball or cube and stored in an appropriate labelled container. The exact weight of each capsule was noted down, since it was obviously not possible to always weigh exactly 1.0 mg of material. Lastly, the rolled-up capsules were handed in to a specialized laboratory at WSL for the analysis.

4.5 Calculation of hydraulic conductivity

For this project, two different corrections of the Hagen-Poiseuille equation (see equation (1) in Chapter 3) were used. For the beech samples, it was utilized the correction for conduits with elliptical transverse sections (2), while for the spruce samples, the correction for conduits with rectangular transverse sections as the majority of the cells of beech and spruce trees are elliptical and rectangular shaped respectively.

(2) $$J_v = -\frac{\pi}{64\mu} * \frac{a^3 b^3}{a^2+b^2} * \frac{\Delta p}{\Delta x};$$

Where J_v indicates the hydraulic conductivity, μ is the viscosity of water, a and b indicate the short and long axes of an ellipsis, and $\Delta p/\Delta x$ is the pressure gradient. For the rectangular transverse shape correction, a different iteration of the Hagen-Poiseuille equation was utilized, namely the Pickard (1981) generalization (3).

(3) $$J_v = -k * \frac{\pi D_h^4}{128\mu} * \frac{\Delta p}{\Delta x};$$

Where k indicates the correction factor due to the shape of the transversal conduit, J_v indicates the hydraulic conductivity, D_h is the hydraulic diameter, μ is the viscosity of water, and $\Delta p/\Delta x$ is the pressure gradient.

However, in order to use this generalization, a few intermediate steps were needed to be calculated. Specifically, the hydraulic diameter D_h (4) and the correction factor k based on the ratio between each cell's long and short axis (Table 2).

(4) $$D_h = \frac{2ab}{a+b};$$

Where D_h is the hydraulic diameter, and a and b are the conduit's short and long sides respectively (Lewis and Boose, 1995; Nonweiler, 1975; Pickard 1981).

Table 2 Correction factors for estimating laminar volume flow rates in rectangular conduits; a is the short side and b is the long side of the conduit (Lewis and Boose 1995).

b/a	k
1.0	1.43
1.1	1.43
1.2	1.43
1.3	1.44
1.4	1.44
1.5	1.44
1.6	1.45
1.7	1.45
1.8	1.46
1.9	1.47
2	1.47
3	1.59
4	1.75
5	1.92
6	2.11
7	2.31
8	2.51
9	2.71
10	2.91
20	5.00
40	9.22
60	13.46
80	17.7
100	21.94

4.6 Outliers' removal for wood anatomy data

Since the microsections that I used for the wood anatomical analysis are considerably big in size, the amount of data is very big for each sample. For this reason, the variability of the values in the dataset is also high, therefore, in order to have reliable results, an algorithm to remove outliers from the dataset is needed (Figure 24).

To achieve this, the detection function from the "boxplot ( )" command in R was used. After the outliers in the dataset were identified, they were selected, and a second data frame was built without them. The "boxplot ( )" function identifies as an outlier every singular value point that lies outside the range of [25th percentile – 1.5*IQR[7] ; 75th + 1.5*IQR]. This process of detection and removal was then repeated for each variable that were to be analyzed. For this reason, the removal process could be slightly different depending on which variable is being plotted.

The outlier removal process resulted in the reduction of about 10% from the total amount of individual values of the original dataset.

[7] The Interquartile Range (IQR) indicates the region of the boxplot from the 25th percentile to the 75th percentile, which corresponds to the rectangle shaped box of a boxplot.

```r
df_list <- list(BT_F1, BT_F2, BT_F3, ST_P1, ST_P2, ST_P3)
treename_list <-c("F1", "F2", "F3", "P1", "P2", "P3")
treeregion_list <- c("Bas","Int1","BoC", "Int2", "Top")
year_list <- c("2017", "2018", "2019")
variab_list <- c("Jv", "lum_perimeter", "lum_area")

for (k in 1:length(df_list)){
  for (year in year_list){
    for (treeregion in treeregion_list){
      for (variab in variab_list){

        outliers_remover(df_list[[k]], treename_list[k], year, treeregion, variab, variab)

      }
    }
  }
}
```

Figure 24 R code depicting the outliers removal function used to reduce the amount of data for the wood anatomy analysis. The removal was applied to the hydraulic conductivity, hydraulic diameter, and lumen area datasets.

5 Results

This section will depict all the relevant results obtained by analyzing the European beech and Norway spruce samples. It will be divided in three main subsections: the results regarding the tree-ring width measurements, those regarding the wood anatomy analysis and those regarding the isotope measurements. It's important to note here that only the most relevant graphs are presented in this section; all other plots will be put in the *Appendix* section at the end of the document.

5.1 Tree-ring analysis

5.1.1 Ring-width curves

From all of the tree-ring measurements for each individual height sample an average ring-width curve was calculated (see *Appendix*). Afterwards they were plotted together species by species, resulting in two plots, one depicting the average ring-width curves of the European beech samples (Figure 25), and one showing the Norway spruces ones (Figure 26).

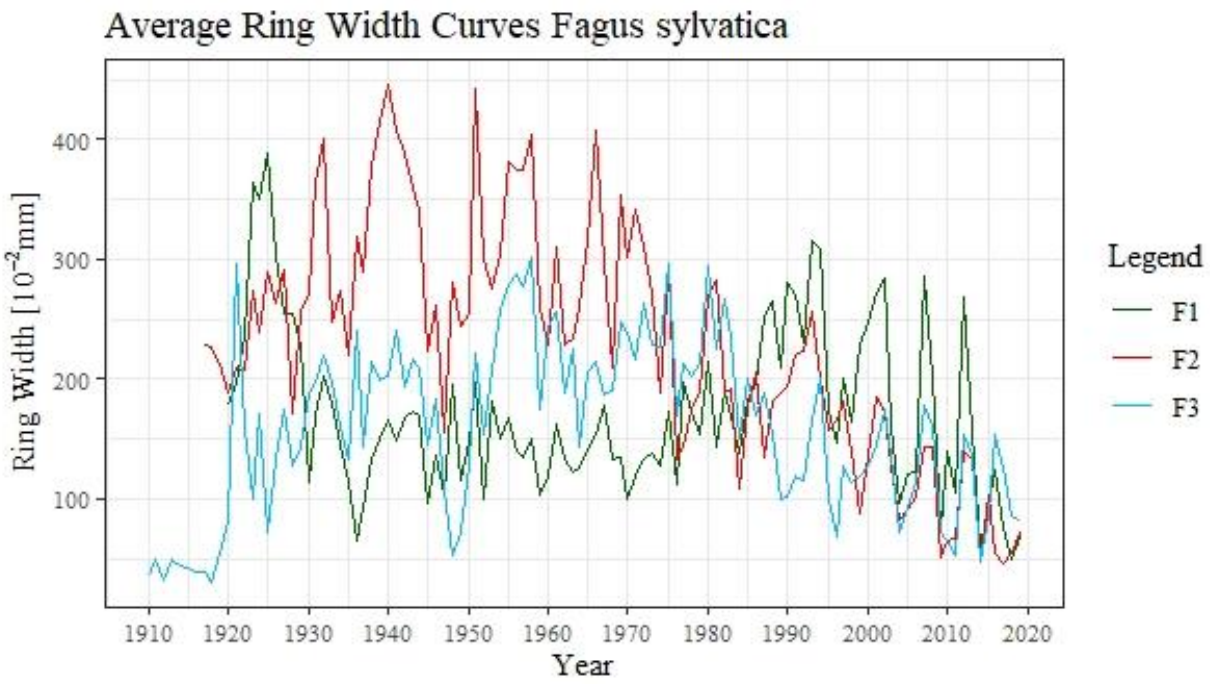

Figure 25 Average ring-width curves of *Fagus sylvatica* trees. The dark green line represents the average ring-width curve of F1, the red one the curve of F2, and the light blue one the curve of tree F3.

In Figure 25, it is noticeable how the three ring-width curves present a similar trend with each other. Even if sometimes the peaks have different magnitude from one curve to another, the high-to-low value trend is comparable for all three curves. F3 is shown to be the oldest beech tree, dating back to 1910, while the other two trees are younger of about 8 – 10 years. F2 shows the highest ring-width peaks of all three beech trees, with the highest values reaching up to 400 μm in 1940 and 1951. Between 1944 and 1951 all three beech trees show a considerable drop in ring-width values. F3 presents the lowest depression point, while F2 registered higher values compared to the other two beech trees.

In Figure 26, on the other hand, the three average curves for the spruce tree closely follow each other throughout the whole chronology; more than the beech trees did. The ages of the trees also seem to be similar; the only small difference is that P2 appears to be younger of about 5 years compared to the other two. The highest recorded ring-width values belongs to both P2 and P3, which is around 620 μm; other than that, all three spruce trees have similar trend everywhere. Also in this case, a considerable region of slowed-down growth was registered. Between 1942 and 1955 all three spruce trees show a substantial decrease in ring width, followed by a sudden increase in the years that closely follow.

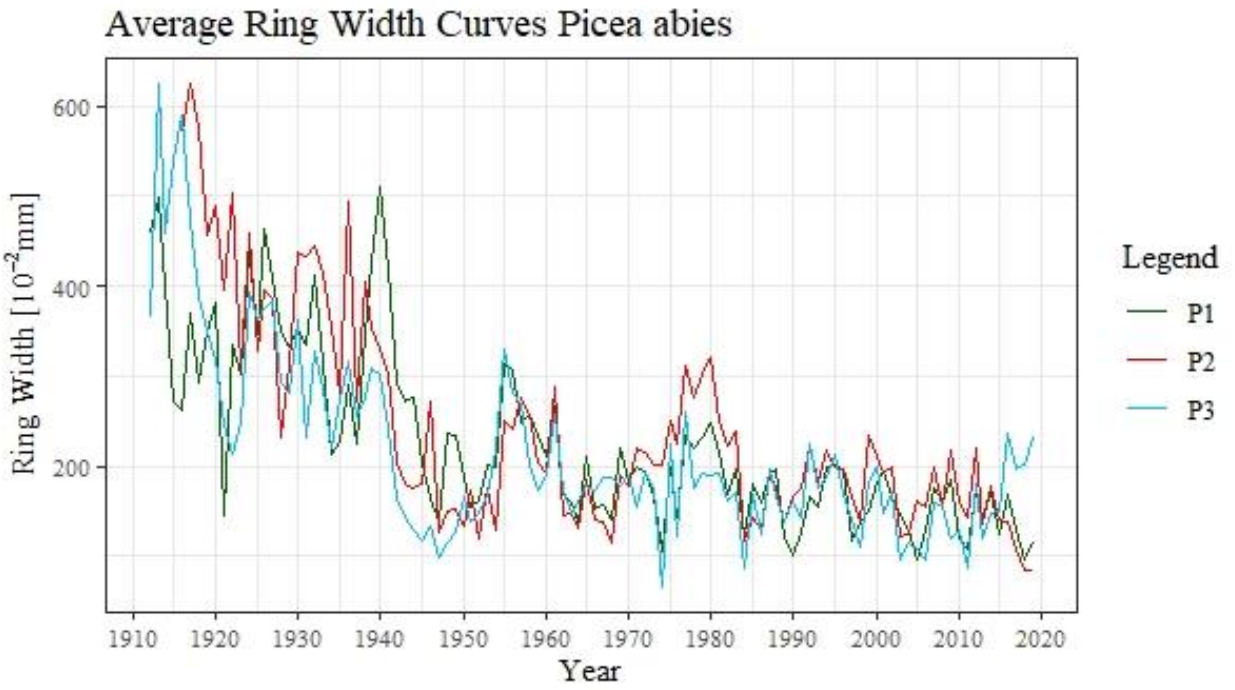

Figure 26 Average ring-width curves of *Picea abies* trees. The dark green line represents the average ring-width curve of P1, the red one the curve of P2, and the light blue one the curve of tree P3.

Next, from each species, an average curve was generated (Figure 27), resulting in two final tree-ring curves, one for the beech trees (made averaging the individual curves from F1, F2, and F3) and one for the spruce trees (made averaging the individual curves from P1, P2, and P3).

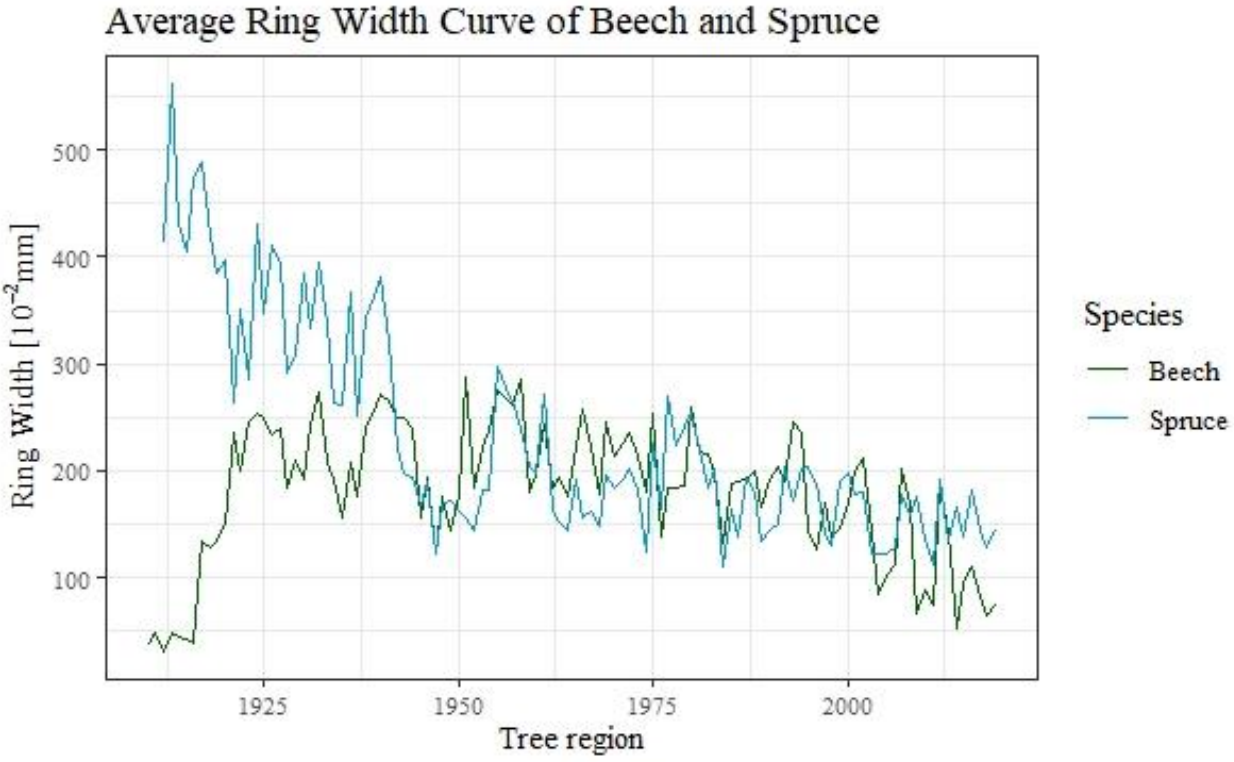

Figure 27 Average ring-width curve of *Fagus sylvatica* and *Picea abies*. The dark green line indicates the average ring-width curve of F1, F2, and F3, while the light blue line represents the average ring-width curve of P1, P2, and P3.

The average curves for the two species show interesting results. Initially the two curves differ from each other quite considerably, to then later follow the same trend in the more recent years. The biggest difference between the two ring-width curves is found in the early stages of the trees' lives. The European beech presents an increase in ring width in the first years, before stabilizing around the 150 – 250 μm-range from 1920 onwards. On the other hand, the Norway spruce shows a contrasting trend showing initially very high values of tree-ring width to then decrease and stabilize around the same 150 – 250 μm-range as the beech samples. However, the two curves reach the before-mentioned range at two different times. Indeed, the Norway spruce converges around 1950, about 30 or so years later compared to the European beech.

As mentioned in Figure 25 and Figure 26, approximately between 1945 and 1955 there is a period where both species were confronted with a substantial decrease in ring width. Interestingly, this phenomenon is also identified in the average curves for each species. Moreover, this period of diminished growth coincides with the moment when the two ring-width curves converge together and start following the same growth trend.

5.1.2 Gleichläufigskeit assessment

In order to generate the average curves from the previous section, each individual samples had to be verified to see whether it cross-dates significantly each other or not. In order to do that, each individual tree-ring curve form each height sample that belongs to the same tree, was compared to every height sample of that specific tree and the Gleichläufigskeit between each pair of ring-width curves was calculated (Table 3). A value of Gleichläufigskeit higher than 75 between two tree-ring curves means that they generally follow the same trend.

Table 3 Gleichläufigskeit (GLK) table of each tree samples. Each height for a single tree is compared within each other and the resulting Gleichläufigskeit is recorded. A value higher than 75 GLK means that the two samples cross date well between each other.

	P1_0m	**P1_8m**	**P1_16m**	**P1_24m**	**P1_32m**
P1_0m		68 (***)	80 (***)	78 (***)	82 (**)
P1_8m	68 (***)		80 (***)	69 (**)	73 (*)
P1_16m	80 (***)	80 (***)		79 (***)	64 ( )
P1_24m	78 (***)	69 (**)	79 (***)		77 (**)
P1_32m	82 (**)	73 (*)	64 ( )	77 (**)	
	P2_0m	**P2_10m**	**P2_18m**	**P2_24m**	**P2_30m**
P2_0m		65 (**)	79 (*)	63 (*)	71 (*)
P2_10m	65 (**)		69 (***)	71 (**)	76 (*)
P2_18m	79 (*)	69 (***)		67 (**)	76 (*)
P2_24m	63 (*)	71 (**)	67 (**)		53 ( )
P2_30m	71 (*)	76 (*)	76 (*)	53 ( )	
	P3_0m	**P3_8m**	**P3_14m**	**P3_24m**	**P3_32m**
P3_0m		70 (***)	76 (***)	66 (**)	60 ( )
P3_8m	70 (***)		77 (***)	63 (*)	77 (*)
P3_14m	76 (***)	77 (***)		70 (**)	63 ( )
P3_24m	66 (**)	63 (*)	70 (**)		80 (**)
P3_32m	60 ( )	77 (*)	63 (*)	80 (**)	
	F1_0m	**F1_12m**	**F1_22m**	**F1_26m**	**F1_30m**
F1_0m		78 (***)	91 (***)	81 (***)	84 (***)
F1_12m	78 (***)		84 (***)	82 (***)	86 (***)
F1_22m	91 (***)	84 (***)		84 (***)	89 (***)
F1_26m	81 (***)	82 (***)	84 (***)		98 (***)
F1_30m	84 (***)	86 (***)	89 (***)	98 (***)	
	F2_0m	**F2_10m**	**F2_18m**	**F2_24m**	**F2_30m**
F2_0m		83 (***)	77 (***)	68 (**)	68 (*)
F2_10m	83 (**)		79 (***)	73 (***)	80 (**)
F2_18m	77 (***)	79 (***)		76 (***)	76 (**)
F2_24m	68 (**)	73 (***)	76 (***)		80 (**)
F2_30m	68 (*)	80 (**)	76 (**)	80 (**)	
	F3_0m	**F3_8m**	**F3_10m**	**F3_24m**	**F3_26m**
F3_0m		79 (***)	82 (***)	61 ( )	80 (***)
F3_8m	79 (***)		82 (***)	71 (**)	74 (**)
F3_10m	82 (***)	82 (***)		73 (**)	73 (**)
F3_24m	61 ( )	71 (**)	73 (**)		77 (***)
F3_26m	80 (***)	74 (**)	73 (**)	77 (***)	

From Table 3, it is noticeable how generally the Fagus sylvatica samples cross-date better with each other, both for GLK values and also for its statistical significance (F1 is by far the tree, whose individual samples cross-date the better). On the other hand, the Picea abies samples cross-date less consistently. Even if sometimes the GLK values are still quite high; they might not be very much significant. Other than that, it can be noted that generally all of the samples cross-date decently enough within the same tree.

5.2 Wood anatomy measurements

This sub-section depicts the results and associated graphs for the wood anatomical analyses. The variable studied in detail here are cell lumen area, hydraulic diameter, and the derived hydraulic conductivity, calculated from anatomical measurements. The complete master table with all other measured variables is available in the *Appendix* at the end of the manuscript.

5.2.1 Lumen area

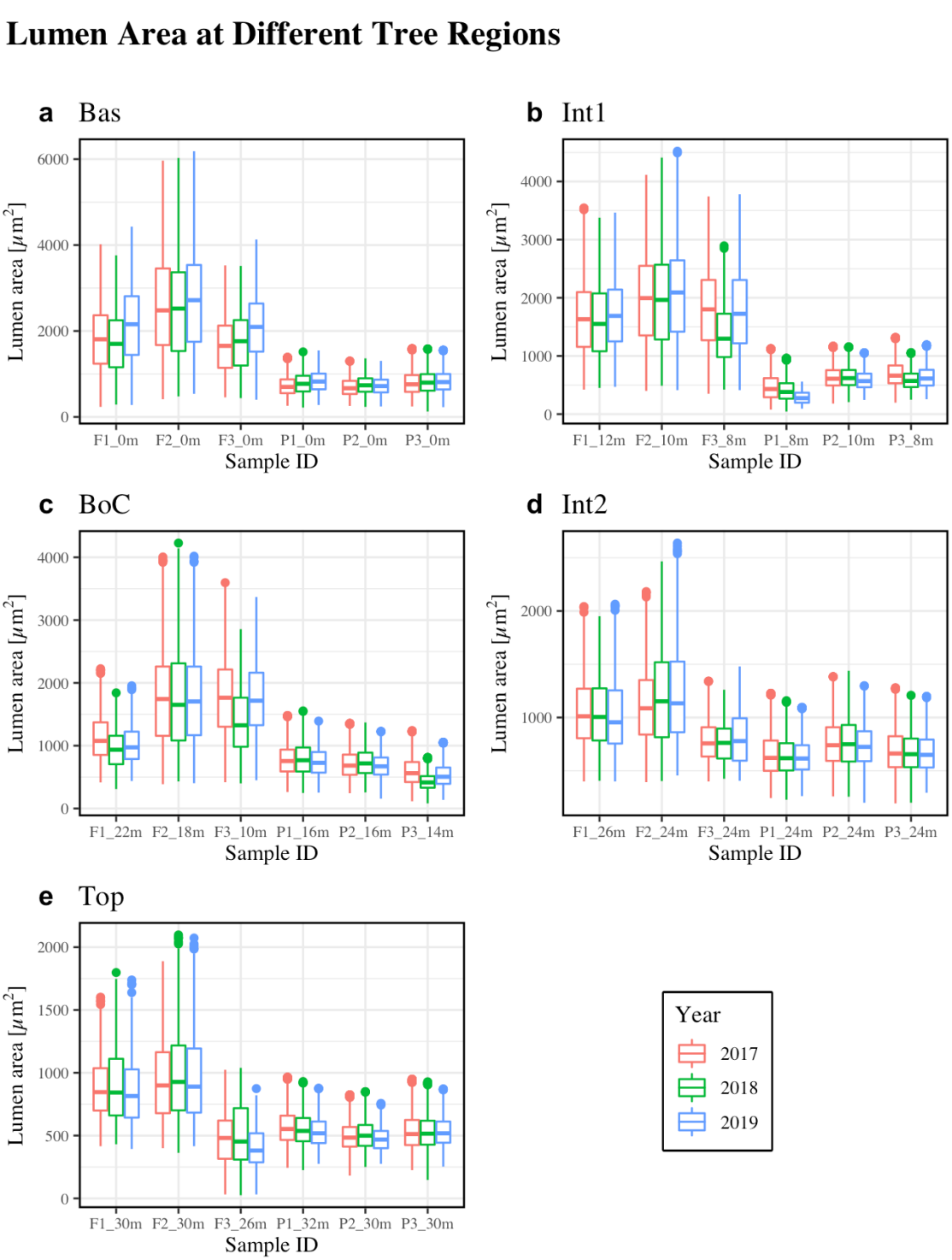

Figure 28 Lumen area at different tree regions. For each tree region (*Bas*, *Int1*, *BoC*, *Int2*, and *Top*), the lumen area for each individual height sample is depicted. Moreover, each height sample represented by three boxplots of distinct color, each for a different reference year: 2017 (shown in red), 2018 (green), and 2019 (blue).

Figure 28 depicts the lumen area of both tree at the different tree regions. From each graph it is easily noticeable that the European beech samples show generally higher lumen area values than the Norway spruce samples. Moreover, the variability of the data, indicated by the extension of the boxplot's boundaries, as well as the length of the error bars, is also generally higher in the European beech compared to the Norway spruce. This difference is decreased in Figure 28d and Figure 28e where the lumen area values for F3 at those heights is

similar to the values for all three spruce trees. Moreover, it is evident that the lumen area values decrease at higher tree regions compared to the ones situated lower on the trees' stems. This finding is also noticeable if we consider the *Bas* tree region (Figure 28a) and the *Top* tree region (Figure 28b). Indeed, the first one presents peak values up to 4000 µm (F2_0m), while the latter presents peaks reaching only up to 2000 µm (F2_30m). Also, the data variability is substantially decreased at higher tree regions, which is evident by the generally reduced extensions of the boxplots' boundaries at these heights. Another important consideration is that for all 5 tree regions it does not seem that there is an evident difference between the measured years. In all of the 5 cases there is not a clear year that constantly has higher (respectively lower) lumen area values.

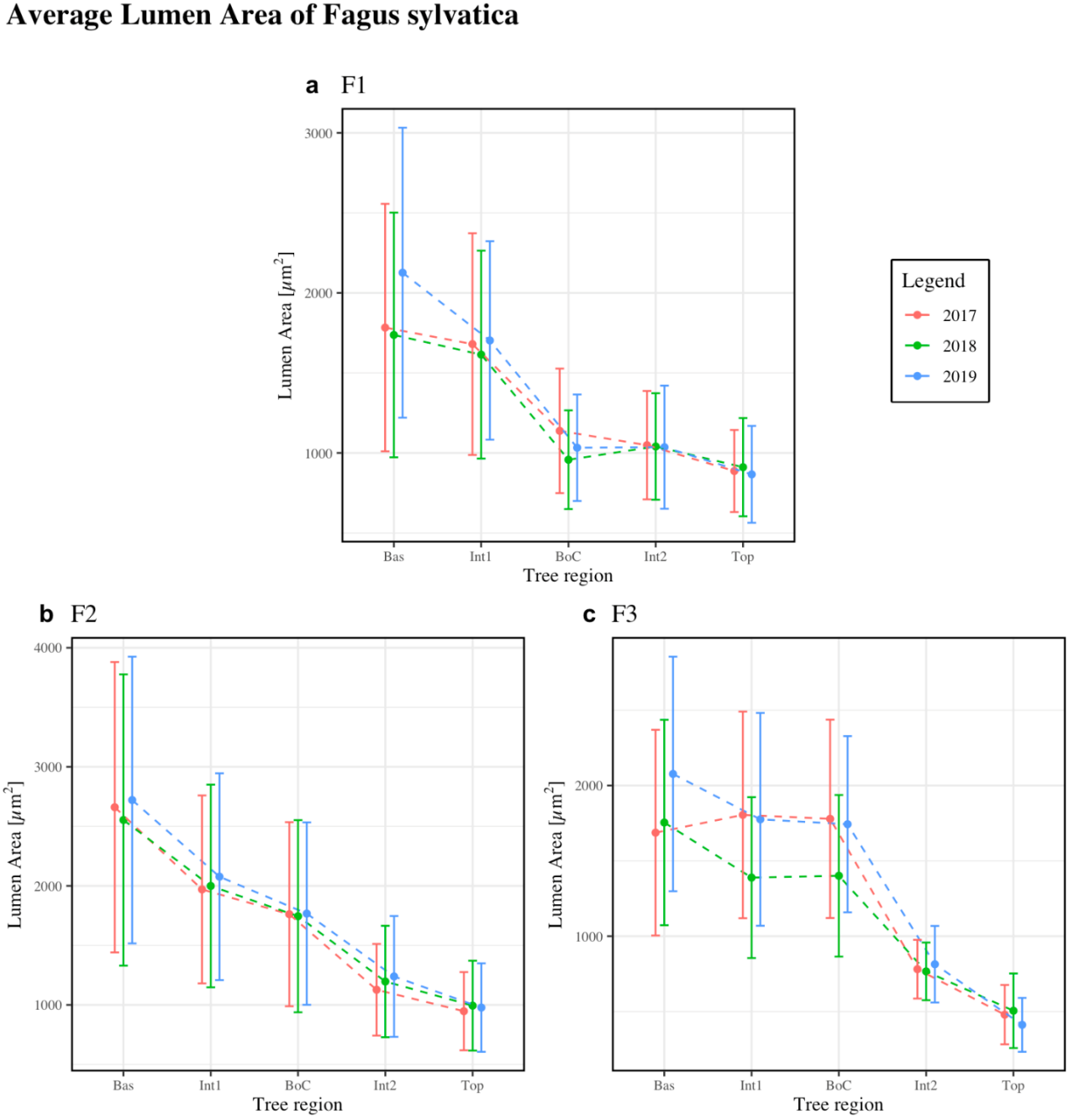

Figure 29 Average lumen area for *Fagus sylvatica* trees (F1, F2, and F3) related to tree region. For each tree region a yearly average was calculated, resulting in three individual points (one for each year) for every tree region. The standard deviation was calculated for each yearly average, and it is depicted by the two-sided error bars.

In Figure 29, it is depicted the average lumen area for the European beech trees related to every tree region. From all three plots, it is noticeable that the lumen area seems to decrease somewhat constantly with height.

In F1 (a) and F2 (b) the decrease seems to be more stable, and constant compared to F3 (c). However, for all three plots there appears to be the same underlying issue: the data variability is very high at every measured height, resulting in uncertain results, which are difficult to assess for truthfulness. Nevertheless, the data variability is decreasing considerably with increasing height; the magnitude of decrease differs from individual tree to the other, but the general trend is found in all of them. Also, in this case there appears to be no relevant annual difference for all three beech trees.

The same cannot be said for the Norway spruce samples (Figure 30). Here is evident that there is not any substantial height related trend. For all three plots, the lumen area appears to be at the same value range, without a real decreasing (respectively increasing) trend. Moreover, the data variability is constantly high also in this case, resulting probably in uncertain and not too reliable results. The only consideration to be made is that it seems that the only decrease in lumen area is found between the upper most regions *Int2* and *Top*. This is visible more in P2 (b) and P3 (c) rather than P1 (a), whose decreasing trend seems to be only slight.

Average Lumen Area of Picea abies

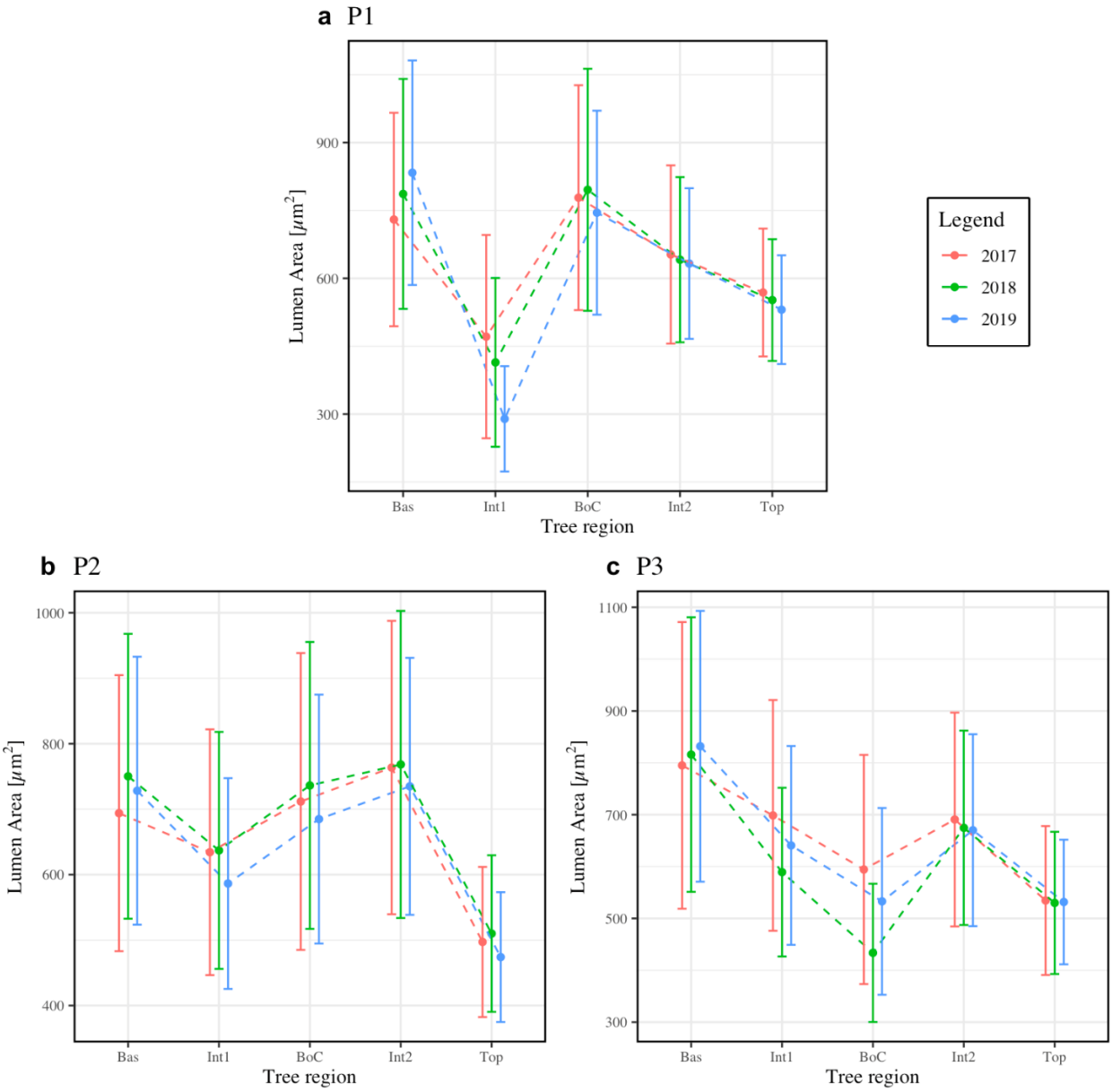

Figure 30 Average lumen area for *Picea abies* trees (P1, P2, and P3) related to tree region. For each tree region a yearly average was calculated, resulting in three individual points (one for each year) for every tree region. The standard deviation was calculated for each yearly average, and it is depicted by the two-sided error bars.

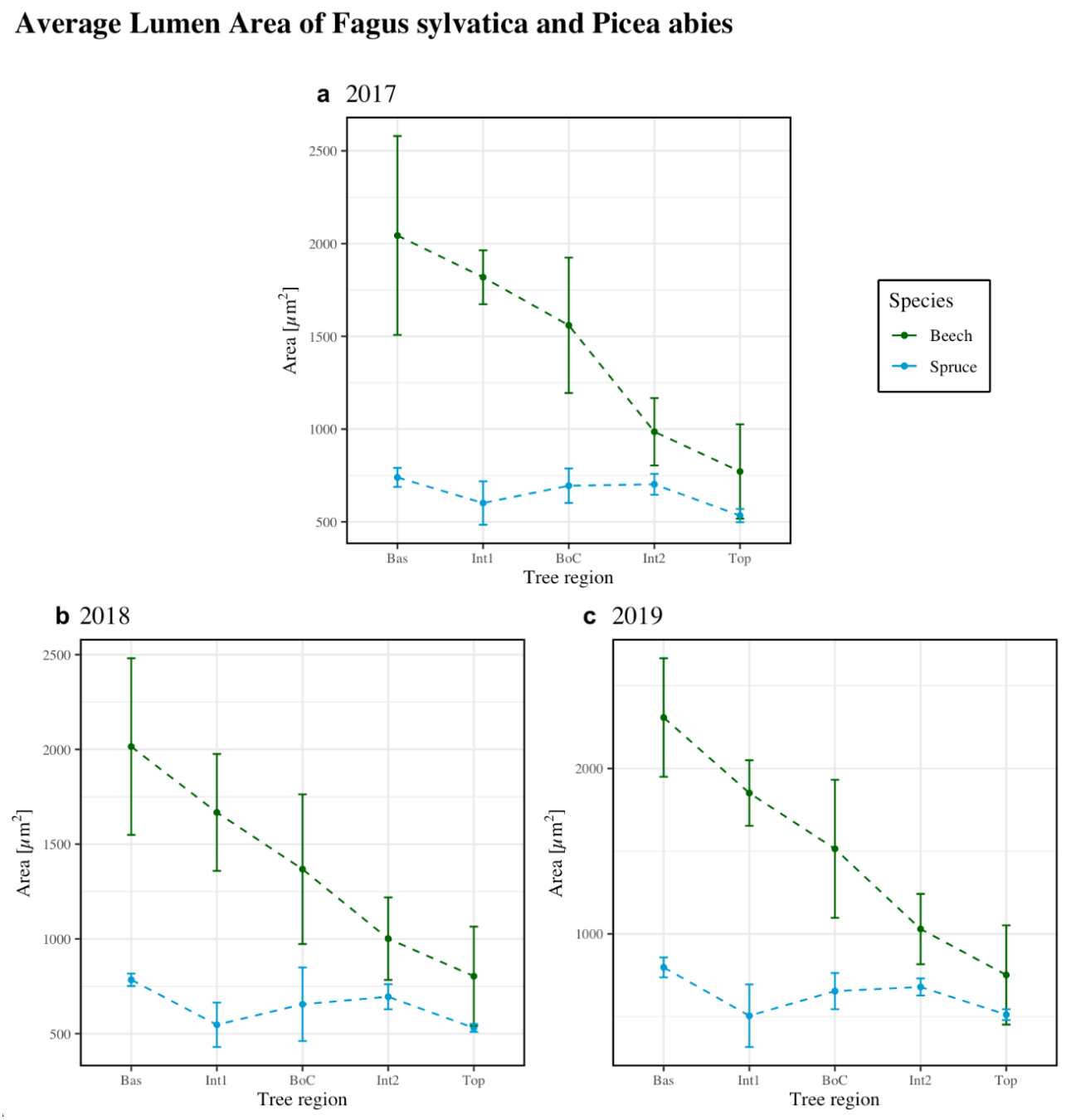

Figure 31 Comparison between average lumen area of *Fagus sylvatica* and *Picea abies* related to the tree regions. For each species averages values for each tree region were calculated and then plotted together for each investigated year. The dark green line represents the Fagus average lumen area, while the light blue line indicated the Picea average lumen area.

Another way to identify this sharp difference between beech and spruce samples is to look at the species' averages for the singular measured years. From Figure 31 it is noticeable how for all three sampled years the beech's lumen area values are always higher than the spruce ones. In general, beech cells appear to be larger in size than spruce cells at every measured tree region. However, this difference is greatly reduced at bigger heights along the tree stem. Comparatively, the difference between beech and spruce lumen area at the tree region *Top* is considerably smaller than at tree region *Bas*. Furthermore, how already mentioned in Figures 29 and 30, it is evident that the lumen area of the spruce samples does not show any height related trend, while the beech ones clearly decrease almost constantly throughout the analyzed regions. Another consideration to be made is that whereas the beech samples have substantially high variability in the values, which also seems to decrease at higher tree regions, the spruce samples seem to have somewhat constantly smaller data

variability, and there is no apparent height related trend regarding it. These considerations are applicable to all three investigated years, with practically no contrasting results.

5.2.2 Hydraulic diameter Dh and hydraulic conductivity Jv

Hydraulic conductivity and hydraulic diameter are two calculated variables that are obtained from the measured wood anatomical data. They serve quite nicely to assess the ability of the plant to transport water through their xylem conduits. Hydraulic diameter is a precursor variable of the hydraulic conductivity, given that the first is needed to calculate the latter. However, it could still be of interest to analyzing them individually, since they might show different results.

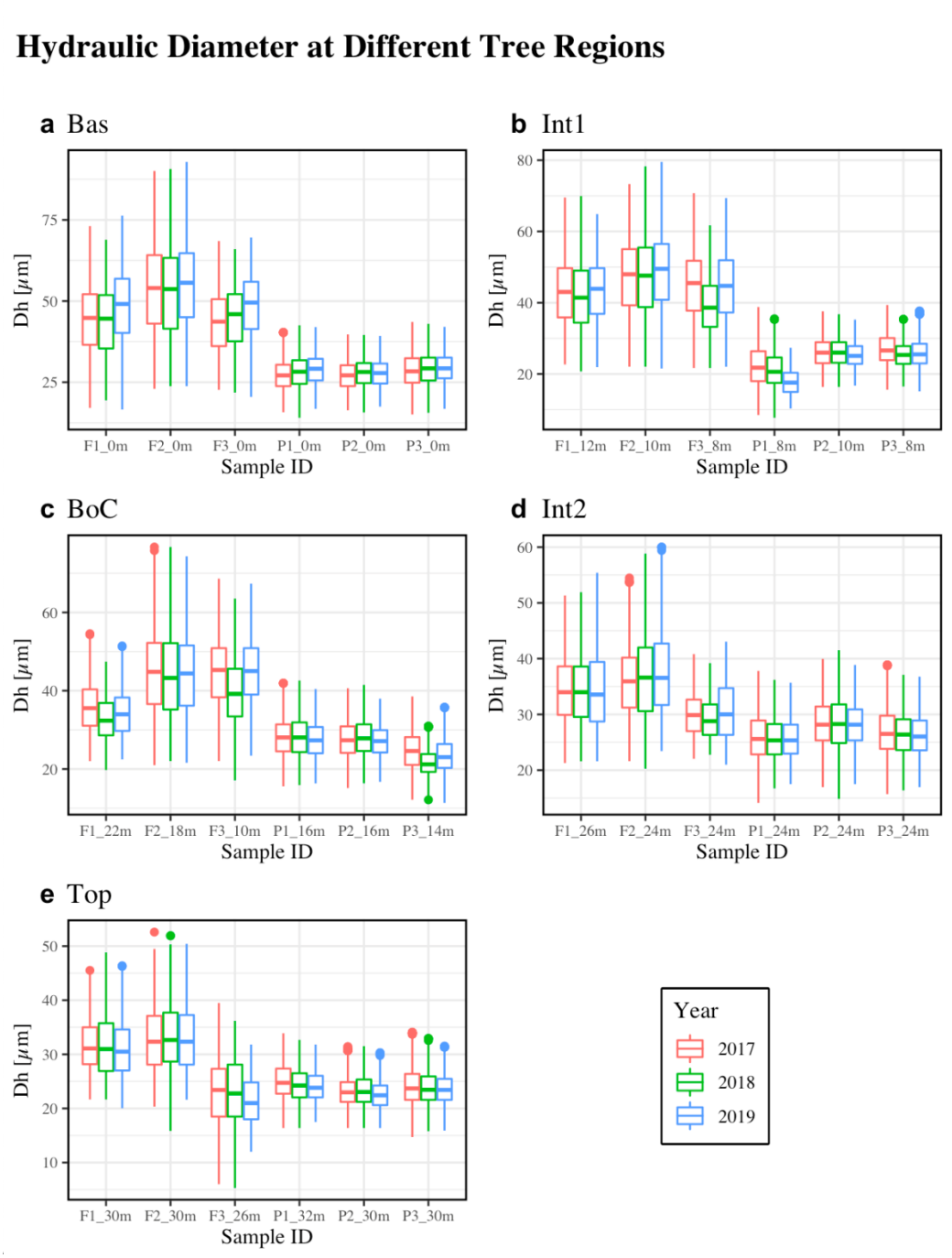

Figure 32 Hydraulic diameter (Dh) at different tree regions. For each tree region *(Bas*, *Int1*, *BoC*, *Int2*, and *Top*), the Dh for each individual height sample is depicted. Moreover, each height sample represented by three boxplots of distinct color, each for a different reference year: 2017 (shown in red), 2018 (green), and 2019 (blue).

In Figure 32 the before mentioned hydraulic diameter (Dh), for each individual tree region is depicted. Similarly, as in Figure 28 with the lumen area, it is noticeable a substantial difference between European beech and Norway spruce samples. Indeed, there is a heavy similarity between the hydraulic diameter and the lumen area, where the species trend seems to be the same in both cases. For example, in both situations the lumen area and the hydraulic diameter are generally higher in the beech samples compared to the spruce ones, and also this difference is grater at lower tree regions, while at higher tree regions the two species seem to assume similar values for both variables. The only slight mismatch is that the difference in magnitude between the two species for the Dh is not so prominent compared to the difference between beech's and spruce's lumen area Furthermore, there seems to be no considerable difference between sampled years, with no apparent trend of one specific year being higher (respectively) lower than the other two.

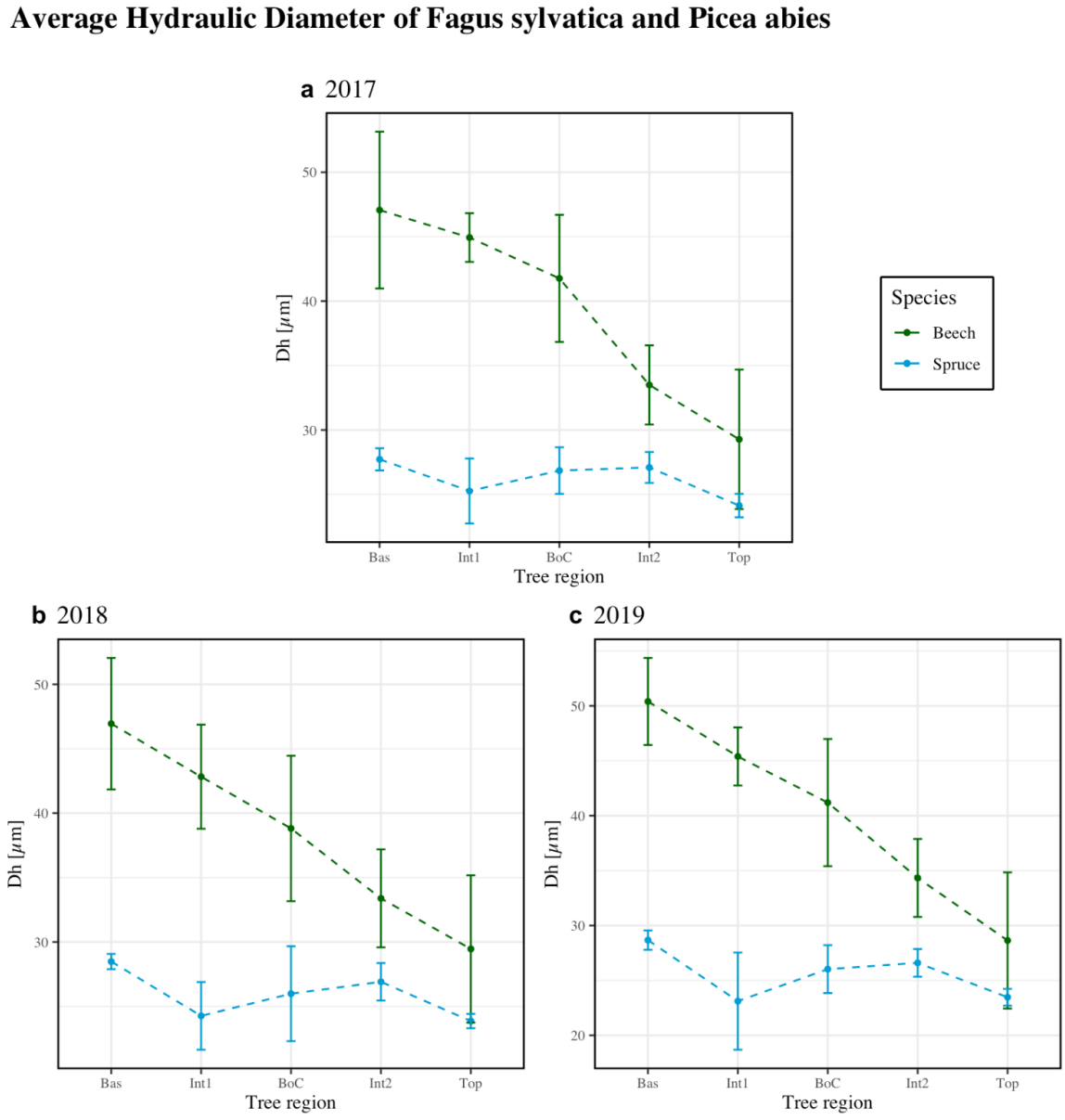

Figure 33 Comparison between average hydraulic diameter (Dh) of *Fagus sylvatica* and *Picea abies* related to the tree regions. For each species averages values for each tree region were calculated and then plotted together for each investigated year. The dark green line represents the Fagus average Dh, while the light blue line indicated the Picea average Dh.

In the same way, taking a look at Figure 33, it is possible to infer that there is a clear discrepancy between the hydraulic diameter of beech and spruce samples. Indeed, the European beech decreases clearly with height, following almost a constant rate of decrease. On the other hand, the spruce Dh fluctuates around the same value range, without showing a clear height related trend.

Furthermore, in all three sampled years the average hydraulic diameter of European beech is always higher than the Norway spruce one at every region along the tree stem.

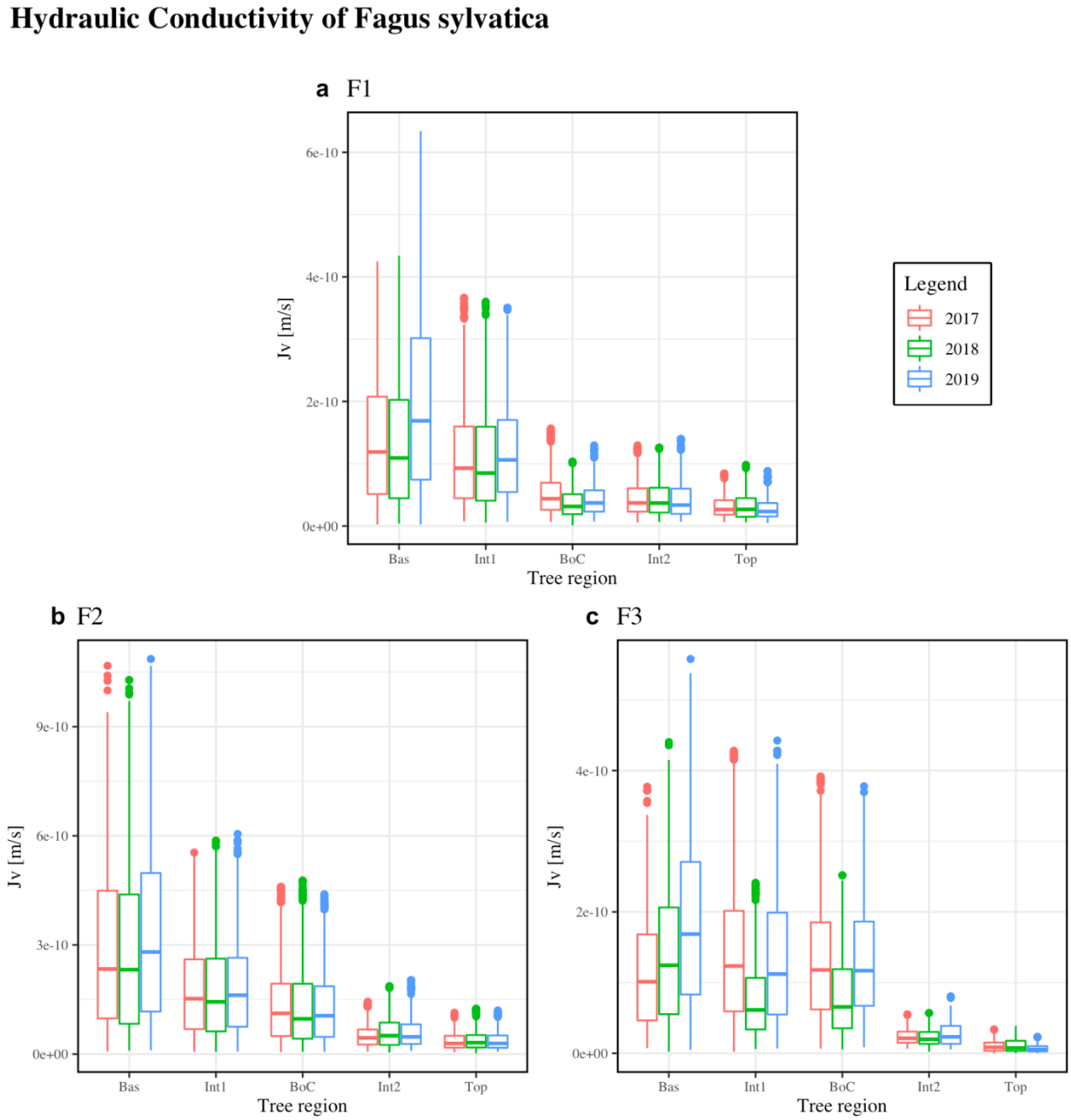

Figure 34 Calculated hydraulic conductivity (Jv) at different tree regions for *Fagus sylvatica*. For each tree region (*Bas*, *Int1*, *BoC*, *Int2*, and *Top*), the hydraulic conductivity of F1, F2, and F3 is depicted. Moreover, each height sample is represented by three boxplots of different color, each for a different reference year: 2017 (shown in red), 2018 (green), and 2019 (blue).

The hydraulic conductivity for European beech (Figure 34) shows clearly a height related trend. For all three trees the hydraulic conductivity decreases at higher tree regions. Furthermore, also the boxplot extension representing the data variability is greatly reduced at higher tree regions. The change for of the beech trees seems to be quite abrupt between the *BoC* tree region and the *Int2* tree region. However, for F1 (a) the abrupt change is found earlier; between tree region *Int 1* and *BoC*. Moreover, in F3 (b) the change in Jv between tree region *BoC* and *Int2* is very severe.

The interannual variability is negligible for all beech trees, even if in F3 it seems to be a small difference. Indeed, the calculated hydraulic conductivity for the tree region *BoC* and *Int2* for the year 2018 appears to be slightly lower than the 2017 and 2019 values.

Furthermore, it is important to state that for the European beech, at the upper most tree regions (*Int2* and *Top*) the hydraulic conductivity takes on very small values; almost reaching zero. The case of this happening is clearer in F3, where the difference in Jv between tree region *Int2* and tree region *Top* is so small that appears to be no difference at all.

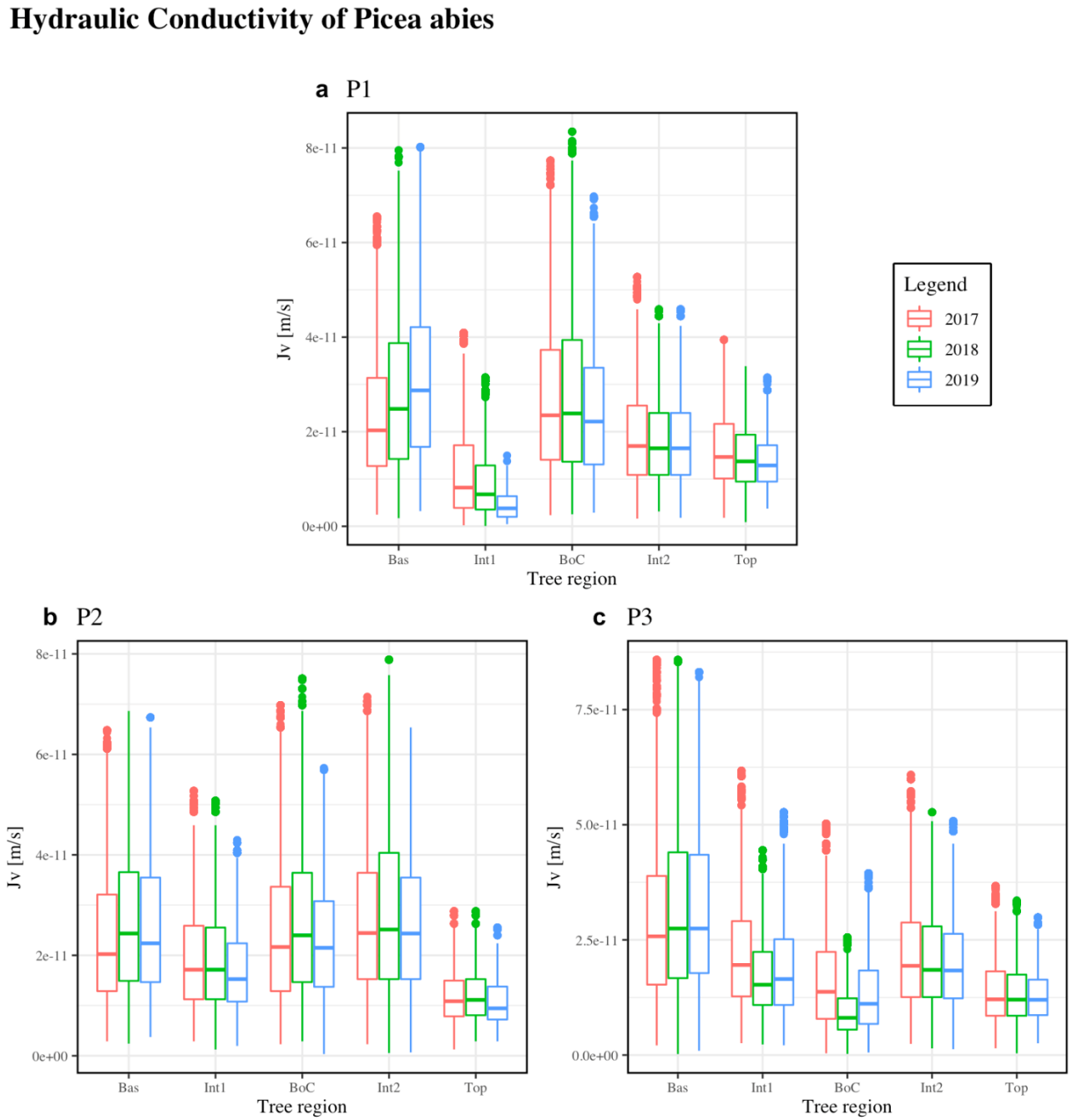

Figure 35 Calculated hydraulic conductivity (Jv) at different tree regions for *Picea abies*. For each tree region (*Bas*, *Int1*, *BoC*, *Int2*, and *Top*), the hydraulic conductivity of P1, P2, and P3 is depicted. Moreover, each height sample is represented by three boxplots of different color, each for a different reference year: 2017 (shown in red), 2018 (green), and 2019 (blue).

On the contrary, the hydraulic conductivity of the Norway spruce trees (Figure 35) does not show any peculiar height related trend. The values seem to be either comparable for every tree region or, in the cases where some

tree regions show lower Jv values than others, there is no clear trend. In P1 (a) for example, the tree region *Int1* represents the tree region with the lowest hydraulic conductivity values for that tree; however, both the previous *Bas* tree region as well as the following tree regions show higher Jv values, which are also not related to each other. In the cases of P2 (b) and P3 (b), the calculated hydraulic is almost constant at every different height region along the tree, apart from maybe the tree region *Top* in F2, which shows the lowest Jv value for that tree.

Also, the variability within the dataset do not show any promising results. Indeed, it is not possible to identify any height related trend in this case as well, since the data variability represented by the extension of the boxplot's boundaries is practically the same along all tree regions belonging to the same tree.

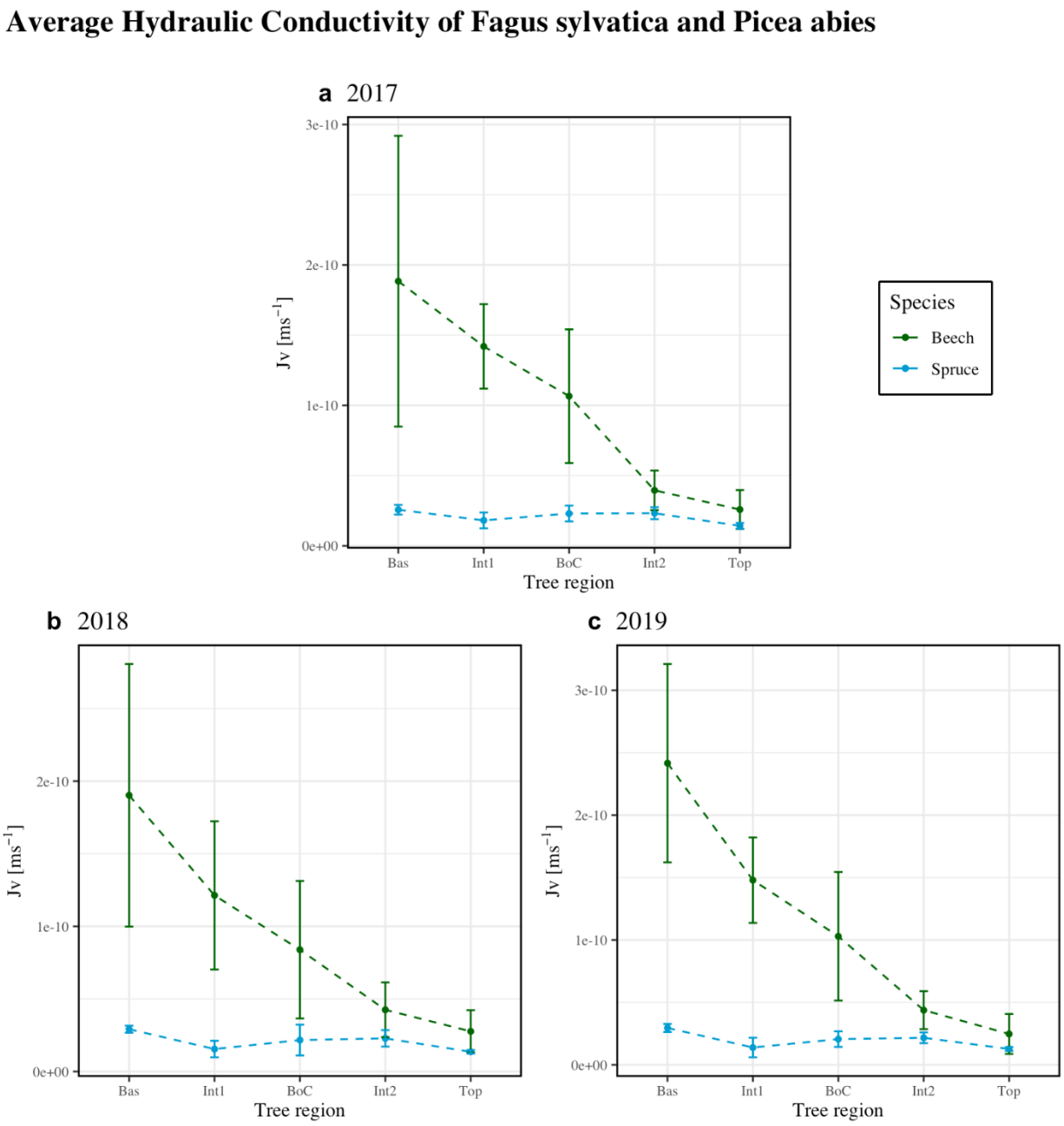

Figure 36 Comparison between average hydraulic conductivity of *Fagus sylvatica* and *Picea abies* related to the tree regions. For each species averages values for each tree region were calculated and then plotted together for each investigated year. The dark green line represents the Fagus average hydraulic conductivity, while the light blue line indicated the Picea average hydraulic conductivity.

If we compare the hydraulic conductivity for the two species (Figure 36), we see clearly a difference between them. For all three years, the spruce's Jv is always lower than the beech's one at every region along the tree

stem. Furthermore, this difference is not constant throughout all the tree regions, but it becomes narrower the higher the samples are. Indeed, at lower heights, the two curves are considerably more diverging than at the upper-most tree regions, where they almost converge to the same hydraulic conductivity values. Moreover, for the beech samples, it is clearly noticeable a height related trend, in which the hydraulic conductivity steadily decreases with each more elevated tree region, whereas the spruce samples do not seem to follow any trend in regard to the tree regions.

Also in this case, the difference in years is negligible, since the curves for all three graphs seems practically the same, apart from maybe a slight difference in the data variability for each averaged Jv values at a particular tree region.

5.3 Isotope meaurements

This sub-section focuses on presenting the results of the isotopic analyses done on the European beech and Norway spruce samples. For comparison purposes with the wood anatomy data presented before, only the results of the $d^{13}C$ and the Nitrogen percentage will be presented in detail in this chapter. The other results will be available in the *Appendix* at the end of the document.

5.3.1 Carbon isotope measurements

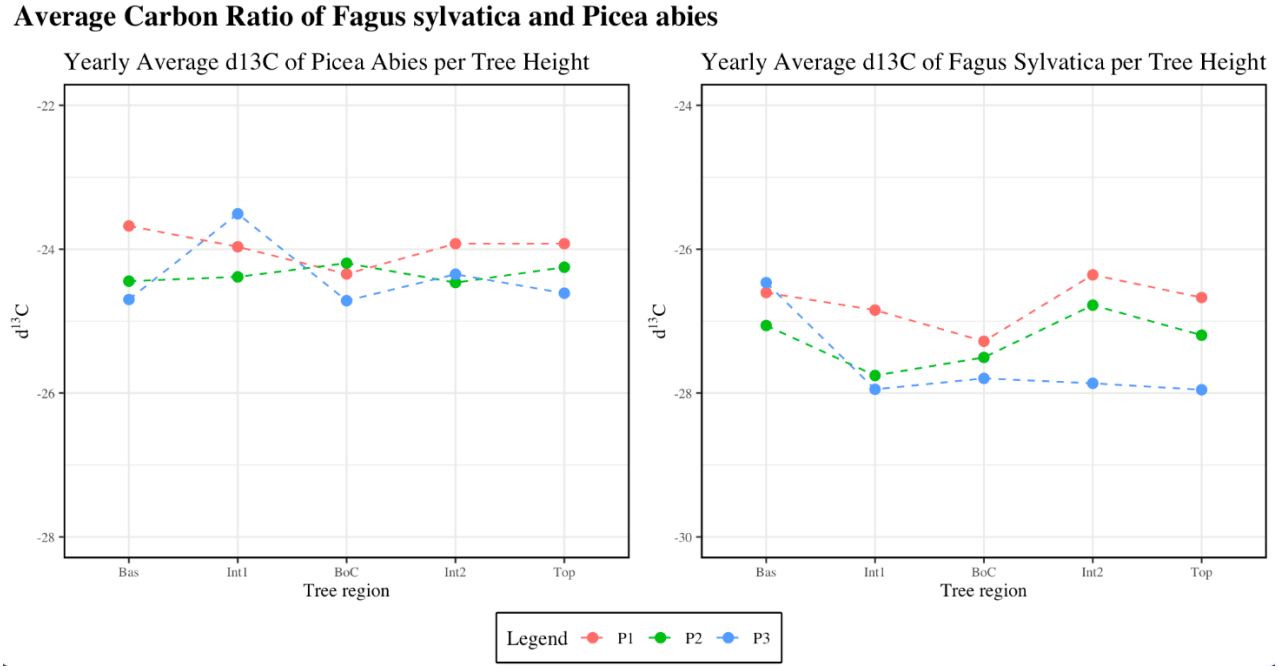

Figure 37 Average delta ^{13}C of *Fagus sylvatica* and *Picea abies* related to each tree region. For each tree region the species average was calculated based on the individual values of F1, F2, and F3 for the *Fagus sylvatica*, and P1, P2, and P3 for the *Picea abies*. For each tree region the values for all three measured years 2017, 2018, and 2019 are depicted.

In Figure 37 is depicted the $d^{13}C$ for Norway spruce (a) and European beech (b). From the two graphs it is evident that each sampled year do not have any considerable difference between each other. Moreover, it is apparent that there is no height related trend in either of the plots. On the contrary both the beech carbon ratio, as well as the spruce carbon ratio remains almost constant (apart for a few very small fluctuations) for every tree regions. Finally, comparing the two graphs it is noticeable that the spruce has generally less negative $d^{13}C$ than the beech.

Yearly Average Carbon ratio of Fagus sylvatica and Picea abies

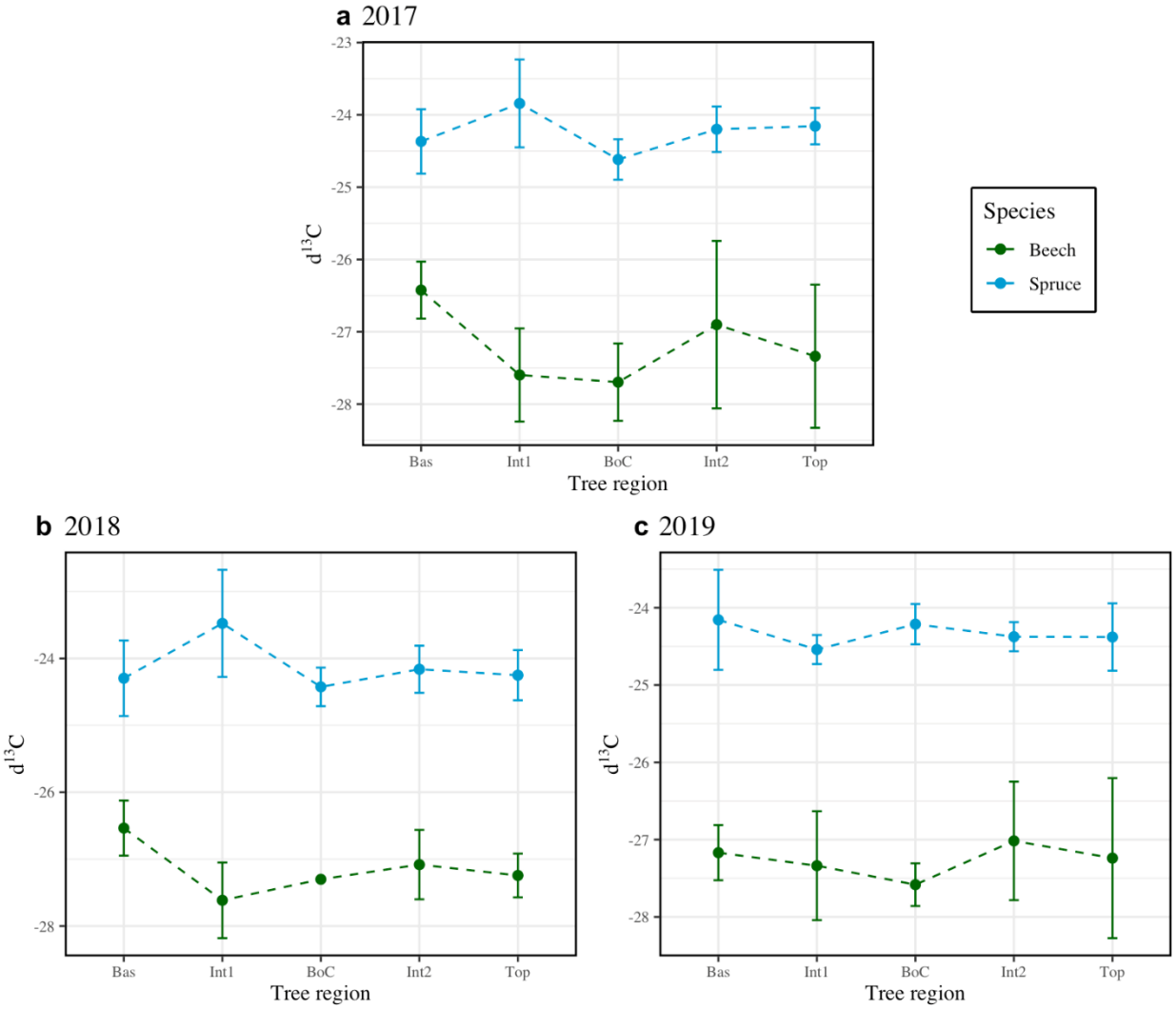

Figure 38 Comparison between average delta ^{13}C of *Fagus sylvatica* and *Picea abies* related to the tree regions. For each species averages values for each tree region were calculated and then plotted together for each investigated year. The dark green line represents the average delta 13C of *Fagus sylvatica*, while the light blue line indicates the average delta ^{13}C of *Picea abies*.

Indeed, in Figure 38 it is evident that for all three years the values of $d^{13}C$ for the European beech is always more negative than the ones for Norway spruce. The biggest difference is reported in Figure 38b, where in 2018 at tree region *Int1*, the average spruce $d^{13}C$ show a peak, while the average for the beech shows a low point. Furthermore, it is also pretty evident that no height related trends are visible in neither of the three studied years. Another aspect to consider is that generally the variability in the carbon ratio for the European beech is bigger than the Norway spruce's variability. This is noticed by the amplitude of the error bars in both cases, where for the beech trees, in all three years, are usually more spread out.

5.3.2 Nitrogen isotope measurements

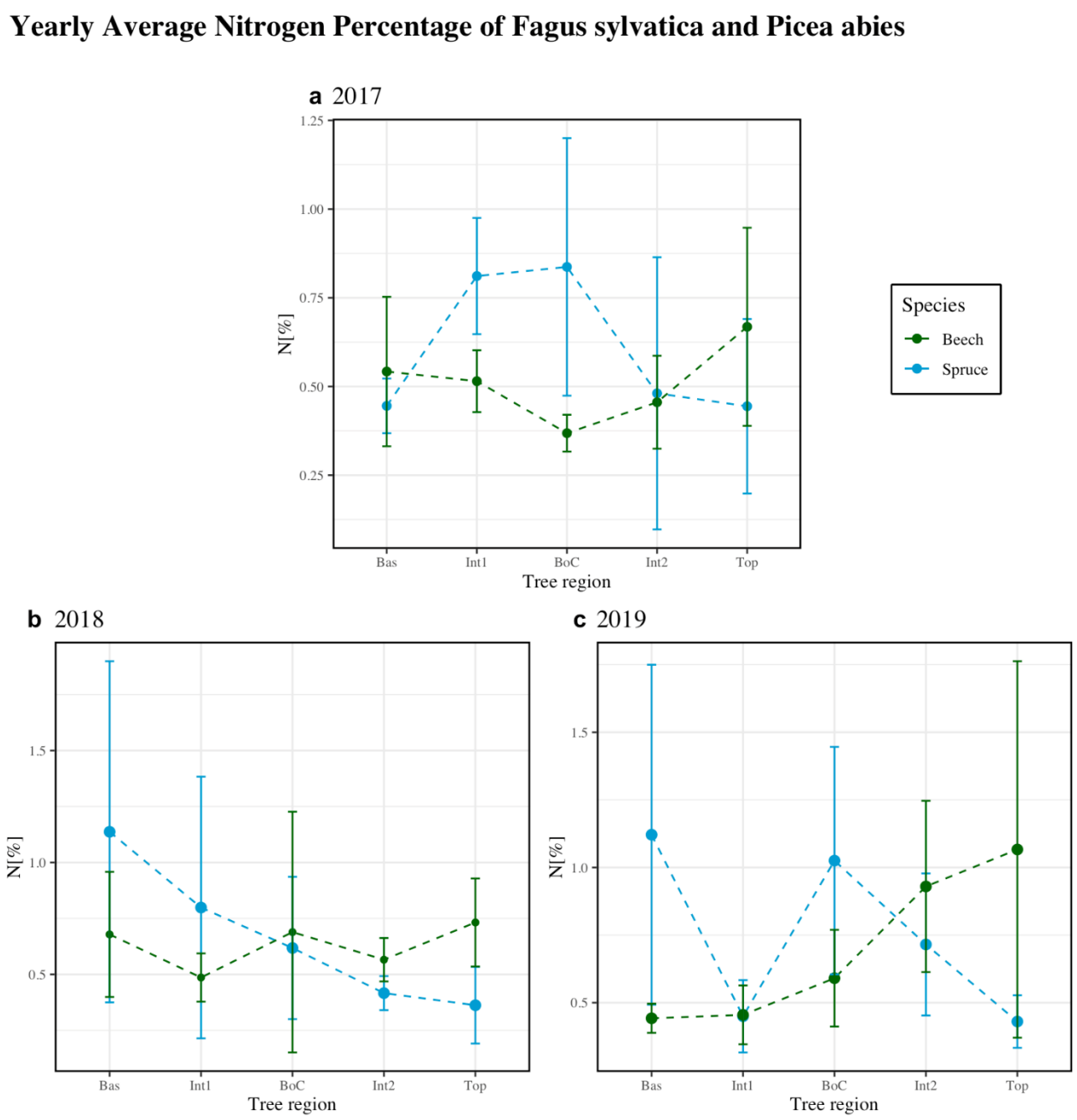

Figure 39 Comparison between average Nitrogen percentage of *Fagus sylvatica* and *Picea abies* related to the tree regions. For each species averages values for each tree region were calculated and then plotted together for each investigated year. The dark green line represents the average N percentage of *Fagus sylvatica*, while the light blue line indicates the average N percentage of *Picea abies.*

Figure 39 show the nitrogen concentration in European beech and Norway spruce related to the tree regions for the usual three studied years: 2017 (a), 2018 (b), and 2019 (c). It is evident that there is no clear species that shows higher or lower values of nitrogen concentration throughout all the measured height regions. Moreover, the height trend is also not clearly visible in all three studies years. One could argue that in 2018 the spruce might show a reduction of nitrogen concentration the higher you go along the tree, but here the data variability is massive, therefore it is not possible to state any conclusion with certainty. This phenomenon of very high variability within the dataset it is present in all three studied years, as well as in both species and in every cases.

5.4 Statistical Analysis

This chapter describes the steps into the statistical analysis conducted for these thesis results. Firstly, for the lumen area, hydraulic diameter and hydraulic conductivity plots, the data were tested for normality between and within each subset using a Shapiro-Wilk test. The initial result was that normality could not be confirmed (p-value < 0.05). For this reason, a base-10 logarithmic correction was applied to the individual subsets to see if normality could be achieved. After having repeated the Shapiro-Wilk test with the corrected values, the results were still that normality could not be inferred (p-value < 0.05). Therefore, since the data were not normal distributed, an ANOVA test could not have been used. Instead, to verify if there was a difference between each measurement years in the datasets, a non-parametric variance test (Kruskal-Wallis test) was used. The result of this test showed that there was indeed a significant difference between each year in each singular subset (p-value < 0.05). However, it can be said that practically speaking this difference is uninfluential since, by looking at Figures 28, 32, 34, and 35, it is not possible to identify individual years there are always higher (or lower) than other.

To verify the presence of a significative relationship between lumen area, hydraulic diameter, and hydraulic conductivity and height, a Spearman's correlation was calculated between said variables and tree region. In order to do that the categories *Bas*, *Int1*, *BoC*, *Int2*, and *Top* were converted back to their original numerical heights. For all three variables the beech samples were found to correlate negatively with tree region ($r_s \approx -1$; p-value < 0.05), meaning that as the tree height increases, lumen area, hydraulic diameter and hydraulic conductivity were found to decrease. On the other hand, for the spruce samples, this correlation was not found ($r_s \approx 0.5$; p-value > 0.05), meaning that is not possible to infer the presence of a height trend.

Similarly, the carbon isotope dataset was firstly tested for normality using the before-mentioned Shapiro-Wilk test. Each tree was individually tested, and the result was that all subsets were found to be normally distributed (p-value > 0.05). It's important to note here that testing each tree individually generates very small subsets composed of only a few values. For this reason, one cannot discard the possibility that the result of the test might not be significant, because of a sample poll too small. Following that, it was decided to test the height trend in the $d^{13}C$ values using the Spearman's correlation (instead of the more precise Pearson's correlation for normally distributed data), which can be used for both normal and non-normal distributed variables. The results indicated how no correlation between carbon ratio and tree region was found for all of the trees ($r_s \approx 0.5$; p-value > 0.05).

6 Discussion

6.1 Interpretation of ring width results

As indicated in Figure 25, the tree-ring curves for all three European beech trees follow more or less the same trend throughout their entire lifespan. This fact make sense if one takes into consideration that all three trees grew in the same study area being only a few meters apart. This is the case because generally trees that grow subjected to the same climatic environmental conditions, most likely will show very similar tree-ring width patterns. Moreover, they belong to the same tree species, meaning that they also have the same basic biological functions (e.g., metabolism, growth rate, etc.). The same can be said for Norway spruce (Figure 26), where also the three trees grew in the same study region and were subject to the same climatic and environmental conditions. Generally, there is no singular factor that influence tree growth, but it is a complex mechanism made of different variables that are intertwined with each other (Gaertner, 1964).

Another consideration is that more or less both average curves for the two species are similar (Figure 27). Indeed, after a certain year (ca. 1950), the two species follow the same tree-ring width trend. The most likely explanation for this delayed convergence in the ring-width curves is the intrinsic difference between the two species, which grew with different competition for light in the early stages or their life. Indeed, the absence or reduced competition leads to unrestricted growth even in later stages of the tree's life. On the other hand, competition for light results in slowed down growth starting very early. The first case scenario is more indicative for the beech trees, where it is noticeable that they could have grown apart from each other, since the width of their rings increase unrestrictedly during the adult stages of their life. On the other hand, the spruce trees show signs of competition form the juvenile stages onwards, which is represented by the sudden decrease and the stabilizing of the ring width. (Rozendaal et al., 2020). Also, as Jarvis and McNaughton (1986) indicate, conifer trees are usually well coupled to the atmosphere thanks to their surface roughness and their high boundary layer conductance of their narrow leaves, leading to more adequate gas exchange with the atmosphere. This finding could also be partially a cause of why the Norway spruce presents higher values of ring-width in their early life stages (i.e., when the plant is still allocating a lot of resources in growth) compared to the European beech.

Looking more in depth at the average curves one can notice a few periods where the two ring-width curves clearly follow the same pattern. This is more clearly noticeable in the before mentioned period of low ring width between 1945 and 1955, as well as two smaller periods around 2003-2005 and 2018-2019. The latter two period are most definitely due to two major drought events that characterized the European climate in those years, namely the 2003 and the 2018 droughts. The fact that the decrease in ring width is prolonged also for a few years following the drought event can be due to sort of a long-lasting effect on tree growth, with both species needing more time to re-adapt to more adequate environmental conditions right after the big droughts (Buras et al., 2019). On the other hand, the 1945-1955 prolonged period of reduced growth can be attributed to the well-known drought period that afflicted Switzerland and the whole of Central Europe between 1945 and 1949 (Hirschi et al., 2013). For the same reason as the 2003 and 2018 droughts the longer period of ring width decrease shown in both beech and spruce can be attributed to a long-lasting effect due to the drought that was afflicting them. In this case, since the drought events were present during a longer period, it is very well possible that the reduction in ring width lasted longer compared to the 2003 and 2018 cases. As stated before (see Chapter 3.1.4), droughts are not the only climatic and environmental phenomenon that can negatively affect tree growth, which will result in a reduction in width in the tree-ring curves. However, for the cases of the ring width reductions shown in these results, drought events seem to be the most plausible cause to explain them.

The inconsistent GLK values (Table 3) found in the Norway spruces samples can be explained by the fact that it could be possible that some (or all three) trees were already growing new rings when they were measured. It is possible that the trees were felt during the start of the growing season, therefore new rings could already have been starting to form. The black circle in Figure 40 indicates a newly formed ring found in sample P1_8m, which was not present in any other height samples used for other analyses. It might be possible that that only tree P1 presents the additional ring, or there is the chance that also the other two spruce tree might have as

well. It is important to note here that there is a considerably high chance that these additional rings might be present in other trees; also from the European beech pool, since all six trees come from the same research site. However, it could be possible that they were not measured depending on where the cross-sections were analyzed. Therefore, there is no complete certainty that the ring-width data are entirely significant and that can explain why the GLK values vary so much from sample to sample.

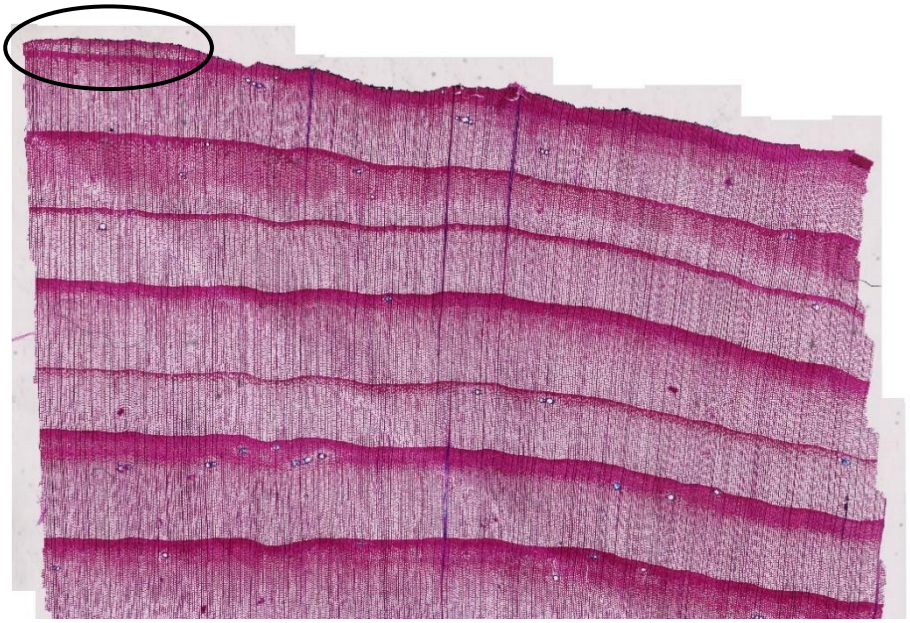

Figure 40 Zoomed in image of sample P1_8m. This scanned micro-section shows the last few rings of sample P1_8m. In the top-left part of the image (black circle), there is a new, smaller ring branching out from the bigger one below (Mattias Barigazzi)

6.2 Interpretation of wood anatomy results

The measurements for wood anatomy were conducted only on earlywood cells for both species. The reasons behind this decision were both because of practicality with cell detection using the WinCell software, and also because of the fact that earlywood conduits were found to transport water more optimally than latewood conduits (Zhu et al., 2021). Also, the high variability shown in pretty much all of the plots for wood anatomy is due to the very high volume of data collected. Indeed, some values were removed using an outlier removal function, but nevertheless, the resulting amount of data still particularly large.

The differences in lumen area shown in Figure 28 are easily explainable by two main factors. The first is based on the biological constitution of their cells. Angiosperm's vessels are usually larger than conifer's tracheids, and, as shown in Figure 41, they have different ways to transport water (Hunt and Manzoni, 2015; Sperry et al., 2006). Moreover, as Choat et al., (2005) indicate, there are considerably large differences between the cellular structure of the xylem of deciduous and evergreen trees. Also, this intrinsic difference is reflected in the hydraulic properties of the two tree classes. For instance, deciduous trees were found to have more efficient water transport than evergreen trees, as indicated by their higher mean vessel diameter. For this reason, it is clear why at every tree region the Norway spruce samples showed lower values of lumen area compared to the European beech ones.

The second factor is related to the tapering of the xylem conduits with height. As Anfodillo et al., (2005) found in their study, all plant species were found to show tapering of the xylem conduits independently from the stand condition that they were found in. Indeed, this trend was found to be applicable to every studied species being either broadleaves or conifers. In the case of Figure 28, comparing the values for lumen area for each sample of the same tree (e.g., F1_0m, F1_12m; F1_22m, F1_26m, F1_30m, etc.), it is evident how for all European beech trees, the lumen size definitely decreases with increasing height. On the other hand, this trend is not visible for the Norway spruce, which presents similar values of lumen area through the entire trees' length. This finding is very interesting since it contradicts the findings from Anfodillo et al., (2005) mentioned above. Furthermore, both the measurements for hydraulic diameter (Figure 33) as well as those for hydraulic

conductivity (Figure 36) show more or less the same exact trend as in the lumen area. Obviously, this is a very logical finding, since the latter two measures are derivate variables which were calculated based on the first one (in reality they were calculated based on the lumen perimeter, but it is practically equivalent as the lumen area). Also, as inferred from the Hagen-Poiseuille law, it was predicted that the wider the vessels, the higher the general hydraulic conductivity should be (Choat et al., 2005). Indeed, looking at Figure 36, it is evident how European beech hydraulic conductivity is always higher than Norway spruce's.

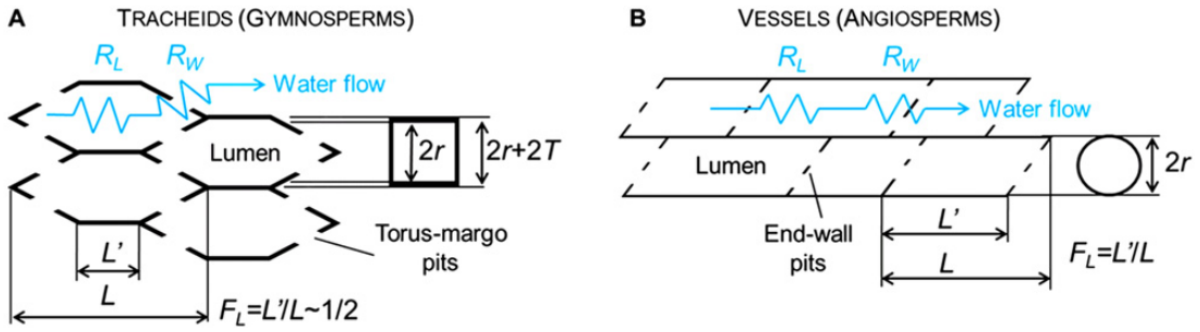

Figure 41 Schematic representation of the anatomical features of tracheids (a) and vessels (b). It is noticeable how tracheids are tubular shaped, and the water flow (blue in the image) passes through a small portion of the cells. On the other hand, the vessels are positioned more regularly one close to the other, making the path for the water flow longer, thus increasing the ability to transport water (Hunt and Manzoni, 2015)

A consideration is needed here: from Figure 36, it is evident how for both species the values of Jv approaches 0 m/s, but without reaching it. Following the literature, it is hypothesized that the reason why both species did not reach a value of 0 m/s in hydraulic conductivity is because they did not reach their maximal height at the time that they were felt down The reason for this is that one can assume that whenever the hydraulic conductivity reaches 0 m/s the plant cannot transport water up to the stem anymore, reaching therefore its maximum vertical height. This can be the case when we take into consideration that hydraulic conductivity is dependent on both the conduit diameter and the water pressure gradient (see equation (1) in Chapter 3.4.3). Therefore, at a certain threshold. where either the conduits are too small or the gravitational pull on the water column is too strong, the value for Jv will likely become 0. (Tyree, 2003; Chelenmuge et al., 2015). Now, this hypothesis could be valid for the European beech, since F1, F2, and F3 showed a reduction of Jv with height as expected from the literature. Contrarily, the same cannot be said with certainty for the Norway spruce, because the values for Jv in P1, P2, and P3 did not show any significant height trend. For this reason, it is possible that either one of the spruce trees might have reached its maximal height, but the hydraulic conductivity results do not show that. Moreover, the literature indicates that European beeches can reach heights of up to 50 meters, while Norway spruces up to 40 meters (Taylor, 1993; Wühlisch, 2008); therefore, it could very much be possible neither one of all of the trees used for this thesis reach their maximum height. Indeed, looking at Table 1 in Chapter 4.1, the highest analyzed cross-section for a beech tree was 30 meters (F1 and F2), and for a spruce tree was 32 m (P1)[8], which is considerably distant from the theoretic maximum heights indicated in the literature. However, it is important to note here that the upper most samples for each tree might not reflect their real maximum height. Indeed, there is the possibility that during sampling at the SCC II some of the apexes of the trees were discarded, given that the cross-sections that were given for this thesis did not include the upper most parts of all of the trees.

As presented in Chapter 3.4, cavitation can be a real issue in drastically reducing hydraulic conductivity in plants. Moreover, according to the literature, there is the possibility that generally larger wood conduits are

[8] There was another sample that was higher than 32 meters. It was at 34 meters and belonged to tree P3 but was discarded in the initial sampling because it was too badly damaged to be used for the ring-width analyses. Anyway, this fact should not influence that fact that all six trees might not have reached their maximum height.

more subject to cavitation compared to smaller ones (Hunt and Manzoni, 2015; Koch et al., 2004; Ryan and Yoder, 1997; Tyree and Sperry, 1988). Since beech's vessels were found to be always larger than spruce's tracheids at every measured tree region, it is possible that the absence of reduction in hydraulic conductivity of the Norway spruces can be attributed to this specific cause. Therefore, assuming that in the spruce's tracheids there were no signs of cavitation. However, this is pure speculation, since Sperry et al., (2006) found that smaller conduits are less susceptible to cavitation, but at the same time they discovered that there is a significant trend, where conifer's conduits were generally at higher risk of cavitation despite having smaller lumen area compared to angiosperm's conduits. Also, it is not possible to verify if in the spruce samples analyzed for this thesis there were actually no signs of cavitation and embolism in the xylem conduits.

Another possible explanation of the fact that the lumen area as well as the hydraulic conductivity in Norway spruce were not found to taper with height, might come from the biological difference between angiosperms' vessels and conifers' tracheids. The latter being elongated and unicellular, consequentially are also smaller in length compared to vessels (Sperry et al., 2006). This finding might be reflected in the wood anatomical features (e.g., lumen area), therefore having an influence during the wood anatomical measurement and the consequent calculation of the hydraulic conductivity. This finding might lead to errors or uncertainties during the image analysis step with WinCell, meaning the measured lumen area for Norway spruce might come from a region along the tracheid which was smaller (or bigger) than in neighboring parts.

From figure 36 it's evident how the vessels from the European beach become smaller from the bottom to the top of the tree, making them comparable to the spruce tracheids. It's then interesting to note that as both trees approach taller heights, the hydraulic conductivity seems to assume values that are comparable between the two species. Usually, the values for hydraulic conductivity for the beach are always higher in value and then the ones from the spruce; however as both species reaches the uppermost tree regions, they start to assume the same values of Jv. Another interesting finding from Figure 36 is that because of this trend between the two species' curves, it could mean that these two different species react differently to maintain water use efficiency along the entire length of the tree. Within each other, it's evident that wood anatomy for the European beach trees changes a lot in order to maintain water use efficiency constantly at a reasonable value at every tree region. On the other hand, this is not the case for the Norway spruce. Indeed, here the values for hydraulic conductivity stay almost the same throughout the whole three length (Jaleel et al., 2008; Sinclair et al., 1984). Moreover, the latter trend is also noticeable in the plot for the lumen area (Figure 31), which is directly comparable to the one for hydraulic conductivity, reinvigorating the hypothesis of water use efficiency difference.

6.3 Interpretation of isotope results

According to the literature, values of delta carbon 13 are expected to become less negative with increasing height, independently from either the studied species or the growing region's conditions (Hultine and Marshall, 2000). Probably, the height difference of $d^{13}C$ in tall trees is caused by the reduction of water potential due to gravity and path length resistance, which results in limited water supply with increasing height, leading ultimately to reduced photosynthesis. The middle step, as discussed in Chapter 3.3, is that photosynthetic activity will proceed with less discrimination by the plant towards the atomically heavier ^{13}C. Therefore, the plots in Figure 38, according to the literature, should show less negative values of carbon ratio with increasing height. (Hultine and Marshall, 2000; Koch et al., 2004). However, the findings in this thesis' results would indicate that there is no difference between d13C from the base samples and the top samples in both studied species.

A possible explanation for the absence of increase in $d^{13}C$ in both species could be reconducted to the fact that wood material consists of a complex mixture of carbon with different turnover times. Furthermore, the structural carbon in deciduous trees (i.e., European beech in this case) is more likely to carry an isotopic signature which is influenced by both the present and also the previous growing seasons. Therefore, it could explain why these findings are like this (Keitel et al., 2006). Also, this phenomenon could happen if we take into consideration the possibility that the selected heights for the analysis were not conclusive enough to concretely see a reduction in $d^{13}C$. Maybe there is the possibility that larger height intervals were needed to

see a conclusive difference. Otherwise, since it transpires form the hydraulic conductivity data (Figure 36) that the trees did not reach maximum height before being sampled, it could be possible that bigger heights were needed to see an actual difference in $d^{13}C$. Nevertheless, in the literature it was found conclusively that all plants should show at least some trend of increasing $d^{13}C$ (i.e., less negative values) with height. (Marshall and Monserud, 1996).

Another hypothesis to why the $d^{13}C$ do not responds to height as theorized in the literature can be that the sugars that come from the wood might have been mixed, and therefore they do to originate from the actual corresponding height region. In this case, it could have happened that some measured $d^{13}C$ values from the uppermost tree regions, might in reality come from further down along the tree. It is not possible to verify this hypothesis, but it was found in the literature that this phenomenon happens quite frequently when investigating height trends along the same analyzed tree. The results of this so-called mixing of sugars are noteworthy uncertainties in the carbon isotope measurements, because it is not possible to clearly identify to which tree region the analyzed wood material really belongs (Gessler et al., 2014).

Regarding the $d^{13}C$ values of European beech and Norway spruce, they seem to coincide with values from the literature. Indeed, Mölder et al., (2010), found in their investigation average values of $d^{13}C$ for European beech between -27% and -25%, while the measured values for this thesis lie around -27% and -28%. Also, for Norway spruce, the average values found in Jäggi et al., (2002), lie around -24% and -25%, which correspond exactly as the average $d^{13}C$ values measured in this thesis. On the contrary, as indicated in Smith and Epstein, (1971), the values of delta carbon 13 for plants of the Fagaceae family (the same as European beech) lie around -26.5%, while the values for the Pinaceae family (the same as Norway spruce) is around -30.8. The study from Smith and Epstein, (1971) was conducted on *Pinus haelpensis*, Mill. as a representative of the Pinaceae family and *Quercus palustris*, Münchh as a representative or the Fagaceae family. It is not clear which of the two findings are more indicative as a comparison with this thesis' results. An educated guess will likely be to consider the findings of Mölder et al., (2010) and Jäggi et al., (2002) as a more accurate reference to assess the validity of the carbon isotope measurements made in this thesis.

Another source of uncertainties can be that the measurements for the $d^{13}C$ data were done using whole wood instead of the more appropriate cellulose extraction. Woody tissues are a mixture of different organic molecules composed of mainly α-cellulose, hemicelluloses, lignin, and other solvent extractable substances such as resins and sugars. Whole wood measurements consist in milling the entire tree-ring, de facto utilizing for the analysis the many components that the latter is made of. On the other hand, the extraction focuses on removing all other wood components, leaving only the α-cellulose to be analyzed. Both methods of measuring carbon isotopes were found to be useful in their own ways, but it was recommended in the literature to prefer cellulose extraction, when possible, since it yields the more reliable results (Epstein et al., 1976; Mischel et al., 2015; Gessler et al., 2014). The main benefits on using cellular extraction are the following; firstly, mobile compounds found in whole wood such as resins and sugars might move along the parenchyma cells and mix between several tree-rings leading potentially to noise from year to year. Also, as mentioned before, mixing can happen also vertically along the tree's stem. Secondly the composition of whole wood is not constant from one year to the other, therefore some tree rings may contain more sugars than other, leading again to more uncertain results. Thirdly, unlike cellulose, lignin usually has inconsistent composition, meaning that the carbon content could vary from the lignin one tree ring to the other. Consequently, cellulose has been defined as the method of choice in $d^{13}C$ analysis even if the procedure is way more time consuming than analyzing with whole wood. (Gessler et al., 2014).

Nevertheless, it was proven in other literature that measurements with whole wood and cellulose extraction are comparable, and they do correlate well with climatic signals (Gessler et al., 2014; Mischel et al., 2015.). In this thesis, the whole wood procedure was chosen mainly because of time management reasons.

Finally, there is the possibility that the absence of height trends in the results are due to errors during the sample preparation process. Maybe the procedure described in Chapter 4.4 were not followed adequately enough to ensure valid results, therefore leading to uncertainties or errors. However, taking into consideration the fact that the raw values of $d^{13}C$ for both Norway spruce and European beech follow the values found in the

literature, one could partially discard the hypothesis of incorrect procedure during the analysis. In this case, there is no certainty that the absence of height trend come from measurement inaccuracies, or it is actually a new finding, and has to be treated as a novelty result.

6.4 Correlating wood anatomy with isotope results

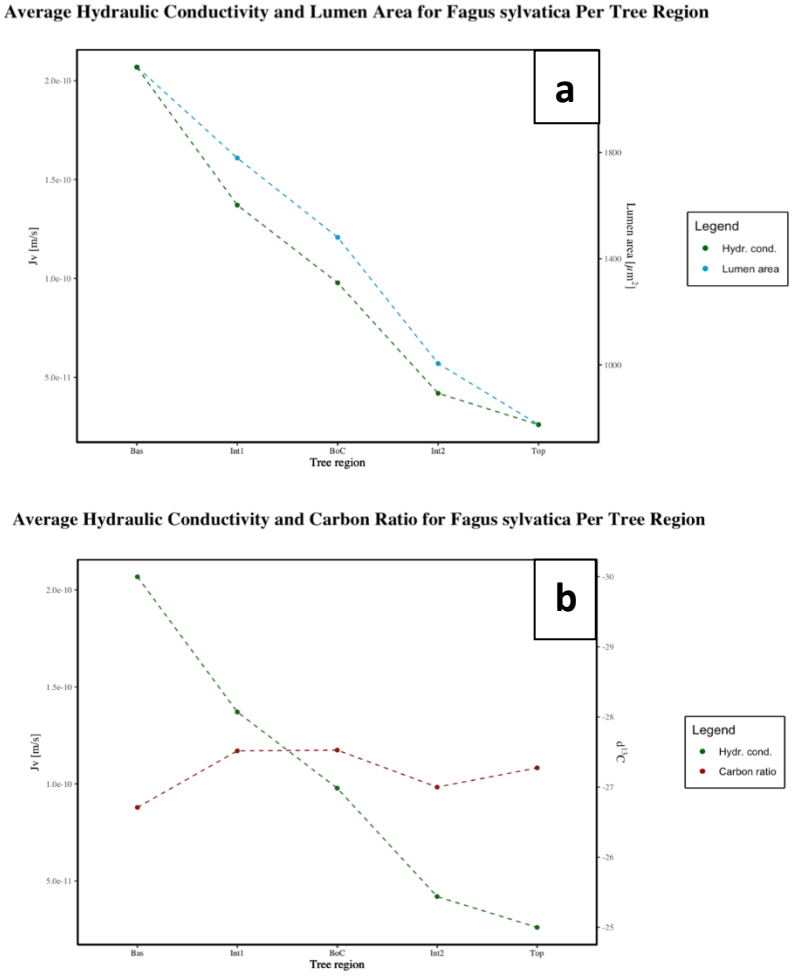

Figure 42 Correlation between hydraulic conductivity and lumen area (a) as well as carbon ratio (b) in *Fagus sylvatica*. The green line indicates hydraulic conductivity, while the blue one represents lumen area and the red one carbon ratio.

As it is shown in Figure 42a, for European beech it is evident how the hydraulic conductivity data correlates perfectly with the wood anatomical measurements (in this case with the lumen area). This makes sense, since one variable is dependent from the other, therefore one should see almost identical trends from the two curves. In Figure 42b, however, the two curves for hydraulic conductivity and $d^{13}C$ do not correlate at all, going against what stated in the literature. In this case, the two curves should show similar trends, since it was found that as the hydraulic conductivity decreases the values for delta carbon 13 should become less negative since at a state of reduced water availability the plant should use the isotope ^{13}C more during photosynthesis compared to a status of standard water availability. (Cherubini et al., 2021; Marshall and Monserud, 1996).

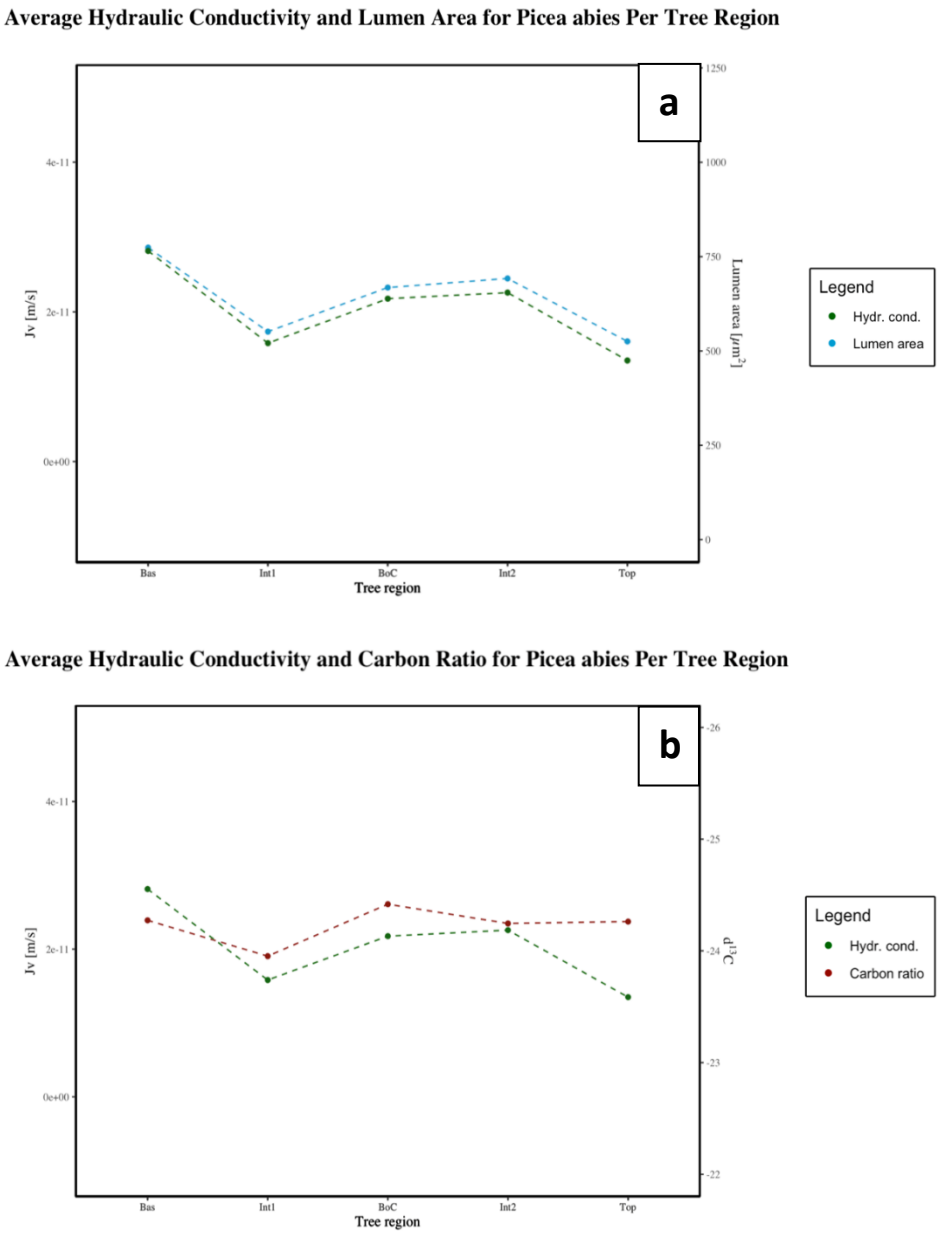

Figure 43 Correlation between hydraulic conductivity and lumen area (a) as well as carbon ratio (b) in *Picea abies*. The green line indicates hydraulic conductivity, while the blue one represents lumen area and the red one carbon ratio.

On the other hand, in the case of Norway spruce, the hydraulic conductivity correlates well with both lumen area and carbon ratio. Figure 43a shows how the curves for Jv and lumen area are almost identical, even more so that the ones for European beech. The same motivation as above is valid here; indeed, the two variables are dependent, therefore showing good correlation between the two curves. In Figure 43b it seems that the hydraulic conductivity correlates well with the $d^{13}C$ measurements, in the sense that both curves remain flat constantly at all tree regions. In this case, it is not possible to assess with certainty if the two curves correlate because of causality or if they show similar trends just because they both do not respond at all with height. As mentioned before, the literature indicated that both curves should show a height related trend. The first should taper with height, while the second should become less negative, and this should apply to all vascular plants.

7 Conclusion

The aim of this thesis was to investigate height trends in wood anatomical and isotope data in two common tree species, namely European beech, and Norway spruce. Further, the focus was on finding possible correlations between the two analyses to see if it were possible to answer questions about tree mortality and maximum height.

Summarizing, the European beech was found to taper with height, meaning that their conduits' size decreased with increasing height and at the same time their hydraulic conductivity followed the same trend. On the other hand, in the Norway spurce samples no particular height trend was found, both for conduit size and also for hydraulic conductivity. Furthermore, for both species the carbon isotope data did not show any height related trend. In particular, $d^{13}C$ remained constant around the same values at each different tree region for all six studied trees. However, it was found in the literature that $d^{13}C$ should show less negative results with increasing height.

Going back to the initial research hypotheses, it is possible to see whether the previously made prediction for this thesis were accurate or not.

Firstly, as already mentioned, hypothesis (**i.**) "*The lumen size of the cells of both plant species will decrease going up towards the top of the tree; at the same time isotopic carbon measurements will reflect this trend as well*" is true only for European beech, in the sense that the lumen size has indeed decreased going upwards from the base to the top of the tree. However, the same cannot be said for Norway spruce. Also, isotopic measurements did not show this trend in both species.

The second hypothesis (**ii.**) "*Interspecific differences will be found between European beech and Norway spruce for both wood anatomy and carbon isotope analyses*" is most likely confirmed. Indeed, for all measurements, the average values for European beech and Norway spruce were found to be considerably different between each other. In the case of lumen area and hydraulic conductivity, European beech showed bigger conduit sizes, and consequently higher hydraulic conductivity than Norway spruce. This difference was more pronounced in tree-regions closer to the base of the tree, while going upwards these differences became always smaller, so that at the upper most tree-regions the values became almost comparable between the two species. These findings matched the ones from the literature. On the other hand, the average values for $d^{13}C$ were higher in Norway spruce than European beech and the trend was constant throughout all investigated tree-regions. Also in this case, the findings matched the literature.

For the third research hypothesis (**iii.**) "*Hydraulic constraints will be found to limit tree height after a certain threshold*" is difficult to say whether it is confirmed or not. Even if one takes into consideration only the European beech, which was found to taper with height, it is still difficult to state with clarity that the decrease in hydraulic conductivity was limiting tree height. The most educated guess is to say that even if at the upper most tree regions, hydraulic conductivity was assuming values close to zero, this did not limit completely tree growth, and as such, maximum tree height was not reached. A possible explanation for this is to look at the theoretical maximum height for European beech at around 50 m. This value is well over the highest point of any of the studied trees, which max out at around 32 m.

As briefly mentioned in the conclusion of hypothesis (**i.),** the fourth and final hypothesis (**iv.**) "*13C/12C will by lower in wood of higher parts of the tree, due to higher consumption of 13C for photosynthesis*" was not confirmed by the results of this thesis. Both theoretically and according to pre-existing literature, this should have been the case. However, in this thesis' results both species presented values for carbon ratio that were constant at every tree height and did not show any noteworthy height trend.

In the end, it can be said that this work produced the expected results only partially. The main issues are found in the wood anatomical data for Norway spruce, as well as the carbon isotope data for both species. On the other hand, the ring-width data for both species and the wood anatomical results for European beech were found to be coherent with the past climatic history and literature.

The next step in this project is to investigate thoroughly where the issues with the unexpected results come from. It is important to verify if the lack of tapering as well as the lack of increase in $d^{13}C$ are due to measurement errors or if they are actually novelty results. The best way to do that will be to redo all measurements for a second time to see if there are discrepancies between the new and the old results. More specifically, to improve the wood anatomical results, it would be better if all microsection will be cut once more, and this time they should be made thinner and smaller in size. This could allow the utilization of the more precise ROXAS software to analyze them. Moreover, during the cell detection process with the software, it should have been more correct to use both earlywood and latewood for the analysis. On the other hand, to improve isotope results, probably the whole procedure has to be repeated, starting with the splitting of the rings. If one were to proceed again with whole wood analysis, it is important to make sure that there is no contamination from the sample to sample and from the outside. Alternatively, there is the possibility to conduct cellulose extraction this time, to see whether there are considerable differences between the two methods and to see if the latter is more truthful than the first.

Lastly, it could be interesting to investigate the validity of the WBE model proposed by West et al., (1999), since it technically states that plants could growth almost indefinitely as long as conditions such as water and nutrient availability are met. It could be of interest to see if it is possible to connect the results from this thesis to those of West and colleagues, with the goal of better understanding maximum tree height.

8 Bibliography

8.1 Literature references

Anfodillo, T., Carraro V., Carrer, M., Fior, C., Rossi, S., 2005, Convergent tapering of xylem conduits in different woody species, *New Phytologist*, Vol. 169, pp. 279-290.

Anfodillo T., Petit, G., 2009, Plant physiology in theory and practice: An analysis of the WBE model for vascular plants, *Journal of Theoretical Biology*, pp. 1-18.

Baltensweiler, W., Weber, U.M., Cherubini, P., 2007, Tracing the influence of learch-bud-moth insect outbreaks and weather conditions on larch tree-ring growth in Engadine (Switzerland), *Oikos*, Vol. 17, No. 2, pp. 161-172.

Becker, A., 2000, The Jura Mountains – an active foreland fold-and-thrust belt?" *Tectonophysics*, Vol. 321, No. 4, pp. 381-406.

Bloos, G., Dietl, G., Schwiegert, G., 2005, Der Jura Süddeutschlands in der Stratigraphischen Tabelle von Deutschland 2002, *Newsletter on Stratigraphy*, Vol. 41, pp. 263-277.

Bose, A.K., Gessler, A., Bolte, A., Bottero, A., Buras A., Cailleret, M., Camarero, J.J., Haeni, M., Heresm A.M., Hevia, A., Lévasque, M., Lineares, J.C., Martinez-Vilalta, J., Matias, L., Menzel, A., Sánchez-Salguero, R., Saurer, M., Vennetier, M., Ziche, D., Rigling, A., 2020, Growth and resilience of Scots pine to extreme droughts across Europe depend on predrought growth conditions, *Global Change Biology*, Vol. 1, pp. 1-17.

Bryant, D.A., Frigaard, N.U., 2006, Prokaryotic photosynthesis and phototrophy illuminated, *Trends in Microbiology*, Vol. 14, No. 11, pp. 488-496.

Buras, A., Rammig, A., Zang, C.S., 2019, Quantifying impacts of the drought 2018 on European ecosystems in comparison to 2003, *Biogeosciences*, pp. 1-23.

Burns, M.J., 1976, A Guide to Measuring Tree-Ring Widths, Laboratory of Tree-Ring Research of the University of California.

Carlón Allende, T., Villanueva Diaz, J., Castro, G.S., Mendoza, M.E., Macías, J.L., 2021, Tree rings as indicators of climatic variation in the Trans-Mexican Volcanic Belt, central Mexico, *Ecological Indicators*, Vol. 120, pp. 1-12.

Carrer, M., Nola, P., Eduard, J.L., Motta, R., Urbinati, C., 2007, Regional variability of climate-growth relationships in *Pinus cembra* high elevation forests in the Alps, *Journal of Ecology*, Vol. 95, pp. 1072-1083.

Carteni, F., Deslauriers, A., Rossi, S., Morin, H., De Micco, V., Mazzoleni, S., Giannino, F., 2018, The Physiological Mechanisms Behind the Earlywood-To-Latewood Transition: A Process-Based Modeling Approach, *Frontiers in Plant Science*, Vol. 9, pp. 1-12.

Cernusak, L.A., Ubirena, N., Winter, K., Holotum, J.A.M., Marshall, J.D., Farquahr, G.D., 2013, Environmental and physiological determinants of carbon isotopes discrimination in terrestrial plants, *New Phytologist*, Vol. 200, pp. 950-965.

Chelenmuge, T., Schuldt, B., Dulamsuren, C., Hertel, D., Leuschner, C., Hauck, M., 2015, Stem increment and hydraulic architecture of a boreal conifer (*Larix sibirica*) under constraining microclimates, 2015, *Trees*, Vol. 29, pp. 623-636.

Cherubini, P., Gärtner, H., Esper, J., Dobbertin, M.K., Kaiser, K.F., Rigling, A., Treydte, K., Zimmermann, N.E., Ulrich Bräker, O., 2004, Jahrringe als Archive für interdisziplinäre Umweltforschung, *Schweizerische Zeitung für Forstwesen*, Vol. 6, pp. 162-168.

Cherubini, P., Battipaglia, G., Innes, J.L., 2021, Tree Vitality and Forest Health: Can Tree-Ring Stable Isotopes Be Used as Indicators? *Current Forestry Reports*, Vol. 7, pp. 69-80.

Choat, B., Ball, M.C., Luly, J.G., Holtum, J.A.M., 2005, Hydraulic architecture of deciduous and evergreen dry rainforest tree species form north-eastern Australia, *Trees*, Vol. 19, pp. 305-311.

Douglass, A.E., 1941, Age of Forestdale Ruins Excavated in 1939, *Tree-Ring Bulletin*, Vol. 8, No. 2.

Entry, J., Emmingham, W.H., 2011, Influence of forest age on nutrient availability and storage in coniferous soils of the Oregon Coast Range, *Canadian Journal of Forest Research*, Vol. 25, No. 1, pp. 114-120.

Epstein, S., Yapp, C.J., Hall, J.H., 1976, The determination of the D/H ratio of non-exchangeable hydrogen in cellulose extracted from aquatic and land plants, *Earth and Planetary Science Letters*, Vol. 30, No. 2, pp. 241-251.

Fan, Z.X., Cao, K.F., Becker, P., 2009, Axial and Radial Variations in Xylem Anatomy of Angiosperm and Conifer Trees in Yunnan, China, *IAWA Journal*, Vol. 30, No. 1, pp. 1-13.

Farjon, A. 2017. Picea abies. The IUCN Red List of Threatened Species 2017: e.T42318A71233492. http://dx.doi.org/10.2305/IUCN.UK.2017-2.RLTS.T42318A7123349.

Fritts, H.C., 1976, Tree Rings and Climate, ISBN: 978-0-12-268450-0.

Gärtner, H., Heinrich, 2013, Dendrogeomorphology, *Enciclopedia of Quaternary Science*, Vol. 2, pp. 91-103.

Gärtner, H., Lucchinetti, S., Schweingruber, F.H., 2014, New perspectives for wood anatomical analysis in dendrosciences: The GSL1-microtome, *Dendrochronologia*, Vol. 32, pp. 47-51.

Gaertner, E.E., 1964, Tree Growth in Relation to the Environment, *Botanical Review*, Vol. 30, No. 3, pp. 393-436.

Caudullo, G., Welk, E., San-Miguel-Ayanz, J., 2017. Chorological maps for the main European woody species. Data in Brief 12, 662-666. DOI: 10.1016/j.dib.2017.05.00.

Gessler, A., Ferrio, J.P., Hommel, R., Treydte, K., Werner, R.A., Monson, R.K., 2014, Stable isotopes in tree rings: towards a mechanistic understanding of isotope fractionation and mixing processes from the leaves to the wood, *Tree Physiology*, Vol. 34, No. 8, pp. 796-818.

Higuchi, T., 1997, Formation of Earlywood, Latewood, and Heartwood, In: Biochemistry and Molecular Biology of Wood, *Springer Series in Wood Science*, Springer, Berlin, Heidelberg, ISBN978-3-642-60469-0.

Hirschi, E., Auchmann, R., Martius, O., Brönnimann, S., 2013; The 1945-1949 droughts in Switzerland, *Weather extremes during the past 140 years*, pp. 81-90.

Huber, B., 1943, Über die Sicherheit Jahrringschronologischer Datierung, *Holz als Roh- und Werkstoff*, Vol. 6, pp. 263-268.

Hunt, A.G., Manzoni, S., 2015, Water transport in plants, In: *Networks on Networks*, Ch. 5, pp. 1-14.

Hultine, K.R., Marshall, J.D., 2000, Altitude trends in conifer leaf morphology and stable carbon isotope composition, *Oecologia*, Vol. 123, pp. 32-40.

Jäggi, M., Saurer, M., Fuhrer, J., Siegwolf, R., 2002, The relationship between the stable carbon isotope composition of needle bulk material, starch, and tree rings in *Picea abies*, *Oecologie*, Vol. 131, pp. 325-332.

Jaleel, C.A., Gopi, R., Sankar, B., Gomathinayagam, M., Panneerselvam, R., 2008, Differential responses in water use efficiency in two varieties of *Catharanthus roseus* under drought stress, *Comptes Rendus Biologes*, Vol. 331, No. 1, pp. 42-47.

Jarvis, P.G., McNaughton, K.G., 1986, Stomatal Control of Transpiration: Scaling Up from Leaf to Region, *Advances in Ecological Research,* Vol. 15, pp. 1-49.

Kahmen, A., Lustenberger S., Zemp, E., Erny, B., 2017, G-08: The Swiss Canopy Crane Experiment II and the Botanical Garden (University of Basel), University of Basel, Schönbeinstrasse 6, 4056 Basel.

Keitel, C., Matzatakis, A., Rennenberg, H., Gessler, A., 2006, Carbon isotopic composition and oxygen isotopic enrichment in phloem and total leaf organic metter of European beech (*Fagus sylvatica* L.) along climate gradient, *Plant, Cell and Environment,* Vol. 29, pp. 1492-1507.

Koch, G.W., Sillett, S.C., Jennings, G.M., Davis, S.D., 2004, The limits to tree height, *Nature,* Vol. 428, 851-854.

Kotowska, M.M., Hertel, D., Rajab, Y.A., Berus, H., Schuldt, B., 2015, Patterns in hydraulics architecture form roots to branches in six tropical tree species form cacao agroforestry and their relation to wood density and stem growth, *frontiers in Plant Science*, Vol.6, Art. 191, pp. 1-16.

Kozlowski, T., Pallardy, S.G., 1997, Physiology of Woody Plants, *Academic Press,* San Diego, 2 Edition.

Leavitt, S.W., 1993, Environmental information from 13C/12C ratios of woods, *Climate Change in Continental Isotopic Records,* Vol. 78, pp 325-332.

Lev-Yadun, S., and Aloni, R., 1995, "Differentiation of the Ray System in Woody Plants." *Botanical Review*, vol. 61, no. 1, 1995, pp. 45–84. *JSTOR*, http://www.jstor.org/stable/4354247. Accessed 8 Jul. 2022.

Lewis, A.M., Boose, E.R., 1995, Estimating volume flow rates through xylem conduits, *American Journal of Botany*, Vol. 82, No. 9, pp. 1112-1116.

Libby, W.F., 1946, Atmospheric helium three and radiocarbon from cosmic radiation, *Physical Review*, Vol. 69, pp. 671-672.

Marshall, J.D., Monserud, R.A., 1996, Homeostatic gas-exchange parmameters inferred from $^{13}C/^{12}C$ in tree rings of conifers, *Oecologia*, Vol. 105, pp. 13-21.

Martinez, L., 1996, Crossdating – The Basic Principle of Dendrochronology, Laboratory of Tree-Ring Research of the University of Arizona, Last Updated: Feb. 2000.

McElrone, A.J., Choat, B., Gambetta, G.A., Brodensen, C.R., 2013, Water Uptake and Transport in Vascular Plants, *Nature Education Knowledge*, Vol. 4, No. 6.

Mencuccini, M., Martinez-Vilalta, J., Vanderklein, D., Hamid, H.A., Korakaki, E., Lee, S., Michiels, B., 2005, Size-mediated ageing reduces vigour in trees, *Ecology Letters*, Vol. 8, pp. 1183-1190.

Miranda, J.C., Calderaro, C., Cocozza C., Lasserre, B., Tognetti, R., Von Arx, G., 2022, Wood Anatomical Responses of European Beech to Elevation, Land Use Change, and Climate Variability in the Central Apennines, Italy, *Frontiers in Plant Science*, Vol. 13, Art. 855741.

Mischel, M., Esper, J., Keppler, F., Greule, M., Werner, W., 2015, δ2H, δ13C and δ18O from whole wood, α-cellulose and lignin methoxyl groups in *Pinus sylvestris*: a multi-parameter approach, *Isotopes in Environmental and Health Studies*, pp. 1-17.

Mölder, I., Leuschner, C., Leuschner, H.H., 2010, $\delta^{13}C$ signature of tree rings and radial increment of *Fagus sylvatica* trees as dependent on tree neighborhood and climate, *Trees*, Vol. 25, pp. 215-229.

Nonweiler, T.R.F., 1975, Flow of biological fluids through non-ideal capillaries, *Encyclopedia of Plant Physiology*, 1, 474-477.

Pesendorfer, M.B., Ascoli, D., Bogdziewicz, M., Hacket-Pain, A., Pearse, I.S., Vacchiano, G., 2021, The ecology and evolution of synchronized reproduction in long-lived plants, *Philosophical Transaction Society B*, Vol. 376.

Petras, R., Bosel, A.M., Mecko, J., Oszalànyi, J., Popa, I., 2014, Height-diameter models for mixed-species forests consisting of spruce, fir, and beech, *Folia Forestalia Polonica*, Vol. 56, No. 2, pp. 93-104.

Petrik, P., Petek-Petrik, A., Kurjak, D., Mukarram, M., Klein, T., Gömöry, D., Strelcova, K., Frydl, J., Konopkova, A., 2022, Interannual adjustments in stomatal and leaf morphological traits of European beech (*Fagus sylvatica* L.) demostrate ist climate change acclimation potential, *Plant Biology*, pp. 1-10.

Pickard, W.F., 1981, The ascent of sap in plants. *Progress in Biophysics and Molecular Biology*, Vol. 37, pp. 181-229.

Pohl, K.A., Hadley, K.S., Arabas, K.B., 2006, Decoupling Tree-Ring Signatures of Climatic Variation, Fire, and Insect Outbreaks in Central Oregon, *Tree-Ring Research*, Vol. 62, No. 2, pp. 37-50.

Prendin, A.L., Mayr, S., Beikircher, B., von Arx, G., Petit, G., 2018, Xylem anatomical adjustments prioritize hydraulic efficiency over safety as Norway spruce trees grow taller, *Tree Physiology*, Vol. 38, pp. 1088-1097.

Rossi, L., Sebastiani, L., Tognetti, R., d'Andria, R., Morelli, G., & Cherubini, P. (2013). Tree-ring wood anatomy and stable isotopes show structural and functional adjustments in olive trees under different water availability. *Plant and Soil*, *372*(1/2), 567–579. http://www.jstor.org/stable/42953083.

Rother, M.T., Huffmann, J.M., Harley, G.L., Platt, W.J., Jones, N., Robertson, K.M., Orzell, S.L., 2018, Cambial Phenology Informs Tree-Ring Analysis of Fire Seasonality in Coastal Plain Pine Savannas, *Fire Ecology, Vol. 14, No. 1, pp. 164-186.*

Rozendaal, D.M.A., Phillips, O.L., Lewis, S.L., Affum-Baffoe, K., Alvarez-Davila, E., Andrade, A., Aragao, L.E.O.C., Araujo-Murakami, A., Baker, T.R., Bánki, O., Brienen, R.J.W., Camargo, J.L.C., Comiskey, J.A., Djuikuouo Kamadem, M.N., Fauset, S., Lovejoy, T., Malhi, Y., Marimon, B.S., Marimon Jr., B.H., Marshall, A.R., Neill, D.A., Vargas, P.N., Pitman, N.C.A., Poorter, L., Reitsma, J., Silveira, M., Sonké, B., Sunderland, T., Taedoumg, H., Steege, H., Terborgh, J.W., Umetsu, R.K., van der Heijden, G.M.F., Vilanova, E., Vos, V., White, L.J.T., Willock, S., Zemagho, L., Vanderwel, M.C., 2020, Competition influences tree growth, but not mortality, across environmental gradients in Amazonia and tropical Africa, *Ecology*, Vol. 101, No.7, pp. 1-11.

Ryan, M.G., Yoder, B.J., 1997, Hydraulic Limits to Tree Height and Tree Growth, *Bioscience Vol. 47, No.4*, pp. 235-242.

Schulze, E.D., Kelliher, F.M., Körner, C., Lloyd J., Leuning, R., 1994, Relationships among maximum stomatal conductance, ecosystem surface conductance, carbon assimilation rate, and plant nitrogen nutrition: A global ecology scaling exercise, *Annual Review of Ecology and Systematics*, Vol. 25, pp. 629-660.

Schweingruber, F.H., 1988, Tree Rings: Basics and Applications of Dendrochronology. *Kluwer Academic Publishers*. ISBN: 9788578110796.

Schweingruber, F.H., 1996, Tree Rings and Environment. Dendroecology. Ed. by S. Swiss Federal Institute for Forest, L. Research. Birmensdorf, p. 609.

Sheldrake, A.R., 2022, Cellular senescence, rejuvenation and potential immortality, *Proceedings Royal Society B*, Vol. 289, pp. 1-9.

Shigo, A., 1986, A new tree biology dictionary, p. 90, *ISBN 0-943563-05-4*.

Sinclair, T.R., Tanner, C.B., Bennet, J.M., 1984, Water-Use Efficiency in Crop Production, *American Institute of Biological Sciences*, Vol. 34, No. 1, pp. 36-40.

Smith, B.N., Epstein, S., 1971, Two Categories of $^{13}C/^{12}C$ Ratios for Higher Plants, *Plant Physiology*, Vol. 47, pp. 380-384.

Speer, J.H., 2010, Fundamentals of tree-ring research. University of Arizona, Ch. 1-3, *ISBN: B00GA42F4O*.

Sperry, J.S., Nicholas, K.L., Sullivan, J.E., Eastlack, S.E., 1994, Xylem Embolism in Ring-Porous, and Coniferous Trees of Northern Utah and Interior Alaska, *Ecology*, Vol. 75, No. 6, pp. 1736-1757.

Sperry, J.S., Hacke, U.G., Pittermann, J., 2006, Size and Function in Conifer Tracheids and Angiosperm Vessels, *American Journal of Botany*, Vol. 93, No. 10, pp. 1490-1500.

Sullivan, J., 1994. "Picea abies". Fire Effects Information System (FEIS). US Department of Agriculture (USDA), Forest Service (USFS), Rocky Mountain Research Station, Fire Sciences Laboratory. Retrieved 18 November 2009.

Taylor, Ronald J. (1993). "Picea abies". In Flora of North America Editorial Committee (ed.). Flora of North America North of Mexico (FNA). Vol. 2. New York and Oxford.

Trillo, N., Fernández, R.J., 2005, Wheat plant hydraulic properties under prolongated experimental drought: Stronger decline in root-system conductance than in leaf area, *Plant and Soil*, Vol. 277, pp. 277-284.

Tyree, M.T., Sperry, J.S., 1988, Do Woody Plants Operate Near the Point of Catastrophic Xylem Dysfunction Caused by Dynamic Water Stress?, *Plant Physiology*, Vol. 88, pp. 574-580.

Tyree, M.T., 2003, The ascent of water, *Nature*, Vol. 423, p. 923.

Visser, R.M., 2021, On the Similarity of Tree-Ring Patterns: Assessing the Influence of Semi-Synchronous Growth Changes on the *Gleichläufigskeitskoeffizient* for Big Tree-Ring Data Sets, *Archaeometry*, Vol 63, No. 1, pp. 204-215.

Von Arx, G., Carrer M., 2013, ROXAS – A new tool to build centuries-long tracheid-lumen chronologies in conifers, *Dendrochronologia*, Vol.32, pp.290-293.

Von Arx, G., Crivellaro, A., Prendin, L., Cufar, K., Carrer, M., 2016, Quantitative Wood Anatomy – Practical Guidelines, *Frontiers in Plant Science*, Vol. 7, pp. 1-13.

Wang, D., Chen, Y., Li, W., Li, Q., Lu, M., Zhou, G., Chai, G., 2021, Vascular Cambium: The Source of Wood Formation, *Frontiers in Plant Science*, Vol. 12, pp. 1-8.

Watson, J.M., Riha, K., 2011, Telomers, Aging and Plants: From Weeds to Methuselah – A Mini Review, *Gerontology*, Vol. 57, pp. 129-136.

West, G.B., Brown, J.H., Enquist, B.J., 1999, A general model for the structure and allometry of plant vascular systems, *Nature*, Vol. 400, pp. 664-667.

Wimmer, R., 2002, Wood anatomical features in tree-rings as indicators of environmental change, *Dendrochonologia*, Vol. 20, No. 1-2, pp. 21-36.

Woodley, E.J., Loader, N.J., McCarroll, D., Young, G.H.F., Robertson, I., Heaton, T.H.E., Gagen, M.H., Warham, J.O., 2012, High temperature pyrolisi/gas chromatography/isotope ration mass spectrometry: simultaneous measurement of the stable isotopes of oxygen and carbon in cellulose, *Rapid Communication in Mass Spectroscopy*, Vol. 26, pp. 109-114.

Wühlisch, G. (2008). "European beech – Fagus sylvatica". *EUFORGEN Technical Guidelines for Genetic Conservation and Use*. Retrieved 07.07.2022.

Yoder, B.J., Ryan, M.G., Waring, R.H., Schoettle, A.W., Kaufmann, M.R., 1994, Evidence of Reduced Photosynthetic Rates in Old Trees, *Forest Science*, Vol.40, No. 3, pp. 513-527.

Zhu, L., Cooper, D.J., Yuan, D., Li, Z., Zhang, Y., Liang, H., Wang, X., 2020, Regional Scale Temperature Rather than Precipitation Determines Vessel Features in Earlywood of Manchurian Ash in Temperate Forests, *Geographical Research: Biogeosciences*, Vol. 125, pp. 1-15.

Zimmermann, J., Link, R.M., Hauck, M., Leuschner, C., Schuldt, B., 2021, 60-year record of stem xylem anatomy and related hydraulic modification under increased summer drought in ring- and diffuse-porous temperate broad-leaved tree species, *Trees*, Vol. 35, pp. 919-937.

8.2 Website references

GESTIS, 2022, O-xylol, Link: https://gestis.dguv.de/data?name=018470, Last visited, 27.09.2022.

Infoflora.ch, 2022a, Fagus sylvatica L., Link: https://www.infoflora.ch/it/flora/fagus-sylvatica.html, Last visited: 21.09.2022.

Infoflora.ch, 2022b, Picea abies L., Link: https://www.infoflora.ch/it/flora/picea-abies.html, Last visited: 21.09.2021.

Meteoblue.com, 2022, Basel-Landschaft, Switzerland, Link: https://www.meteoblue.com/en/weather/historyclimate/climatemodelled/h%C3%B6lstein_switzerland_2660311, Last visited: 03.08.2022.

Royal Botanic Garden, 2017, Fagus sylvatica L., in: Plants of the World Online, Link: https://powo.science.kew.org/taxon/urn:lsid:ipni.org:names:305836-2, Last visited: 15.08.2021.

Sigma Aldrich, 2022a, Astra Blau, Link: https://www.sigmaaldrich.com/CH/de/product/sial/363405, Last visited: 27.09.2022.

Sigma Aldrich, 2022b, Safranin O, Link: https://www.sigmaaldrich.com/CH/de/product/sial/s2255, Last visited: 27.09.2022.

Sigma Aldrich, 2022c, Toluidinblau O, Link. https://www.sigmaaldrich.com/CH/de/product/sial/t3260, Last visited: 27.09.2022.

Sigma Aldrich, 2022d, Kanadabalsam, Link: https://www.sigmaaldrich.com/CH/de/substance/canadabalsam123458007474, Last visited: 27.09.2022

Swiss Canopy Crane II, Department for Environmental Sciences, Link: https://ppe.duw.unibas.ch/en/sccii/, Last visited: 03.08.2022.

University of Basel, Swiss Canopy Crane II, Department for Environmental Sciences, Link: https://ppe.duw.unibas.ch/en/sccii/, Last visited: 03.08.2022.

9 Appendix

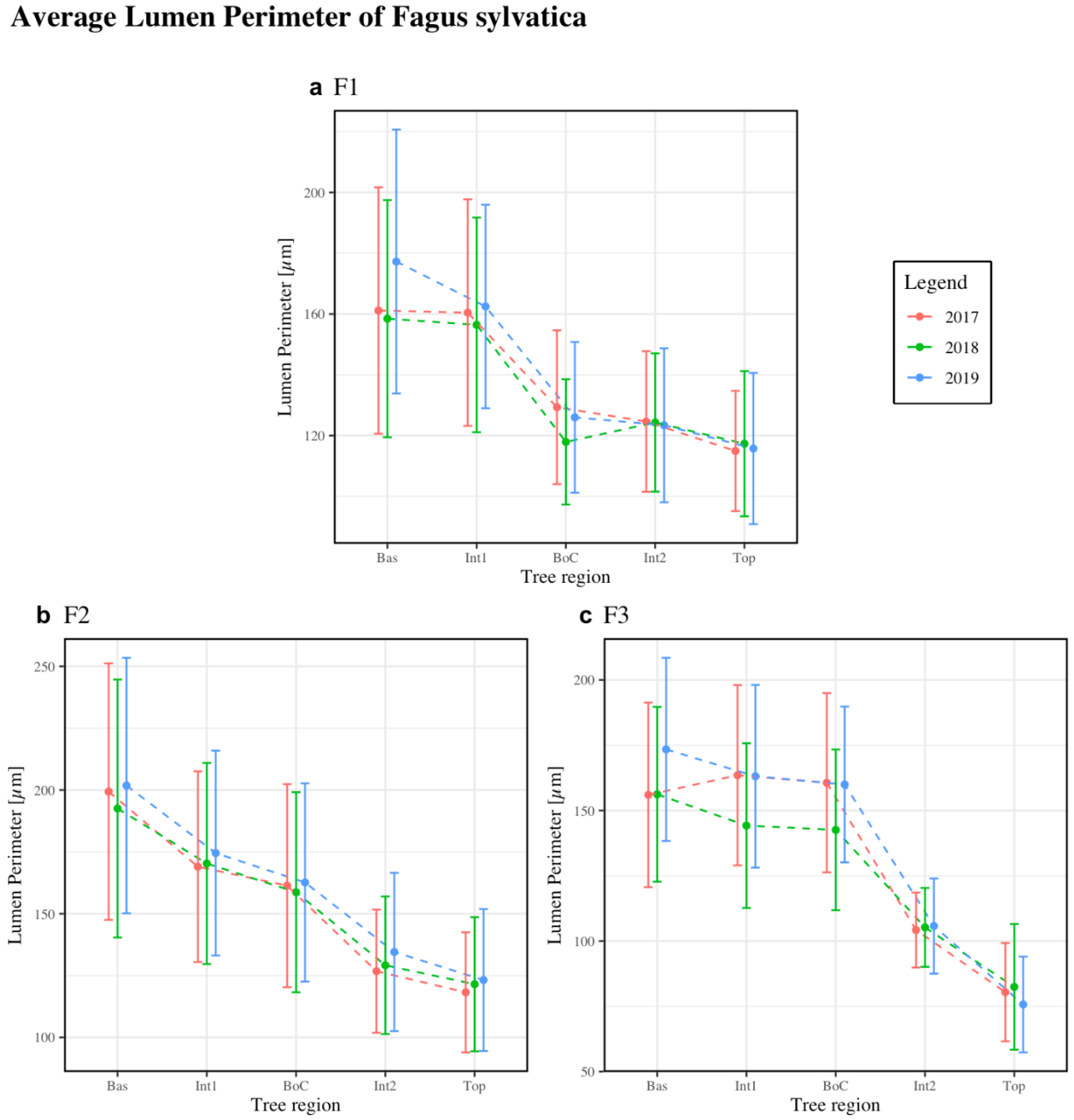

Figure 44 Average lumen perimeter for *Fagus sylvatica* (F1, F2, F3) for the years 2017, 2018, and 2019.

Average Lumen Perimeter of Picea abies

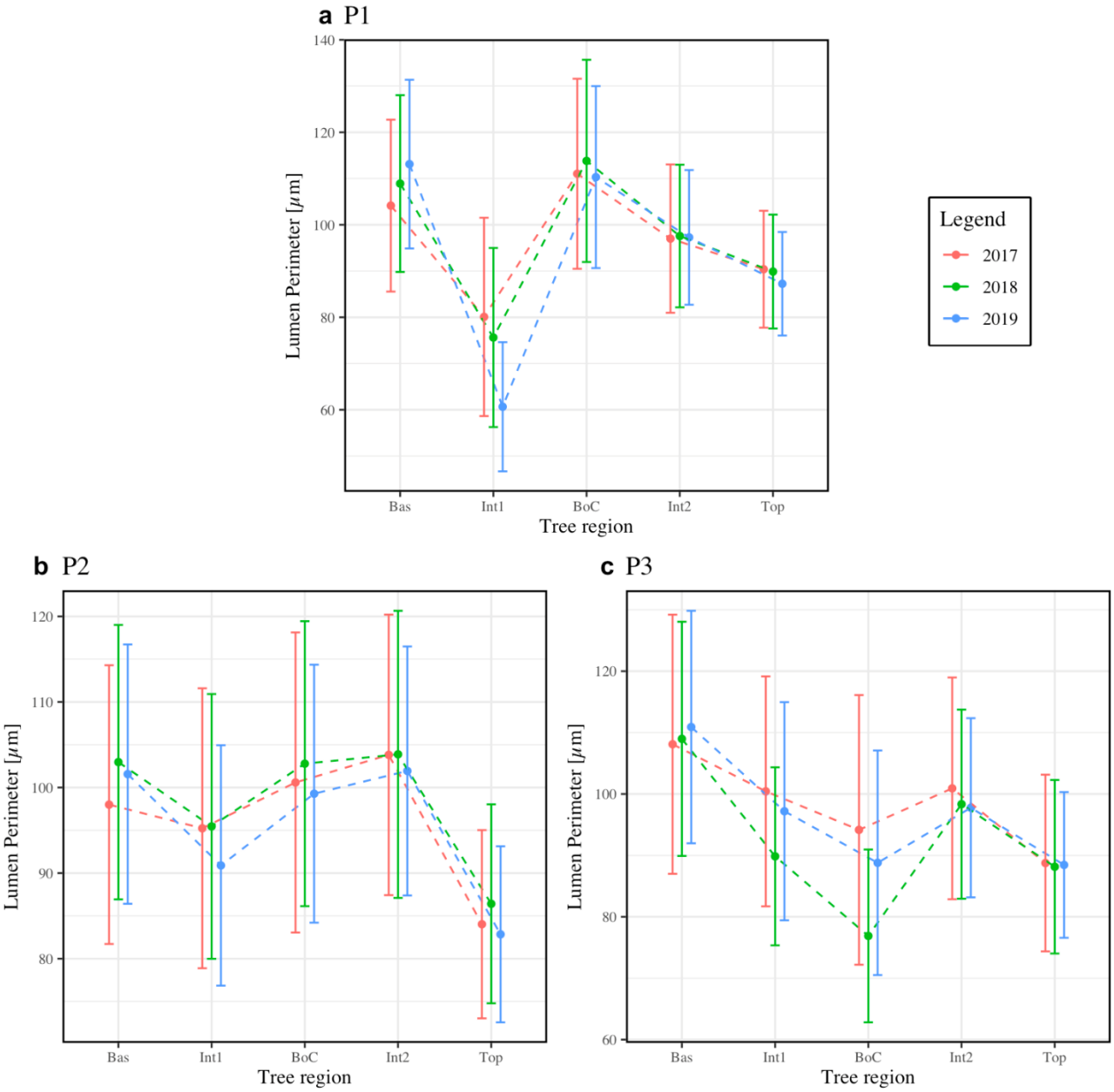

Figure 45 Average lumen perimeter for *Picea abies* (P1, P2, P3) for the years 2017, 2018, and 2019.

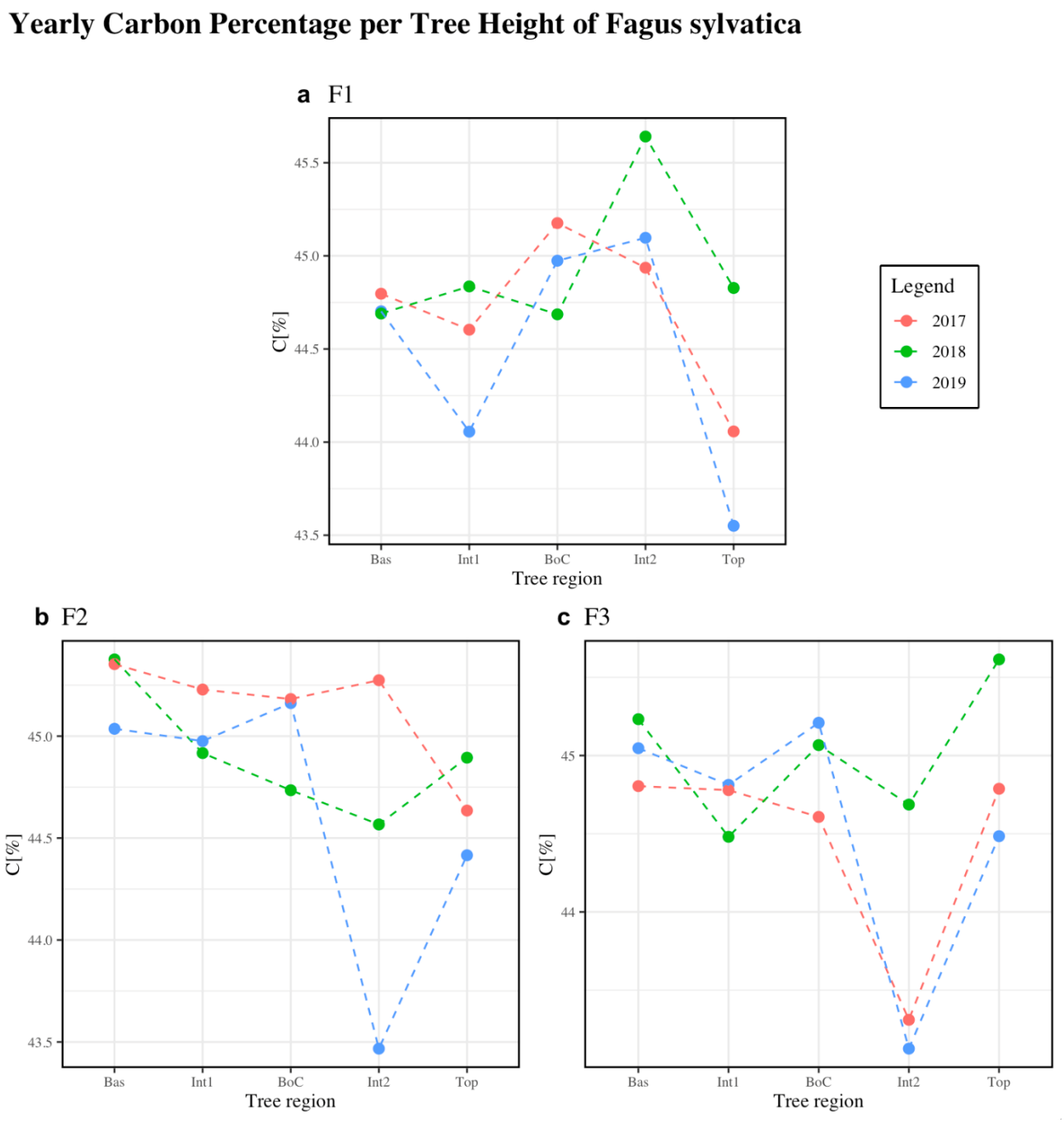

Figure 46 Carbon percentage for *Fagus sylvatica* (F1, F2, F3) for the years 2017, 2018, and 2019.

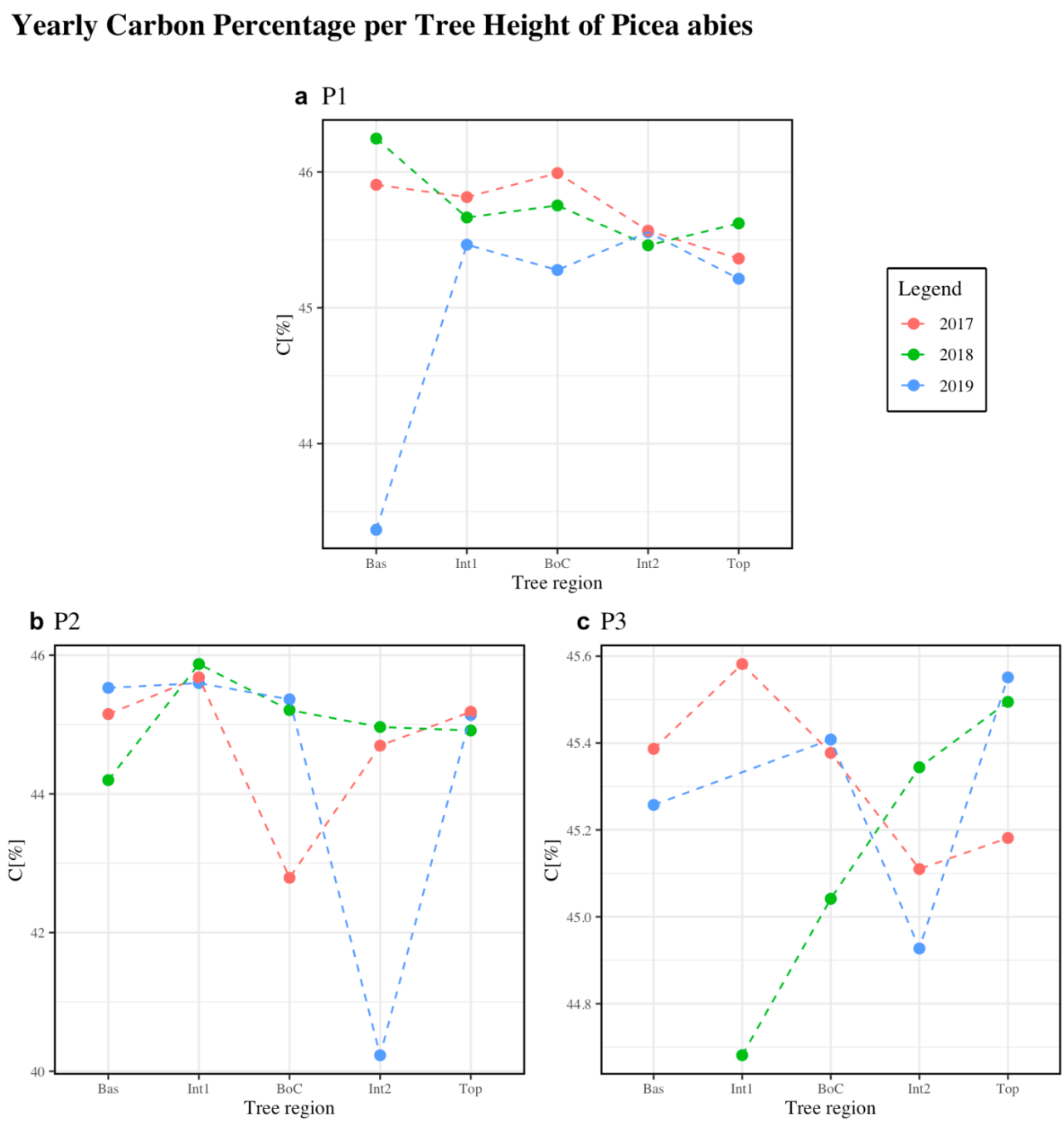

Figure 47 Carbon percentage for *Picea abies* (P1, P2, P3) for the years 2017, 2018, and 2019.

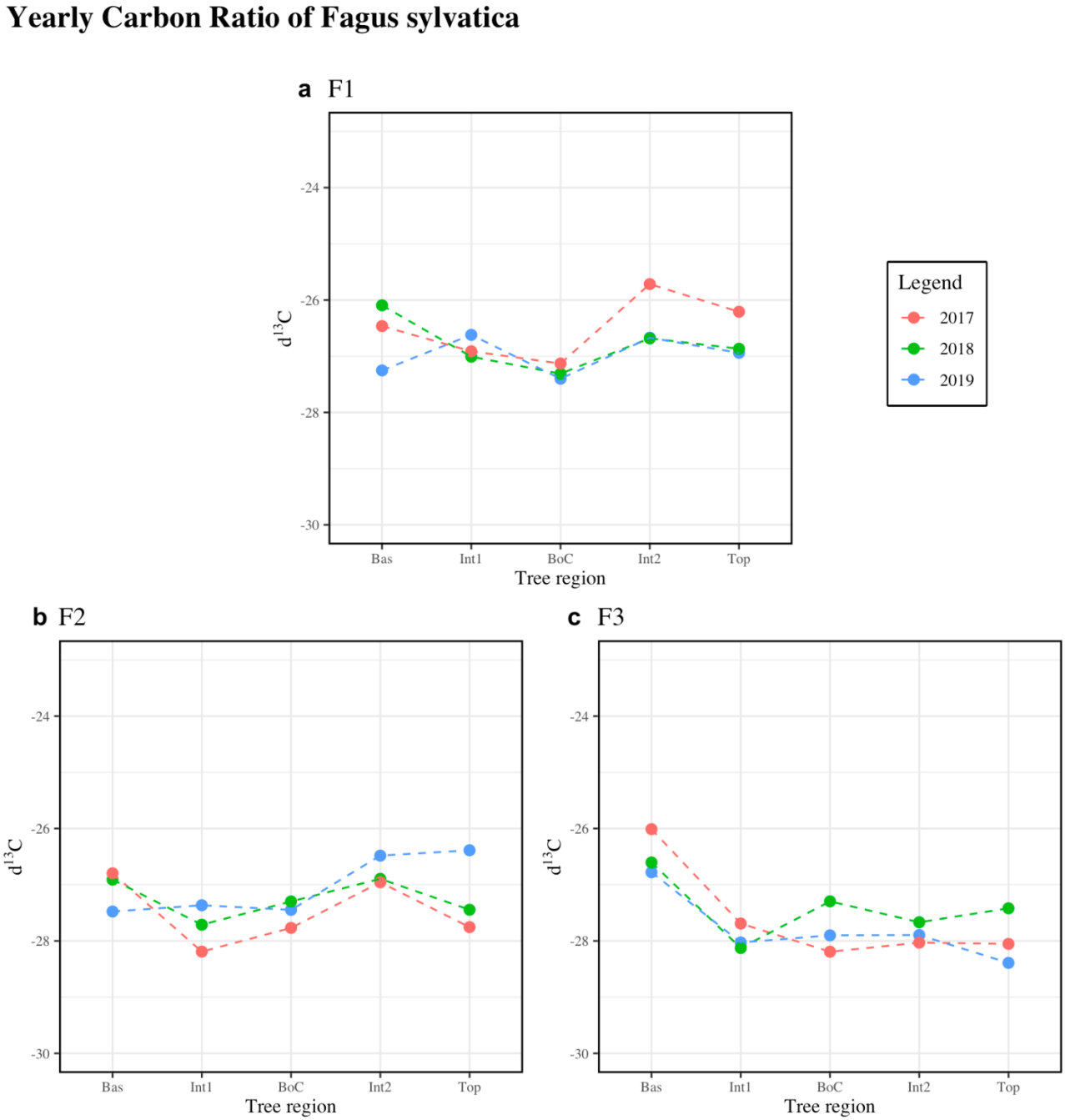

Figure 48 Carbon ratio ($d^{13}C$) for *Fagus sylvatica* (F1, F2, F3) for the years 2017, 2018, and 2019.

Yearly Carbon Ratio of Picea abies

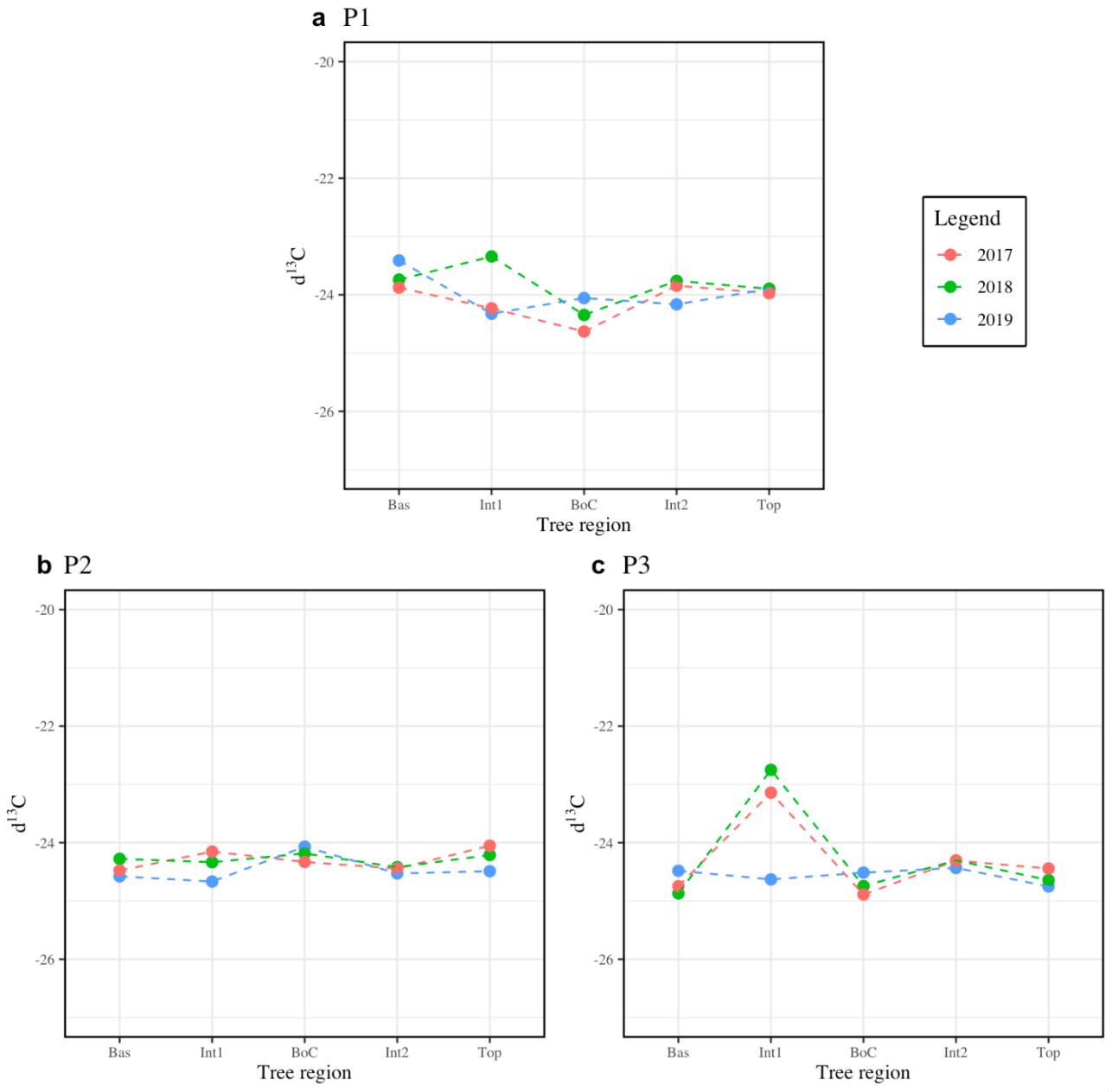

Figure 49 Carbon ratio ($d^{13}C$) for *Picea abies* (P1, P2, P3) for the years 2017, 2018, and 2019.

Figure 50 *Fagus sylvatica* Samples after being sorted and labelled (old names are shown, Mattias Barigazzi)

Figure 51 *Picea abies* samples after being sorted and labelled (old names are show, Mattias Barigazzi)

Table 4 Isotope analysis master table

samp_no	samp_ID	samp_year	treeregion	samp_weight [mg]	$d^{13}C$	C [%]	$d^{15}N$	N [%]	outlier
1	P2_0m	2019	Bas	0.957	-24.58	45.53	4.51	0.73	NO
2	P2_0m	2018	Bas	1.025	-24.28	44.20	5.74	1.68	NO
3	P2_0m	2017	Bas	1.025	-24.48	45.15	1.56	0.47	NO
4	P2_10m	2019	Int1	1.023	-24.67	45.60	-3.30	0.36	NO
5	P2_10m	2018	Int1	0.968	-24.33	45.87	1.56	0.60	NO
6	P2_10m	2017	Int1	1.002	-24.15	45.68	2.37	0.73	NO
7	P2_16m	2019	BoC	0.972	-24.07	45.36	5.51	1.50	NO
8	P2_16m	2018	BoC	1.050	-24.18	45.21	-5.26	0.27	NO
9	P2_16m	2017	BoC	0.982	-24.33	42.79	4.65	1.23	NO
10	P2_24m	2019	Int2	1.029	-24.53	40.23	3.24	0.93	NO
11	P2_24m	2018	Int2	1.033	-24.42	44.96	-1.89	0.33	NO
12	P2_24m	2017	Int2	1.043	-24.44	44.70	2.90	0.92	NO
13	P2_30m	2019	Top	0.976	-24.49	45.14	0.28	0.53	NO
14	P2_30m	2018	Top	1.038	-24.21	44.91	-6.29	0.26	NO
15	P2_30m	2017	Top	1.017	-24.05	45.18	-0.59	0.36	NO
16	P1_0m	2019	Bas	0.986	-23.41	43.37	0.60	0.79	NO
17	P1_0m	2018	Bas	0.978	-23.74	46.25	-0.72	0.60	NO
18	P1_0m	2017	Bas	1.035	-23.88	45.91	-1.24	0.36	NO
19	P1_8m	2019	Int1	1.015	-24.32	45.46	-0.79	0.54	NO
20	P1_8m	2018	Int1	1.008	-23.34	45.66	4.02	1.46	NO
21	P1_8m	2017	Int1	0.998	-24.23	45.81	4.30	1.00	NO
22	P1_16m	2019	BoC	0.981	-24.06	45.28	1.94	0.69	NO
23	P1_16m	2018	BoC	0.986	-24.35	45.75	2.71	0.89	NO
24	P1_16m	2017	BoC	1.027	-24.63	45.99	0.55	0.52	NO
25	P1_24m	2019	Int2	0.990	-24.16	45.56	1.97	0.80	NO
26	P1_24m	2018	Int2	1.029	-23.76	45.46	-0.32	0.49	NO
27	P1_24m	2017	Int2	1.012	-23.84	45.57	-4.91	0.25	NO
28	P1_32m	2019	Top	0.963	-23.90	45.21	-2.72	0.42	NO

29	P1_32m	2018	Top	1.019	-23.90	45.62	-4.10	0.27	NO
30	P1_32m	2017	Top	0.999	-23.97	45.36	-6.63	0.25	NO
31	P3_0m	2019	Bas	1.000	-24.48	45.26	4.45	1.85	NO
32	P3_0m	2018	Bas	0.993	-24.87	60.43	-6.85	0.30	YES
33	P3_0m	2017	Bas	0.974	-24.75	45.39	0.04	0.51	NO
34	P3_8m	2019	Int1	1.030	-24.63	23.60	3.19	0.57	YES
35	P3_8m	2018	Int1	0.989	-22.75	44.68	0.60	0.34	NO
36	P3_8m	2017	Int1	1.044	-23.14	45.58	2.22	0.71	NO
37	P3_14m	2019	BoC	1.023	-24.51	45.41	2.82	0.89	NO
38	P3_14m	2018	BoC	0.974	-24.74	45.04	1.36	0.69	NO
39	P3_14m	2017	BoC	1.046	-24.89	45.38	0.95	0.76	NO
40	P3_24m	2019	Int2	0.968	-24.43	44.93	-2.24	0.42	NO
41	P3_24m	2018	Int2	1.024	-24.30	45.34	-1.69	0.43	NO
42	P3_24m	2017	Int2	1.018	-24.31	45.11	-6.15	0.27	NO
43	P3_32m	2019	Top	0.990	-24.75	45.55	-2.18	0.34	NO
44	P3_32m	2018	Top	0.968	-24.64	45.49	1.56	0.56	NO
45	P3_32m	2017	Top	0.979	-24.44	45.18	1.71	0.72	NO
46	F2_0m	2019	Bas	1.035	-27.48	45.04	-3.79	0.49	NO
47	F2_0m	2018	Bas	1.013	-26.91	45.38	-4.78	0.43	NO
48	F2_0m	2017	Bas	0.979	-26.80	45.35	1.68	0.71	NO
49	F2_10m	2019	Int1	1.002	-27.37	44.98	-3.30	0.58	NO
50	F2_10m	2018	Int1	1.002	-27.71	44.92	-4.66	0.41	NO
51	F2_10m	2017	Int1	1.011	-28.19	45.23	-4.49	0.49	NO
52	F2_18m	2019	BoC	1.046	-27.45	45.16	-3.90	0.45	NO
53	F2_18m	2018	BoC	1.014	-27.30	44.73	3.46	1.30	NO
54	F2_18m	2017	BoC	0.981	-27.77	45.18	-4.95	0.42	NO
55	F2_24m	2019	Int2	0.994	-26.48	43.47	0.41	1.26	NO
56	F2_24m	2018	Int2	0.978	-26.90	44.57	-2.70	0.67	NO
57	F2_24m	2017	Int2	1.015	-26.96	45.27	-3.53	0.48	NO
58	F2_30m	2019	Top	0.987	-26.39	44.42	3.75	1.87	NO
59	F2_30m	2018	Top	1.034	-27.45	44.89	-1.23	0.93	NO

60	F2_30m	2017	Top	0.964	-27.75	44.63	-4.86	0.59	NO
61	F3_0m	2019	Bas	1.013	-26.78	45.05	-4.24	0.39	NO
62	F3_0m	2018	Bas	0.979	-26.60	45.23	0.37	0.63	NO
63	F3_0m	2017	Bas	0.984	-26.01	44.80	-5.99	0.31	NO
64	F3_8m	2019	Int1	0.955	-28.03	44.81	-4.50	0.38	NO
65	F3_8m	2018	Int1	0.977	-28.13	44.48	1.50	0.61	NO
66	F3_8m	2017	Int1	1.029	-27.69	44.78	-1.85	0.45	NO
67	F3_10m	2019	BoC	1.012	-27.90	45.21	1.64	0.79	NO
68	F3_10m	2018	BoC	0.962	-27.30	45.07	-7.30	0.30	NO
69	F3_10m	2017	BoC	1.035	-28.19	44.61	-3.97	0.32	NO
70	F3_24m	2019	Int2	1.023	-27.89	43.13	-1.52	0.62	NO
71	F3_24m	2018	Int2	0.960	-27.67	44.69	-2.77	0.47	NO
72	F3_24m	2017	Int2	1.000	-28.03	43.31	-6.73	0.31	NO
73	F3_26m	2019	Top	1.000	-28.39	44.48	-3.65	0.60	NO
74	F3_26m	2018	Top	0.972	-27.42	45.61	-1.76	0.54	NO
75	F3_26m	2017	Top	1.030	-28.05	44.79	-2.27	0.44	NO
76	F1_0m	2019	Bas	0.983	-27.25	44.70	-5.75	0.45	NO
77	F1_0m	2018	Bas	0.994	-26.09	44.69	2.55	0.98	NO
78	F1_0m	2017	Bas	1.018	-26.46	44.80	-1.47	0.61	NO
79	F1_12m	2019	Int1	1.043	-26.62	44.06	-4.63	0.41	NO
80	F1_12m	2018	Int1	0.987	-27.01	44.84	-4.77	0.44	NO
81	F1_12m	2017	Int1	1.016	-26.91	44.60	-0.19	0.61	NO
82	F1_22m	2019	BoC	0.968	-27.40	44.97	-2.62	0.53	NO
83	F1_22m	2018	BoC	0.983	-27.31	44.69	-3.13	0.47	NO
84	F1_22m	2017	BoC	1.037	-27.13	45.18	-4.92	0.36	NO
85	F1_26m	2019	Int2	1.042	-26.67	45.10	0.74	0.91	NO
86	F1_26m	2018	Int2	0.951	-26.68	45.64	-4.73	0.56	NO
87	F1_26m	2017	Int2	0.958	-25.72	44.94	-2.04	0.57	NO
88	F1_30m	2019	Top	0.965	-26.94	43.55	-3.11	0.73	NO
89	F1_30m	2018	Top	0.973	-26.87	44.83	-0.43	0.72	NO
90	F1_30m	2017	Top	1.012	-26.21	44.06	2.57	0.98	NO

Table 5 Wood anatomy master table

samp_ID	treeregion	samp_year	lum_area [µm²]	SD_lum_area	lum_length [µm]	SD_lum_length	lum_width [µm]	SD_lum_width	lumperi	SD_lumperi
F1_0m	Bas	2017	1786.6	772.6	52.13	14.93	39.66	10.35	160.76	40.48
F1_0m	Bas	2018	1753.0	782.1	50.62	14.32	40.18	11.22	158.98	39.23
F1_0m	Bas	2019	2126.5	904.2	57.43	16.11	43.38	11.42	177.60	44.70
F1_12m	Int1	2017	1716.6	743.3	50.77	14.61	39.60	9.19	162.41	40.00
F1_12m	Int1	2018	1621.5	665.9	48.14	12.86	39.19	9.54	156.84	36.24
F1_12m	Int1	2019	1710.0	628.6	50.66	12.57	40.12	9.16	163.40	34.81
F1_22m	BoC	2017	1182.5	454.2	41.21	10.03	33.85	7.15	129.68	25.98
F1_22m	BoC	2018	968.6	322.8	36.61	7.83	31.12	6.46	118.21	20.83
F1_22m	BoC	2019	1094.4	432.2	40.11	10.94	32.61	6.48	127.49	27.76
F1_26m	Int2	2017	1104.1	435.6	40.68	9.84	32.00	6.92	127.07	27.39
F1_26m	Int2	2018	1062.1	368.2	39.04	9.39	32.13	6.55	125.74	25.21
F1_26m	Int2	2019	1077.0	452.9	39.14	10.01	32.40	7.57	126.23	34.81
F1_30m	Top	2017	917.5	301.0	35.76	7.41	30.43	5.94	116.38	22.40
F1_30m	Top	2018	911.5	307.9	36.28	8.55	29.76	5.91	117.23	23.74
F1_30m	Top	2019	925.2	391.7	36.37	9.51	29.78	6.49	118.32	29.58
F2_0m	Bas	2017	2699.1	1310.1	63.59	17.64	49.81	14.05	200.21	53.72
F2_0m	Bas	2018	2580.9	1277.7	60.56	18.49	49.42	14.35	193.20	53.32
F2_0m	Bas	2019	2806.0	1363.1	63.93	18.53	51.53	14.60	204.02	55.69
F2_10m	Int1	2017	1968.1	792.3	52.86	14.12	44.05	10.65	168.96	38.86
F2_10m	Int1	2018	2020.6	882.2	53.16	14.62	44.69	11.22	170.90	41.21
F2_10m	Int1	2019	2109.8	925.1	53.66	15.06	46.13	11.50	176.16	45.53
F2_18m	BoC	2017	1831.2	899.4	50.57	14.69	42.23	11.38	163.97	46.21
F2_18m	BoC	2018	1801.5	930.7	49.52	15.43	42.07	11.61	162.24	50.48
F2_18m	BoC	2019	1854.5	943.5	51.81	15.83	41.48	11.06	169.19	57.49
F2_24m	Int2	2017	1174.9	462.3	40.18	10.10	34.73	7.61	128.86	29.14
F2_24m	Int2	2018	1214.6	503.5	41.37	10.35	34.68	8.29	131.30	32.04
F2_24m	Int2	2019	1344.3	652.8	43.52	12.29	36.19	9.50	139.25	39.20

F2_30m	Top	2017	1004.5	427.8	37.28	8.88	31.65	7.51	120.14	28.28
F2_30m	Top	2018	1045.0	469.6	38.37	10.86	32.02	7.28	122.94	29.49
F2_30m	Top	2019	1018.0	435.5	37.79	10.04	31.65	7.32	124.53	30.82
F3_0m	Bas	2017	1700.3	693.3	49.56	12.58	40.30	9.47	155.92	35.19
F3_0m	Bas	2018	1759.3	688.7	50.07	12.15	41.61	9.43	156.47	33.91
F3_0m	Bas	2019	2071.3	773.1	55.24	13.26	44.75	10.11	172.48	36.20
F3_8m	Int1	2017	1813.7	695.6	52.39	13.50	41.03	9.00	164.01	35.38
F3_8m	Int1	2018	1405.8	561.4	44.83	11.66	36.88	8.20	144.64	32.52
F3_8m	Int1	2019	1780.2	710.3	51.06	13.32	41.17	9.37	163.81	35.82
F3_10m	BoC	2017	1781.2	666.2	51.94	13.14	40.64	8.29	160.91	35.10
F3_10m	BoC	2018	1409.8	545.2	45.10	11.58	36.98	8.01	143.18	31.55
F3_10m	BoC	2019	1758.9	605.6	50.99	11.52	41.65	8.59	161.23	32.15
F3_24m	Int2	2017	788.6	210.3	32.57	5.67	29.01	5.09	105.00	16.15
F3_24m	Int2	2018	777.3	194.7	33.76	7.15	27.41	4.53	106.29	15.66
F3_24m	Int2	2019	804.5	254.7	33.23	6.46	28.94	5.27	105.08	18.40
F3_26m	Top	2017	485.2	208.5	25.61	6.82	22.07	5.99	80.54	19.38
F3_26m	Top	2018	496.4	253.8	26.14	9.19	21.45	6.85	81.21	25.25
F3_26m	Top	2019	427.0	187.6	24.36	6.44	20.42	5.45	76.09	19.58
P1_0m	Bas	2017	745.5	259.0	31.98	7.09	24.83	5.71	104.75	19.93
P1_0m	Bas	2018	793.9	265.3	33.24	7.12	25.54	5.85	109.43	20.21
P1_0m	Bas	2019	836.1	252.1	34.95	7.20	25.62	5.43	113.47	19.17
P1_8m	Int1	2017	480.8	240.3	22.24	6.44	23.96	6.99	80.54	22.23
P1_8m	Int1	2018	431.6	214.7	23.80	6.80	20.37	5.88	76.31	20.42
P1_8m	Int1	2019	287.7	125.0	17.03	3.92	19.49	5.01	59.97	13.99
P1_16m	BoC	2017	793.1	271.4	30.66	6.26	27.34	6.84	111.95	22.09
P1_16m	BoC	2018	801.5	276.3	30.12	6.39	27.99	7.31	114.77	23.34
P1_16m	BoC	2019	750.1	232.4	29.00	5.31	27.20	6.55	111.47	21.55
P1_24m	Int2	2017	662.9	212.6	27.44	5.69	25.74	5.55	97.36	16.81
P1_24m	Int2	2018	650.1	196.3	26.72	5.20	25.92	5.78	97.85	15.95
P1_24m	Int2	2019	643.3	182.1	26.60	4.94	25.58	5.31	97.66	15.15
P1_32m	Top	2017	577.0	154.2	26.13	4.87	24.97	4.58	90.73	13.17

P1_32m	Top	2018	561.4	149.8	25.03	4.36	25.04	4.99	90.35	13.06
P1_32m	Top	2019	537.1	131.5	24.57	3.88	24.71	4.63	87.62	11.86
P2_0m	Bas	2017	698.6	217.2	30.39	6.04	25.31	5.17	98.09	16.40
P2_0m	Bas	2018	750.5	218.7	32.83	6.34	25.16	4.97	102.90	16.20
P2_0m	Bas	2019	731.6	208.6	32.17	5.81	24.98	4.97	101.77	15.50
P2_10m	Int1	2017	645.2	203.9	28.57	5.78	25.07	5.08	95.84	17.30
P2_10m	Int1	2018	643.6	191.0	28.03	5.31	25.36	5.08	95.91	16.18
P2_10m	Int1	2019	594.0	172.0	26.26	4.63	25.26	4.98	91.31	14.71
P2_16m	BoC	2017	717.9	234.7	29.36	6.15	27.02	5.94	100.94	18.21
P2_16m	BoC	2018	739.0	222.8	29.21	5.84	27.91	5.91	103.09	17.24
P2_16m	BoC	2019	691.5	199.6	28.18	5.12	27.09	5.59	99.80	16.09
P2_24m	Int2	2017	767.2	228.5	30.45	6.12	27.48	5.47	104.23	17.05
P2_24m	Int2	2018	768.3	234.5	30.19	5.92	27.88	5.76	104.08	17.09
P2_24m	Int2	2019	737.9	200.2	29.85	4.80	27.08	5.47	102.41	15.40
P2_30m	Top	2017	506.5	129.9	24.53	3.68	22.81	4.45	84.74	12.34
P2_30m	Top	2018	519.1	132.8	24.64	3.96	23.06	4.54	87.10	13.02
P2_30m	Top	2019	481.7	114.2	23.30	3.32	22.70	4.35	83.67	13.91
P3_0m	Bas	2017	808.0	294.4	31.93	7.69	27.32	6.23	108.43	21.68
P3_0m	Bas	2018	820.6	271.5	31.59	6.49	28.13	6.31	109.31	19.89
P3_0m	Bas	2019	843.4	277.3	32.61	6.67	27.78	6.06	111.39	19.75
P3_8m	Int1	2017	705.8	231.8	28.52	6.39	26.95	5.24	101.26	20.01
P3_8m	Int1	2018	599.0	177.4	25.59	4.56	26.07	5.05	90.54	15.63
P3_8m	Int1	2019	655.5	213.0	30.33	7.03	23.73	4.59	97.84	18.78
P3_14m	BoC	2017	601.0	230.7	28.99	7.86	22.67	5.10	94.89	23.14
P3_14m	BoC	2018	451.2	161.7	22.16	4.66	22.62	5.05	77.79	15.59
P3_14m	BoC	2019	542.2	195.2	29.51	7.48	20.35	4.25	89.71	19.83
P3_24m	Int2	2017	697.8	215.9	28.37	6.17	26.61	5.23	101.69	19.22
P3_24m	Int2	2018	681.7	198.0	27.71	5.46	26.47	5.14	98.95	16.35
P3_24m	Int2	2019	676.1	193.7	27.51	4.80	26.09	5.54	98.12	15.21
P3_30m	Top	2017	545.3	159.9	25.54	5.22	23.85	4.95	89.75	16.48
P3_30m	Top	2018	538.2	149.3	24.47	4.23	24.12	4.93	89.43	16.39

P3_30m	Top	2019	536.7	127.7	24.05	3.60	23.93	4.56	89.80	14.47

Personal declaration: I hereby declare that the submitted Thesis is the result of my own, independent work. All external sources are explicitly acknowledged in the Thesis.

Location, Date: Zürich, 30.09.2022 Signature: